Deformed soft matter under constraints

Martin Bertrand

Thesis submitted to the
Faculty of Graduate and Postdoctoral Studies
In partial fulfillment of the requirements
For the Ph.D. degree in Physics

Department of Physics
Faculty of Science
University of Ottawa

To Édouard and Élizabeth, hope it inspires you to follow your dreams.

SUMMARY

In the last few decades, an increasing number of physicists specialized in soft matter, including polymers, have turned their attention to biologically relevant materials. The properties of various molecules and fibres, such as DNA, RNA, proteins, and filaments of all sorts, are studied to better understand their behaviours and functions. Self-assembled biological membranes, or lipid bilayers, are also the focus of much attention as many life processes depend on these. Small lipid bilayers vesicles dubbed liposomes are also frequently used in the pharmaceutical and cosmetic industries. In this thesis, work is presented on both the elastic properties of polymers and the response of lipid bilayer vesicles to extrusion in narrow-channels. These two areas of research may seem disconnected but they both concern deformed soft materials. The thesis contains four articles: the first presenting a fundamental study of the entropic elasticity of circular chains; the second, a simple universal description of the effect of sequence on the elasticity of linear polymers such as DNA; the third, a model of the symmetric thermophoretic stretch of a nano-confined polymer; the fourth, a model that predicts the final sizes of vesicles obtained by pressure extrusion. These articles are preceded by an extensive introduction that covers all of the essential concepts and theories necessary to understand the work that has been done.

SOMMAIRE

Depuis plus d'une décennie, un nombre croissant de physiciens spécialisés en matière molle, incluant les polymères, s'attardent aux matériaux dit biologiques. Les propriétés de diverses molécules et fibres, tels l'ADN, l'ARN, les protéines et filaments de toutes sortes, sont étudiées afin de mieux comprendre leurs comportements et fonctions. Par ailleurs, plusieurs chercheurs se concentrent sur les membranes lipidiques, ces structures auto-assemblées fascinantes, comme elles semblent fondamentalement nécessaires à la vie cellulaire et sont, sous forme de vésicules, largement utilisées dans les industries pharmaceutiques et cosmétiques. Ainsi, cette thèse vous présente les fruits de travaux de recherche sur les propriétés élastiques des polymères et sur le comportement de vésicules lipidiques en extrusion dans des canaux de taille nanoscopique. Ces deux sujets peuvent sembler déconnectés, mais ils ont un dénomiteur commun : la matière molle sous déformation. La thèse contient quatre articles : le premier présente une étude fondamentale de l'élasticité entropique d'une chaîne ciruclaire ; le deuxième, une description simple et universelle de l'effet de la séquence sur l'élasticité linéaire de polymères tel l'ADN ; le troisième, un modèle de l'élongation symétrique d'un polymère nano-confiné soumis à des forces thermophorétiques ; le quatrième, un modèle prédisant la taille finale de vésicules obtenues par extrusion sous pression. Ces articles sont précédés d'une introduction extensive couvrant les théories et concepts essentiels à leur compréhension.

STATEMENT OF ORIGINALITY

I hereby certify that, to the best of my knowledge, the research presented in this thesis is original. I have defined the questions, conducted the studies, and wrote the papers under the supervision of Dr. Béla Joós. Martin Forget, co-author of the paper on circular chains, was an undergraduate student that I helped supervise and who conducted some of the initial molecular dynamics simulations of this particular system. The same can be said for Daniel O'Keeffe, co-author of the paper on the elasticity of heteropolymers. I constructed various models and ran simulations to describe the elastic properties of polymer chains and the rheology of lipid bilayer vesicles extruded in narrow channels, sometimes explaining experimental results and confirming established theories, often making new predictions that could be tested experimentally.

ACKNOWLEDGEMENTS

The journey through the land of doctoral studies is not one to walk alone. Many I have met who explicitly or even implicitly helped me go forward. I fear establishing any list of names since I wish to not forget anyone. Those colleagues and friends who supported me, I thank you all from the bottom of my heart. There are however very special persons that I would like to name and thank. I cannot find the proper words to describe how grateful I feel to have worked under the supervision of Béla Joós. He has been a patient and very understanding guide, teacher, and friend. He has supported me through some very rough times and still is to this date. He trusted me, gave me plenty of latitude in research, and offered all the academic opportunities I could dream of. Also, I would like to thank my son Édouard and my daughter Élizabeth. Let me say it with simple words: they make me happy and fill me with pride, amazement, and wonder. And last but not the least, I could not have done it without Karine, my partner in life, my muse, my love.

FOREWORD

As one starts writing a scientific thesis, especially one by articles, the following dreaded question inevitably comes: who's going to read this anyway? Colleagues and other scientists are mostly going to be interested in the articles, as they should. Referees will read it of course, but who else? I say students are.

Indeed, I myself remember having consulted the thesis of those preceding me in the groups of Dr. Gary Slater and Dr. Béla Joós. I found both enjoyment and much needed information in some of the best written ones. I therefore dedicate my introduction to those students coming after me. I have made sure that all the knowledge needed to understand the context and the contributions of the articles making up the main body of this thesis is covered. I have strived to explain concepts and theories in the most intuitive way possible, as I always do. I thus made heavy use of carefully crafted images to strongly convey ideas, and employed a tone that borrows from popularization works as much as possible.

If you happen to be familiar with some of the basic topics I cover and do not wish to go through a review, I strongly advise you at least skim these more tedious parts since lots of useful information about the articles is embedded in the introduction. But my sincere hope is that no matter how versed you are in the subjects I present, you will enjoy how they are conveyed in this present document.

All that's left to say is: enjoy your reading !

Table of contents

1

Introduction

C'est l'inconnu qui m'attire. Quand je vois un écheveau bien enchevêtré, je me dis qu'il serait bien de trouver un fil conducteur.
-Pierre-Gilles de Genne

From the title, you must have guessed that the concept of soft matter is central to this work. However, you might be wondering what characterizes a matter as soft as opposed to hard. If this is your case, you will find answers in the first sections of this introduction. I also try to contextualize my research in the framework of biological physics. In addition, you will receive relevant information regarding the physics of these materials studied in the subsequent articles. And since all my work combines theory to computational tools, it is only natural that I elaborate on those in the last sections. I have kept the style of this introduction as light as possible with plenty of illustrations as they often convey more information than even the best wording could achieve and calling upon equations only when necessary.

1.1 Soft *vs* Hard

If I were to ask "Can you give me examples of both soft and hard matter?", I have no doubt that you'd be successful in doing so. That's because in our daily routines we constantly interact with objects made of either one. We have constructed intuitive definitions for both through our experimentations with the world surrounding us. We quite readily classify liquids, foams, gels,

and the such as being soft, whereas we find metals, wood, and glass to be hard. However, the physical differences between hard and soft matter are not readily exposed by our intuition. Let us establish a contrast that should help better define soft matter.

Some hard materials - most metals - are found in a crystalline form at room temperature[1], that is the molecules or atoms constituting their bulk are bound to each other on a lattice and remain so at all scales (Fig. 1.1): remember in high school when we were told that no matter how small a cube of salt is fractured it still looks like a cube. These materials do have some elastic properties, the steel cables of a suspended bridge stretch under tension for example, but beyond a certain load, atomic bonds are broken and cracks start to propagate. To study their mechanical properties, microscopic or macroscopic, one has to focus on atomic interactions as they govern responses at all scales.

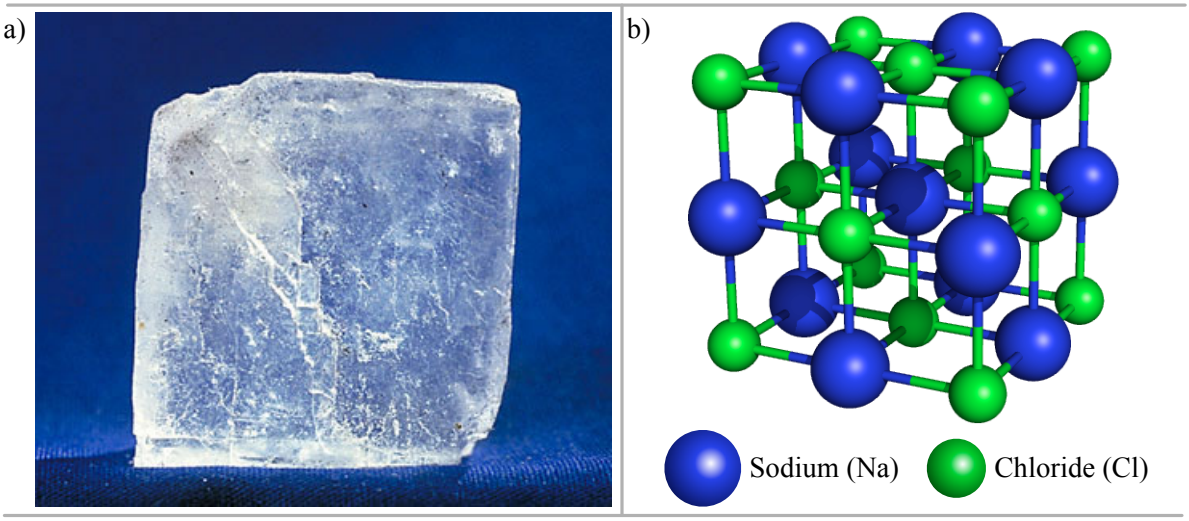

FIGURE 1.1 A simple example of hard matter: common table salt which goes under the code name *Sodium Chloride* alias NaCl. In a) we show a real life picture of a salt cube (origin unknown) and in b), the atomic structure where atoms are arranged on lattice sites.

By opposition, we will then define soft materials as those whose microscopic molecular constituents are loosely bound together. In fact they are constantly jiggled around by what we call thermal forces which often dominate molecular interactions at the microscopic scale. But at the mesoscopic scale, just between micro and macro, these can often shape into structures whose

[1] Hard materials can be found in an amorphous form, that is the constituents are not arranged in a regular lattice, but the small scale fluctuations in soft materials contrast better with the order found in crystals.

interactions influence the mechanical properties of the material on the macroscopic scale. One simple example of such a material is foam (Fig. 1.2): the microscopic fibres or polymers are thermally agitated and form bubbles under given conditions, and it's the properties of these bubbles and their interactions which set the overall characteristics of the material. One complex example could be our muscle fibres: smaller molecules under thermal agitation find each other and form mesoscopic structures such as proteins, special fibres, and lipid membranes which are themselves the constituents of mesoscopic objects that we call cells whose interactions result in macroscopic muscle functions. Soft materials often exhibit unusual mechanical properties. For example, the famous Silly Putty bounces back when thrown but slowly flows down a slope if left undisturbed for a while. We find that whether the material exhibits an elastic or a viscous response depends on the magnitude and duration of the applied load. We say it is **viscoelastic**. Patrick Oswald wrote a superb book about soft matter **rheophysics**, that is how it deforms when subject to some constraint, that I highly recommend to the curious reader [1].

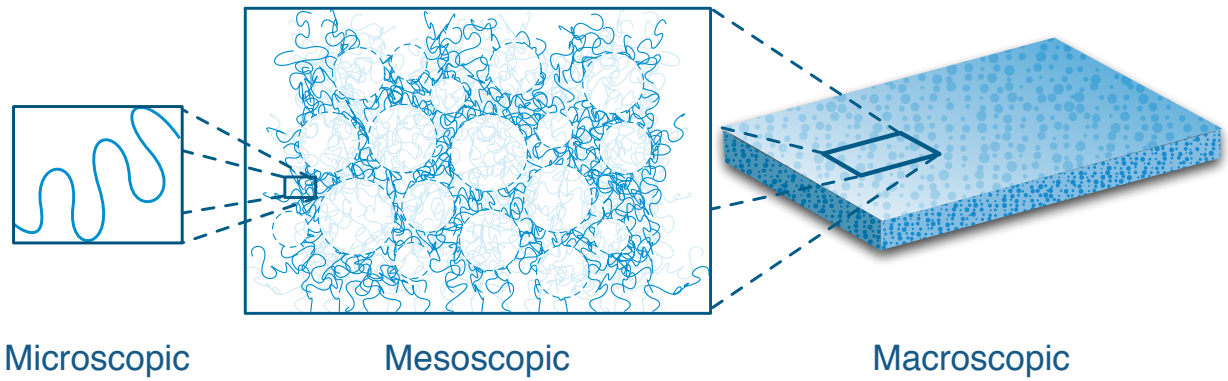

FIGURE 1.2 A simple example of soft matter: a generic foam. In this specific depiction of a foam, on the microscopic scale there are fibres which are then arranged in a manner that allows bubbles to appear on a mesoscopic scale, and these structures result in macroscopic properties.

Thus comes our definition of soft matter: a material is soft when it is characterized at small scales by an interplay between **enthalpic** and **entropic** forces close to room temperature. Enthalpic forces are simply those due to atomic or molecular interactions, whereas entropic forces are the result of thermal agitation. The rest of this chapter is dedicated to our exploration of two types of soft mesoscopic materials mostly related to biological systems: polymer chains such as DNA and proteins, and lipid bilayer vesicles. In particular, we will elaborate on the rheophysics of these. But first, let us talk about the relationship between physics and biology.

1.2 Biological physics

Physicists have always been intrigued by biological systems. Some of our greatest have tried to provide answers to fundamental problems in biology such as Erwin Schrodinger in his 1944 book entitled *What is life?* [2][2]. Throughout the 20-th century, there has been a steady rise in the number of physicists engaging in research related to biological systems. Loofbourrow in 1940 wrote one of the earliest reviews of the application of physical methods in biological sciences [3]. He cited 1203 references in biological physics while today the number of papers in the field is in the hundreds of thousands. However, it's only in the last decade or so that physics departments really started to be populated by a breed of scientists who often refer to themselves as biophysicists, since up until the mid-nineties, most academic positions were held by physicists working in traditional sub-fields of physics [4]. Today, the *Biophysical Society*, www.biophysics.org, counts 9000 members and annually gathers around 6000 of those to share results and ideas.

So what is biological physics? I will borrow the words of Andrew Rutenberg from the website for *Quantitative Biology in Canada*, www.qbio.ca, as he puts it more succinctly than I would: "Physics is the quantitative study of nature, with an impulse towards control and simplicity. Biological physics (or physical biology or biophysics) is that study of biological systems." If biophysics is a sub-field of physics, it also has a vast set of sub-fields itself. One could go right down to the molecular level and study the properties of the very basic components of life (DNA, RNA, proteins, etc.), whereas another could try to understand the behaviour of entire bacterial colonies (see Fig.1.3). Philip Nelson's [5] and Henrik Flyvbjerg et al. [6] books are both great introductions to the many problems physicists tackle in biology, the former being geared more towards the beginner while the latter is addressed to an advanced crowd.

A popular and well funded area of research in biophysics is biomedical physics. Here, the quantitative approach of physics is used to better understand how to interact with biological matter with the objectives to prevent and/or treat medical conditions. Within this sub-sub-field, a multitude of problems are addressed by physicists. Imaging techniques were some of the earliest applications of physics to the medical field. One only has to remember the discovery and use of X-rays by Roentgen at the beginning of the 20-th century. Later came radiation therapy techniques which to this date are still being improved. Nowadays, physicists participate in the development of novel faster and cheaper DNA sequencing techniques for genetic studies and therapies [7], lab on

[2] We now know he was mostly wrong. Nevertheless he convinced a great many physicists to study biological systems

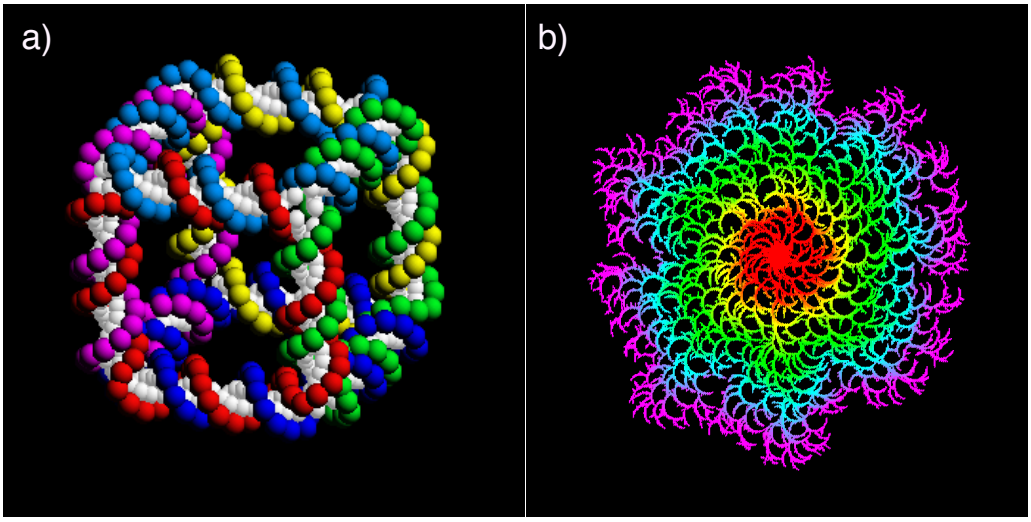

FIGURE 1.3 a) The study of the properties of DNA has led to the creation of nanoscopic structures such as this cube (image courtesy of Prof. Ned Seeman). These could be useful in the design of nano-devices, nano-robots, and DNA based computers. b) Growth simulation of a colony of *P. dendritiformis* bacteria (image courtesy of Prof. Eshel Ben-Jacob).

chips for diagnostic or synthesis purposes [8], drug delivery systems [9], and revolutionary cancer therapies based on the properties of nano-particles [10] just to name a few. And it goes without saying that our better understanding of biological systems in general can lead to biomedical applications.

Of course, to engage in meaningful research biophysicists need not only to collaborate with one another but also with members of other disciplines. Physicists, biologists, chemists, health scientists are all mingling and cooperating to unravel the mysteries of life, its inner workings, and to improve our ability to prevent and treat illnesses.

The studies presented in the articles that make up the body of this document are all related to the mechanical properties of soft materials found in the human body. Hence they fall in the sub-field of biological physics with possible biomedical applications. The first three focus on the mechanical response of single isolated polymers to applied constraints. In all cases the polymers are idealized but could represent DNA, proteins, or other relevant microstructures in the body. The last article revolves around the rheological properties of lipid bilayer vesicles flowing in narrow nano-capillaries. It could impact the production of vesicles for drug encapsulation and delivery, but could also improve our understanding of the deformation and flow of cells such as erythrocytes

and platelets in the smallest channels of our vascular system. The next sections are dedicated to the introduction of key concepts in polymer and lipid bilayer physics with explanations regarding the numerical tools used to prepare the reader for the following chapters.

1.3 Essential concepts

Before we discuss the physics of the specific soft materials we will encounter in the main body of this document, the reader is invited to a short introduction covering some essential concepts: random walks, diffusion, entropy, and free-energy. The goal here is to refresh the memory more than to teach which explains why many details are skipped.

1.3.1 Random walks and diffusion

The **random walk** (RW) is often referred to as the "drunkard's walk" and indeed it does resemble the stereotypical manner in which someone very drunk moves [5]. Random walks are encountered in almost every field of research and serve to model various phenomenon. To generate a RW in 1,2, or 3 dimensional space is fairly easy: take N successive steps of length b, each step being in a random direction as in Fig. 1.4. If one were to generate a number of RWs of the same length all starting from a single origin, one would find the mean square distance travelled to be:

$$\langle R^2 \rangle = Nb^2 \tag{1.1}$$

I here refer the reader to the Wikipedia entry for random walk as a starting point to explore its many possible uses, RW. We will consider only two of these: 1) the RW model of particle diffusion, the topic of this subsection; 2) the RW model of an ideal chain.

Thermal agitation, that we referred to earlier, results in the **diffusion** of particles in gases and liquids, a motion called Brownian. The story goes that it is the botanist Robert Brown in 1827 that discovered this motion while observing pollen grains at the surface of water under the microscope and it so happens that it was a RW. In 1905, Einstein connected the dots, yet again. He used the central limit theorem, which states that any random process occurring over a sufficiently large ensemble or long interval of time can be described by Gaussian statistics, and first derived an equation for the mean square distance travelled by a particle (or a collection of particles) in a time t [11]:

$$\langle R^2 \rangle = 2dDt, \tag{1.2}$$

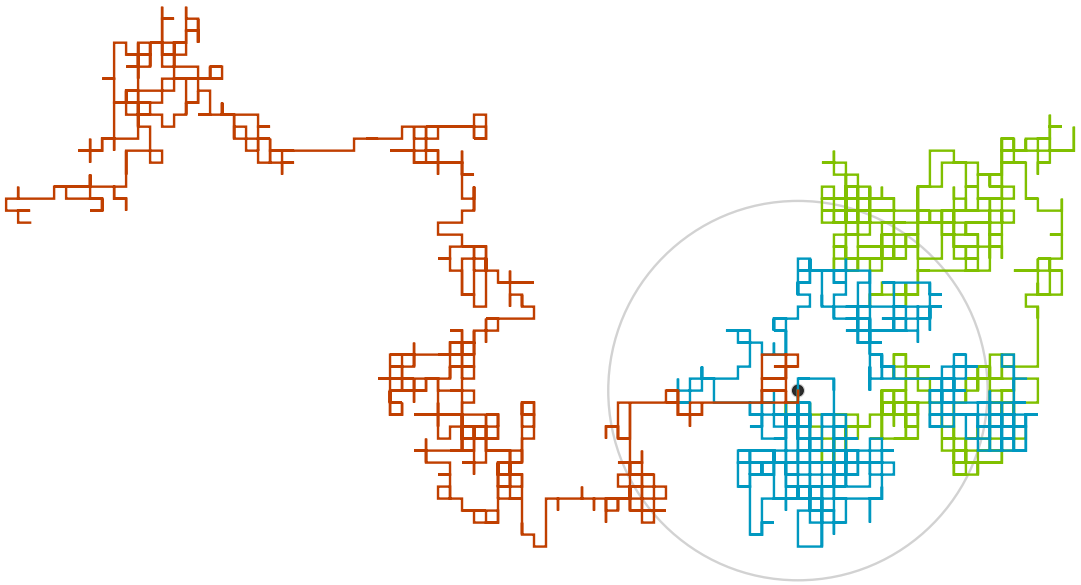

FIGURE 1.4 Random walks on a 2-dimensional lattice. This is a sample of only three RWs of a 1000 steps all originating from the same point as it gets messy quickly. The grey circle outlines the root mean square distance $N^{1/2}b$ one would expect to obtain for many walks. It is important to observe that a single RW does not necessarily travel such a distance.

where d is the number of dimensions (let us limit this discussion to cases where $d = \{1, 2, 3\}$), and D is called the diffusion coefficient. Putting Eqs. 1.1 and 1.2 together we get that $D = Nb^2/2dt$. Einstein went further, and derived a relationship between diffusion D, thermal energy k_BT (k_B is the Boltzmann constant and T, the temperature), and friction with the surroundings ζ:

$$D = \frac{k_BT}{\zeta}. \tag{1.3}$$

In technical jargon, Eq. 1.3 is a fluctuation-dissipation relation. It relates an intrinsic property of the system, in this case the diffusion coefficient D, with a linear response coefficient, in this case the friction coefficient ζ. In more intuitive words, Eq. 1.3 says that the thermal energy of a particle, which leads to its diffusion, is dissipated through friction with the surroundings. Friction itself arises because a diffusing particle collides with its neighbours with $\bar{t}_f$ being the mean time of flight between two collisions and b, the mean free path travelled. We thus find the number of steps taken in a time t to be $N = t/\bar{t}_f$. In the context of polymer physics, even though the monomers are connected to each other, they diffuse, that is they undergo Brownian motion. It is this internal motion that allows the entire chain to explore its many possible configurations in space which make up what we call configurational entropy. In the context of a lipid bilayer membrane,

the constituents, that is the lipids, first find each other through diffusion in solution and then are able to diffuse in the two-dimensional membrane itself giving it the ability to reorganize constantly and fluidly.

1.3.2 Entropy and free-energy

Entropy, denoted S, is a concept central to all the systems we will discuss in this document. Its very formal definition goes as follows: if the probability of finding a system in the i-th state is P_i, then its entropy is [12]:

$$S = -k_B \sum_i P_i \ln P_i. \tag{1.4}$$

More intuitively, entropy can be thought of as a measure of the number of ways a system can be arranged given some conditions. In fact, if the system is totally closed, we find that all states are equally probable with $P_i = 1/\Omega$ where Ω is the number of states. Eq. 1.4 then simplifies to $S = k_B \ln \Omega$, an expression that closely matches our intuitive definition and can even be found engraved on Ludwig Boltzmann's tombstone. The second law of thermodynamics states that an isolated system in equilibrium has its entropy maximized. Thus, in the process of reaching that equilibrium entropy increases and since there are many more ways to put things in disorder than in order, the latter is often only achieved by paying in the energy currency[3]. We could go on for many pages on entropy alone and the curious reader is advised to pick the excellent book by Brian Greene *The Fabric of the Cosmos* [13] for an entertaining discussion on the topic.

The second law of thermodynamics seems to imply that something like life, that necessitates highly structured systems, cannot exist. The key out of this trap lies in the word **isolated**. Indeed, living organisms and their subsystems are not isolated but are rather deeply connected to their environment. This is the case for all the systems considered in the articles to come. For them, we will consider the following conditions to hold: the number of particles N is constant and so is the volume V, while the temperature T is equal to that of the heat bath to which it is connected. In thermodynamics, we say the system is in the canonical or NVT ensemble [12]. The main difference, between such a system and the isolated one, is that heat (energy) can be exchanged with the environment. This situation requires that we take into account not only the entropy S, but also the potential energy U of the system, or energy of interaction between the constituents.

[3] I often think of that when comes the time to put things where they belong in our home.

Hence, the concept of **free-energy** is introduced. We calculate this new quantity A in the following way:

$$A = U - TS. \tag{1.5}$$

A system in the NVT ensemble is in equilibrium when the free-energy is minimized. If the entropy decreases but concords with a more important decrease in potential energy, the second law of thermodynamics is still observed. That's because the lost energy has been dissipated in the form of heat transferred to the bath, and since a variation of heat equals entropy, the entropy of the bath plus the system increases. Life is possible!

1.4 Polymer physics

Let us delve into the physics of single isolated polymers as the three first articles you will get to read concern such structures. Polymers do not behave the same way whether they are isolated in solution, in denser solutions, in melts and gels, or rubber. To thoroughly discuss polymer physics necessitates writing an entire book and fortunately for us some very good ones have already been produced. I give you here my favourites or those I consulted the most: *Polymer Physics* by Rubinstein and Colby [14], *Polymer Solutions* by Teraoka [15], and *The Physics of Polymers* by Strobl [16]. Most of what is covered in this section can be found in one of these books in one form or another. None of these books address the issue of electrostatic interactions and neither will we. Although most polymers of biological relevance are charged in solution, a great deal can be learned about their mechanical properties without explicitly taking into account these interactions.

So then what is a **polymer**? A quick search on the etymology of the word itself reveals that it comes from the combination of two words in Ancient Greek, *polus* meaning "many" and *meros* meaning "part". A polymer is thus a collection of many - poly - similar elements - **monomers** - strung together much like train cars. Some of the most notable biopolymers are DNA, RNA, and proteins. But really, any biological fibre made of smaller constituents can be considered a polymer. I should also stress that synthetic and petroleum derived polymers are frequently used in industry. We are literally surrounded with polymeric products, mostly plastics and rubbers. The chemical details keeping the monomers bound together on the atomic scale will be overlooked as the behaviours of the polymers considered here are largely independent of these [17]. We will first discuss the ideal chain model of a polymer isolated in solution and then move on to more realistic models, *i.e.* the real flexible chain and the semi-flexible chain. We will finish this section with a

discussion of the deformation of polymers under constraints, whether they be external forces or confining geometries.

1.4.1 The ideal chain

The simplest model of the configuration of a polymer in solution at a given instant is the RW. Let us assume that the chain is made of N connected monomers of length b such that its total length, or contour length, is $L_c = Nb$. Then by generating a RW of N steps of length b, we sample one of the possible configurations of the polymer. Of course, this is overly simplistic and not realistic, since non-adjacent monomers do not interact which allows for the possibility of monomer superposition in space (see Fig. 1.5). Nevertheless, this model of a polymer that we call the **ideal freely-jointed chain** (IFJC), is mathematically tractable and makes for a good introduction to polymer physics.

Over time, the IFJC explores its configurational space through Brownian motion as explained in the previous subsection which amounts to generating a multitude of RWs. Thus, the mean square end-to-end distance of the polymer is simply given by Eq. 1.1. You might wonder what does the chain looks like on average, a question that can only be fully answered using the concept of configurational entropy. The latter is equivalent to enumerating all possible RWs of N steps of length b that can be generated, a large amount by all account. But I do not need this number to tell you that it spends more time in a coil-like configuration. Let me guide your intuition here: take a piece of string, fully stretch it and observe how many configurations are possible for your string disregarding rotations around its center; now coil it in your palm many times over and observe the various ways you can achieve this. Just like the string you manipulated (or pictured in your mind), there are many more ways to coil a polymer than to fully stretch it.

The surprising consequence of this, is that if you were to stretch the chain, it would appear to resist since it goes against its tendency to be coil-like. This is why polymers are often referred to as entropic springs. Since the ideal chain's configurations can be described by RWs, they obey Gaussian statistics. One can use this to calculate its free-energy A as given by Eq. 1.5 where only entropy is important since the potential energy does not change, and then use this result to estimate the force with which the chain opposes being in a stretched configuration ($f = -\partial A/\partial R$). One finds a Hookean relationship:

$$\vec{f}_{\text{sp}} = \frac{3k_BT}{Nb^2}\vec{R}, \tag{1.6}$$

where $\vec{R}$ is the end-to-end vector. The entropic spring's constant is thus $k_{\text{sp}} = 3k_BT/Nb^2$.

The coiled chain rotates around its center of mass and occupies, on average, a spherical space whose radius of gyration is R_g. Its square is defined as the mean value over many configurations of the average square distance between the monomers and the center of mass. If $\vec{R}_i$ is the position of the i-th monomer, and $\vec{R}_{\rm cm}$ is the center of mass, we can write:

$$R_g^2 = \left\langle \frac{1}{N} \sum_i \left(\vec{R}_i - \vec{R}_{\rm cm} \right)^2 \right\rangle . \tag{1.7}$$

For a long ideal chain we find that $R_g^2 = Nb^2/6 = R^2/6$. Despite its simplicity, the ideal chain model well describes polymers in the melt, real flexible chains in a θ-solvent, and long semi-flexible chains. We will discuss the two last cases shortly.

1.4.2 The real chain

The monomers of a realistic chain cannot occupy the same spot in space as imposed by Pauli's exclusion principle on the electron clouds. One models a **real FJC** (RFJC) by introducing some interaction potential between the monomers that includes a short range hard-core repulsive force to keep them from overlapping. But we'd also like it to have an attractive part at longer range since monomers often prefer their own company than that of the solvent particles. The Lennard-Jones (LJ) potential matches these requirements and is considered a good approximation for inter-molecular interactions [18]:

$$U_{\rm LJ}(r) = 4\epsilon \left[\left(\frac{\sigma}{r} \right)^{12} - \left(\frac{\sigma}{r} \right)^{6} \right] . \tag{1.8}$$

In the above, r is the inter-molecular distance, while ϵ gives the depth of the potential and σ, the distance at which it is equal to zero. The LJ potential is repulsive up to $r = 2^{1/6}\sigma$ and then becomes attractive. Each monomer making up our real chain occupies a volume where all other monomers are excluded. Compared to its ideal counterpart, the real chain thus looks swollen at sufficiently high temperatures as will soon be discussed. If one knows the **excluded volume** v, it is fairly easy to construct a real chain by performing a self-avoiding random walk (SAW): a RW that allows the placement of a monomer only if it does not fall too close to another one (see Fig. 1.5).

It appears that we need a value for v to be able to describe the configurations of a real chain. The excluded volume depends on the differences between monomer-solvent, monomer-monomer, and solvent-solvent interaction energies. It depends on the temperature through a Boltzmann factor

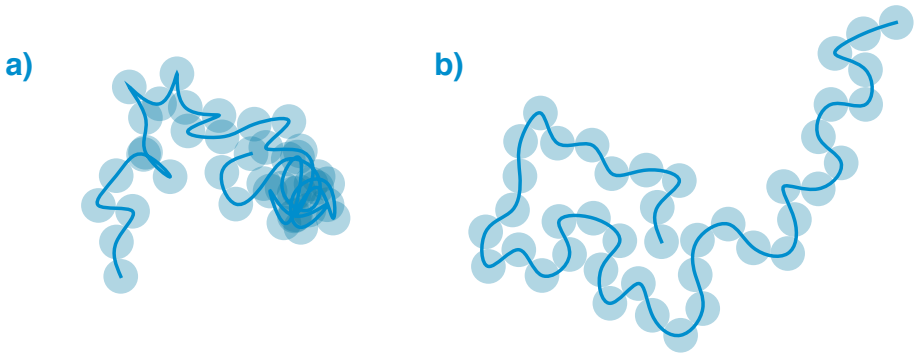

FIGURE 1.5 Two-dimensional polymers (N=40): a) an ideal chain generated by RW where one can clearly see the monomers overlapping; b) a real chain generated by SAW where the monomers do no overlap.

of the form $\exp(-U(r)/k_BT)$ where $U(r)$ is an effective monomer-monomer interaction of the form given in Eq. 1.8. One can derive a simple equation for $v(T)$ [14]:

$$v(T) = \int [1 - \exp(-U(r)/k_BT)]\, d^3r \approx \frac{T-\theta}{T} v_\infty, \tag{1.9}$$

where θ is a transition temperature, and v_∞, the high temperature limit of v. For a real chain made of spherical monomers of size b, like single-stranded DNA (ssDNA), $v_\infty = b^3$, while for one made of cylindrical monomers of length b and diameter d, like double-stranded DNA (dsDNA), $v_\infty = b^2 d$ [19]. For temperatures well above θ, we say the solvent is athermal, just above θ, it is good, and in both cases the repulsive part of Eq. 1.8 dominates. At $T = \theta$, we have a θ-solvent, the repulsive and attractive part sort of cancel out, and the chain size scales like an ideal one. Below θ, the solvent is poor, the attractive part of Eq. 1.8 dominates, and the chain starts to collapse on itself in a globular configuration with a negative value for the excluded volume v. A coil to globule transition thus happens as the temperature is lowered across the θ value.

With the excluded volume known, it should now be possible to determine the average size of a real chain in solution. Flory estimated the contributions of molecular interactions to the free-energy of the real chain A_{int} using a mean-field approximation [20]. He assumed the concentration of monomers to be the same in the entire volume occupied by the chain, $c_m \sim N/R_F^3$ where R_F is the Flory radius and $N \gg 1$. Doing so gives:

$$A_{\text{int}} \approx kT \left[v\frac{N^2}{R_F^3} + w\frac{N^3}{R_F^6} \right], \tag{1.10}$$

where the first term, involving the excluded volume, models the contribution of two-body interactions, whereas the second term accounts for three-body interactions with $w = b^6$ and $w = b^3d^3$ for spherical and cylindrical monomers respectively. Notice that Eq. 1.10 does not carry any numerical factors as we are in the realm of approximations and all we really wish to recuperate are the correct scaling laws and ball park estimates for observables. The real chain is still an entropic spring and Flory approximated its response to be much like an ideal chain to first order whose contribution to the free-energy A_{ent} is:

$$A_{\text{ent}} \approx kT \left[\frac{R_F^2}{Nb^2} + \frac{Nb^2}{R_F^2} \right], \tag{1.11}$$

where the first term represents the response to stretch that we've already encountered and the second one, the response to compression.

For a chain in an athermal or good solvent, three-body interactions are negligible since the monomer concentration is not high enough, and the entropic response to compression is negligible as the chain swells because of **excluded volume interactions** (EVI). Thus combining the appropriate terms of Eqs. 1.10 and 1.11 we get an approximate free-energy of the chain:

$$A \approx kT \left[\frac{R_F^2}{Nb^2} + v\frac{N^2}{R_F^3} \right]. \tag{1.12}$$

At equilibrium the above is minimized and one finds the Flory radius of the swollen real chain:

$$R_F \approx v^{1/5} b^{2/5} N^{3/5}. \tag{1.13}$$

This result agrees very well with experiments, simulations, and other more complicated theories such as renormalization group theory. This is surprising because we now know that Flory overestimated EVI by assuming a homogeneous concentration of monomers in the volume occupied by the chain whereas it is heterogeneous, and he also overestimated the entropic response to stretch by considering the one of an ideal chain. Nevertheless, it appears that these errors cancel out which explains why Flory's approach is still used to this date with great success (see Chapter 4). For a chain in a θ-solvent, interactions are completely negligible, and minimizing Eq. 1.11 leads to $R_F \approx bN^{1/2}$, the size of an ideal chain. And finally, for a chain in a poor solvent, the entropic response is negligible, and minimizing Eq. 1.10 gives $R_F \approx (wN/|v|)^{1/3}$, the size of the globular chain. Thus in general we write that $R_F \propto N^{\nu}$, where ν is the Flory exponent and corresponds to the type of solvent the chain is in.

The excluded volume v also defines the size of a **thermal blob** ξ_T, that is the chain size for which EVI, as defined by the first term of Eq. 1.10, equate the thermal energy k_BT:

$$k_BT|v|\frac{g_T^2}{\xi_T^3} \approx k_BT. \tag{1.14}$$

Below that size, the g_T monomers contained in each thermal blob behave mostly like an ideal chain, $\xi_T \approx bg_T^{1/2}$, while above, EVI become important for blob interactions. We therefore find:

$$\xi_T \approx \frac{b^4}{|v|}. \tag{1.15}$$

For a polymer in an athermal solvent ($T \gg \theta$) and in a literally bad solvent ($T \ll \theta$), the thermal blob size is that of the monomers b. In molecular dynamics (MD) simulations, polymers are often modelled like beads strung together with springs, the Kremer-Grest approach [21]. The springs model the entropic elasticity of the ideal sub-chains contained in the thermal blobs while the interactions between the beads account for the EVI between the blobs themselves. MD simulations of polymers will be covered in a later section.

The first article you will read concerns isolated **circular real chains** under deformations (see Chapter 2). Many circular polymers are encountered in biological physics whether it be circular DNA molecules in some bacteria [22] or circular structures in some proteins. In addition, cyclic peptides are often looked for or synthesized in the pharmaceutical industry since they are more stable than their linear counterparts [23]. In terms of equilibrium properties, the scaling laws we've just introduced also work for circular chains in the limit where $N \gg 1$. It gets more interesting when forces are applied to these objects and we shall elaborate on the topic in section 1.4.4.

1.4.3 The semi-flexible chain

Up to until now, we have only looked at chains that are fully flexible (FJC models), the only rotational constraints imposed on the monomers of real chains originating from coarse EVI (RFJC model). However, many biopolymers are semi-flexible in nature, the obvious example being ds-DNA. The constituents along the backbone of a semi-flexible polymer cannot freely rotate due to steric hindrance (see Fig. 1.6). Thus the directionality of the chain persists beyond the size of its molecular building blocks.

If s is a curvilinear coordinate that follows the backbone, then the autocorrelation of the tangential unit vector $\hat{t}(s)$ (shown on Fig. 1.6) decays exponentially:

$$\langle \hat{t}(0) \cdot \hat{t}(s) \rangle = \exp(-s/l_p), \tag{1.16}$$

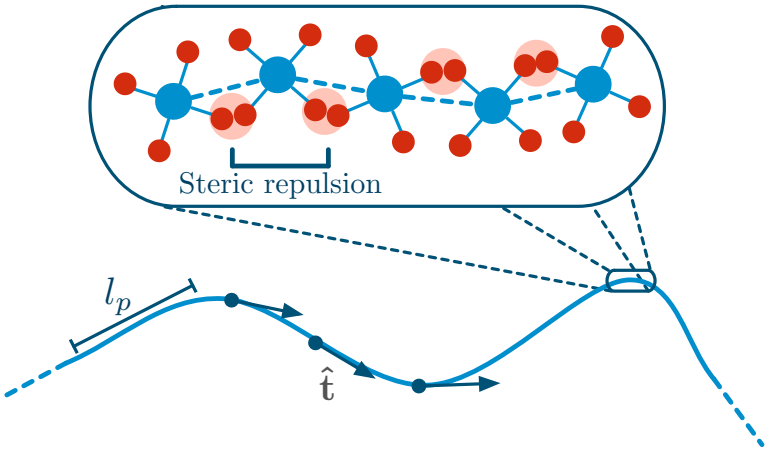

FIGURE 1.6 Cartoon representation of a semi-flexible chain with a close-up on the structure of the backbone where one can see the steric repulsion between the constituents limiting their rotational freedom. The characteristic length scale of the chain, the persistence length l_p is shown, so is the change in the direction of the tangential unit vector $\hat{t}$.

where l_p is the **persistence length**, the characteristic length scale of a semi-flexible chain. Eq. 1.16 is the central piece of the worm-like chain (WLC) model, or Kratky-Porod chain, used to describe semi-flexible chains. The end-to-end vector of a WLC is $\vec{R} = \int_0^{L_c} \hat{t}(s)ds$ where L_c is the contour length. Thus the mean size of a WLC as given by its mean square end-to-end distance is:

$$\langle R^2 \rangle = \langle \vec{R} \cdot \vec{R} \rangle = 2l_p L_c \left[1 - \frac{l_p}{L_c} \left(1 - e^{-L_c/l_p} \right) \right]. \tag{1.17}$$

We are here considering an ideal WLC in the sense that nothing prevents far apart segments of the chain to overlap. In the case where $L_c \gg l_p$, Eq. 1.17 reduces to $\langle R^2 \rangle \cong 2l_p L_c$, and if one introduces the concept of Kuhn segments of length $b_K = 2l_p$, it further reduces to:

$$\langle R^2 \rangle \cong b_K^2 N_K, \tag{1.18}$$

where $N_K = L_c/b_K$ is the number of Kuhn segments in the chain. In other words, in the limit where the WLC is long compared to its persistence length, it behaves like a flexible ideal chain of N_K Kuhn segments of length b_K and indeed, this is true in reality [19]. Semi-flexible chains are often better modelled using cylindrical monomers of diameter d than spherical ones which are better suited for real flexible chains. This is best showcased by the following example: dsDNA whose Kuhn length is $b_K \cong 132\text{nm}$ and diameter, $d \cong 2.0\text{nm}$ is semi-flexible and modelled with cylindrical monomers whereas ssDNA whose Kuhn length is $b_K \cong 1.2\text{nm}$ and diameter,

$d \cong 1.0\text{nm}$ is a real flexible chain made of roughly spherical monomers [19].

For semi-flexible chains such as dsDNA, whose backbone can be made of any sequence of its four fundamental building blocks A,C,G, and T, the persistence length l_p can be a function of s, that is it can vary along the chain [24]. In this sense, DNA is a heterogeneous polymer. Thus, the measured experimental persistence length of such a chain is an effective value L_p (notice the capital L) [25]. For sufficiently long chains, the sequence becomes irrelevant and all should have the same effective persistence length $L_{p,\text{eff}}$. But for shorter chains, L_p will vary from one sequence to another. It is this variability that the article presented in Chapter 3 attempts to quantify.

1.4.4 The response of polymers to applied external forces

A classical case of soft matter deformation under a constraint is the uniaxial extension of a polymer chain under the action of an applied force [5]. One can essentially pull on both ends of a polymer with a force f (or pin one down) and measure the resulting mean extension, an experiment performed in the constant stress ensemble. Conversely, in the constant strain ensemble, one maintains the two ends at a fixed mean distance from one another and tracks the recoil force exerted by the polymer. In either cases, there is a departure from the preferred coil-like configuration of the polymer which means the origin of the force that resists extension is at least partly entropic. Pulling on a nanoscopic chain might seem like a boring thing to do, but there is a great deal one can learn about the elastic properties of the molecule itself while performing these force spectroscopy measurements [26]. The acquired knowledge can be used to uncover the folding pathways of proteins, to better understand how DNA packs in the nucleus and how it translocates out of it, or to precisely manipulate single biopolymers and expose their backbone to study the binding activity of enzymes for example.

Deformed ideal chain

Let us first discuss the response of an **ideal** FJC being stretched (constant stress ensemble). We already said the chain acts like an entropic spring with a response force given by Eq. 1.6 which allows the chain to extend indefinitely (see Fig. 1.7a). This is rather unrealistic as we expect the end-to-end distance to smoothly saturate towards the contour length of the chain $L_c = Nb$ (see Fig. 1.7b). In fact, a thorough derivation of the magnitude of the scaled mean extension $H = \langle h \rangle / Nb$

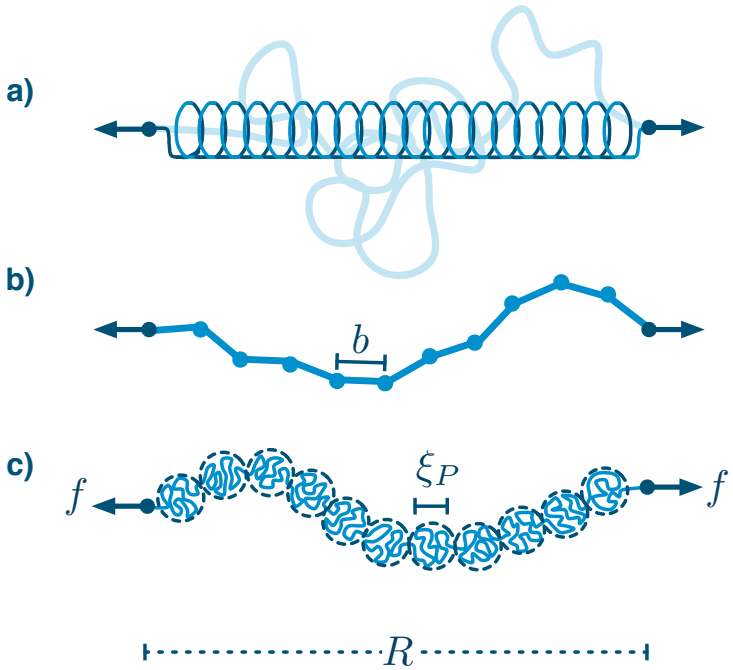

FIGURE 1.7 Chains being stretched by a force f: a) ideal chain modelled as a simple Hookean entropic spring; b) ideal chain with monomers of length b (long semi-flexible chain where $b_K = b$); c) real chain made of a sequence of Pincus blobs of size ξ_P.

as a function of the scaled applied force $F = fb/k_BT$ using statistical mechanical tools yields [14]:

$$H = \coth F - \frac{1}{F}. \tag{1.19}$$

The right hand side of Eq. 1.19 is what we call a Langevin function. For small forces $F \ll 1$, Eq. 1.19 simplifies to the linear relationship given in Eq. 1.6. For large forces $F \gg 1$, it simplifies to $H = 1 - 1/F$ which asymptotically approaches unity as the force increases. In the constant strain ensemble, the force F as a function of the extension H can only be approximated [27]:

$$F \cong \frac{3(1-1/N)H - (1+1/N)H^3}{1-H^2}. \tag{1.20}$$

In the Kremer-Grest approach to the molecular dynamics simulation of polymers [21], the springs linking the beads together, dubbed Finitely Extensible Non-linear Elastic (FENE) springs, have

a recoil force of the form given by Eq. 1.20 where often N is taken to be very large such that $1/N \to 0$.

Deformed real chain

What about the response to stretch of **real flexible** chains with EVI? There is no exact statistical mechanical calculation that can be performed here to give us the extension *vs* force relationship. One can at best describe what happens using scaling arguments, an art that Pierre-Gilles de Gennes, one of the fathers of polymer physics, was highly proficient at (see his book [17]). We've already talked about the thermal blob size ξ_T below which the excluded volume interactions are irrelevant (see Sect. 1.4.2). We can use similar arguments to determine the size of a blob below which the action of a uniaxial extension force is not felt:

$$f\xi_P \approx k_B T. \tag{1.21}$$

We are going to call ξ_P the **Pincus blob** size after the name of Philip Pincus who introduced it [28]. The sub-chain within a Pincus blob adopts the configuration of an undisturbed real chain which ends up being a succession of such blobs (see Fig. 1.7c), and assuming the thermal blob size to be that of a monomer ($\xi_T \approx b$), we find $\xi_P \approx b g_P^{3/5}$. If the chain is only slightly perturbed ($\xi_P \sim bN^{3/5}$ and $fb \ll k_B T$), there is only one Pincus blob roughly the size of the chain and we expect a simple Hookean elastic response:

$$H \approx \frac{bN^{3/5}}{k_B T} f = N^{3/5} F. \tag{1.22}$$

When the force becomes sufficiently strong to considerably extend the chain ($\xi_P < \langle h \rangle \ll Nb$ and $fb < k_B T$), the extension of the chain is simply $\langle h \rangle \approx N_P \xi_P$ where N_P is the number of Pincus blobs $N_P \approx N/g_P$:

$$H \approx F^{2/3}. \tag{1.23}$$

When the force is so strong that EVI can be neglected ($\xi_P \sim b$ and $fb \sim k_B T$), then the extension of a real chain corresponds to that of its ideal counterpart given in Eq. 1.19.

The article presented in Chapter 2 and entitled *Entropic elasticity of dilated and contorted idealized circular chains* summarizes the results of a study about the deformation of a particular real chain whose topology is circular. The linear elasticity of such an object has already been studied [29] and so the questions tackled, complementary in a sense, concerned the dilation of the

circle or ring and its subsequent contortion. We found the first deformation to be akin to stretching a linear chain of equal contour length, while for the second, we found a Hookean elastic response to torsion. Surprisingly, the linear relationship extends to large angular deformations.

Deformed semi-flexible chain

We now briefly discuss the elasticity of the WLC. Let us assume we are in the constant stress ensemble and that the chain is stretched by a force f. For small forces $fl_p \ll k_BT$, the extension still follows a simple Hookean law with $\langle h \rangle / L_c \sim fl_p/k_BT$ while for large forces $fl_p \gg k_BT$ Marko and Siggia found $\langle h \rangle / L_c = 1 - 1/\sqrt{4fl_p/k_BT}$ [30]. They constructed an approximate function of force *vs* extension from these two extremes that describes well results of stretch experiments performed on WLCs:

$$F \approx H + \frac{1}{4(1-H)^2} - \frac{1}{4}, \tag{1.24}$$

where $F = fl_p/k_BT$. We are often interested in an expression of extension *vs* force, the inverse of Eq. 1.24, like in the article of Chapter 3. In a personal communication with Stigter and Bustamante [31], Zimm has provided a piecewise approximation that does a very good job:

$$H \approx \begin{cases} \dfrac{0.6667F + 0.8080F^2 + 0.10365F^3}{1 + 1.1118F + 1.1076F^2 + 0.10365F^3} & \text{for } F \leq 9 \\ 1 - \dfrac{1}{2\sqrt{F}} & \text{for } F > 9, \end{cases} \tag{1.25}$$

There is an interesting question that arises when considering the elasticity of WLCs such as dsDNA: what is the effect of sequence? We talked about the variability of the persistence length l_p in the previous subsection. This inevitably affects the elastic response but to what degree? A number of studies have been devoted to the topic and the interested reader is directed to the article of Chapter 3 conveniently entitled *Universal measure of the effect of sequence on the elasticity of heteropolymers* and the references therein . This article presents a particularly simple and elegant way to quantify the effect of the sequence on the elasticity of WLCs with variable persistence length.

1.4.5 Polymers confined in a channel

We have only discussed unconfined and isolated polymers in free-solution. But often, polymers evolve in confined geometries. For example, a virus' RNA is found confined in its capsid, spring

loaded and ready to be injected [32], while DNA molecules are often manipulated in channels and slits [33]. In the former case, the polymer is confined in all three dimensions, whereas in the latter cases, in two and only one dimensions respectively. No matter the degree of confinement, there is an inevitable free-energy cost incurred. Rubinstein and Colby's book [14] covers all these situations and describes the corresponding characteristic configurations using scaling arguments. We will only discuss the 2D case, confinement in a channel, often referred to as biaxial compression, as it pertains to Chapter 4.

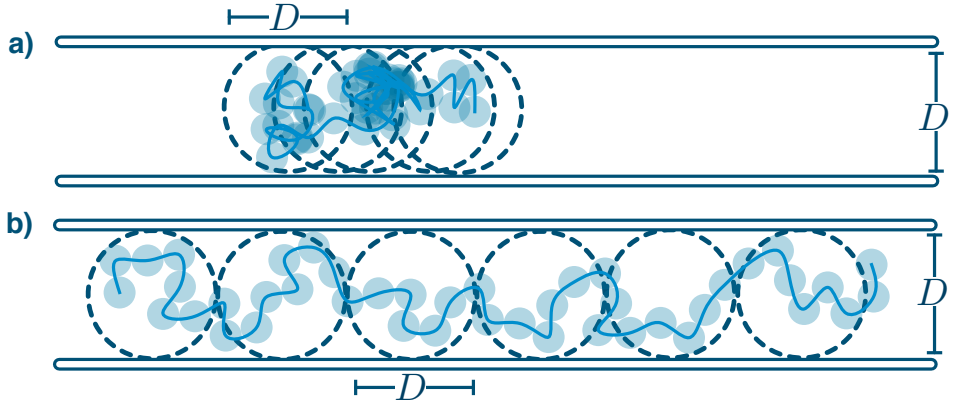

FIGURE 1.8 Two-dimensional chains confined in a channel of width D: a) ideal chain; b) real chain with excluded volume.

Let us describe ideal and real chains in an athermal solvent confined to a channel of diameter D as shown in Fig. 1.8. Within **compression blobs** of size D where $D < R_g$, each containing g monomers, one can assume the sub-chains to be undisturbed such that $D \approx bg^{1/2}$ and $D \approx bg^{3/5}$ for ideal and real chains respectively. In the case of the ideal chain, these blobs do not see each other and the mean length of the chain along the tube's axis $R_\parallel$ is found to be that of a 1D random walk of blobs (see Fig. 1.8a):

$$R_\parallel \approx D\left(\frac{N}{g}\right)^{1/2} \approx bN^{1/2}. \tag{1.26}$$

The above is equivalent to the root mean square end-to-end distance of an unconstrained ideal chain: all three dimensions are decoupled here since there are no EVI and biaxial compression does not affect the longitudinal span of the chain. This is not the case for a real chain whose blobs cannot overlap because of EVI (see Fig. 1.8b). The length $R_\parallel$ is then given by the number of blobs times their size D:

$$R_\parallel \approx D\frac{N}{g} \approx Nb^{5/3}D^{-2/3}. \tag{1.27}$$

Thus this real chain naturally extends along the length of the channel it is confined to ($R_{\parallel} > bN^{3/5}$), a property that can be exploited by experimentalists to better study its local properties or the binding activity of chemical agents to specific sites for example [34]. The free-energy cost of biaxial compression is estimated as k_BT per compression blob:

$$F_{\text{conf}} \approx k_BT\frac{N}{g} \approx k_BT\left(\frac{bN^{\nu}}{D}\right)^{1/\nu}, \tag{1.28}$$

where ν is the appropriate exponent, $1/2$ for the ideal chain, $3/5$ for the real one.

Describing a semi-flexible chain such as dsDNA confined to a nano-channel poses some problems since the channel size D is often times comparable with the persistence length l_p of the chain. As a very crude approximation, we will consider that when $D > l_p$, in the De Gennes and De Gennes extended regimes, the chain's conformation can be described using the blob approach as done above, while for $D < l_p$ one has to use Odjik's approach [35].

What happens if in addition to being confined to a channel, the polymer is subjected to other forces? The case of longitudinal stretching or compressing forces has already been dealt with [36] so let us make it a bit more complicated: what if these forces are not uniform along the length of the channel? The article presented in Chapter 4 and entitled *A theory of the thermophoretic stretch of nano-confined polymers* answers this question for a confined polymer in a thermal gradient whose monomers are subject to thermophoretic forces. The last subsection is then dedicated to the introduction of thermophoresis, in the context of polymer physics of course.

1.4.6 Thermophoresis

If in electrophoresis the motion of a particular electrolyte is induced by an electric field, in thermophoresis a particle moves because it is in a thermal gradient. For an intuitive explanation of what is thermophoresis and how it works, we better turn to suspended aerosols in gases for enlightenment. Here, much can be explained using the kinetic theory of gases. Maxwell has shown that there are no gradient of pressure associated with a gradient of temperature in a rarefied gas [37]. In Fig. 1.9a, the gas molecules on the warmer side of a suspended particle are depicted with more momentum than those on the cooler side, whereas the density is greater in the former than in the latter. As a consequence, the suspended particle feels no net force due to the normal component of the stress tensor at its surface. The thermophoretic force thus arises from imbalances in the tangential component of the stress tensor for elements of the particle's surface with a component along the direction of the temperature gradient. In essence, gas molecules collide inelastically

and thermalize with the surface which results in momentum transfer [38]. Those coming from the warm side give more than those coming from the cool side which pushes the particle towards the right as in Fig. 1.9a. It helps to imagine that this also happens for the monomers of a polymer in solution such as shown in Fig. 1.9b where one can see that it stretches non-uniformly (this problem is tackled in Chapter 4), although the origins of the net thermophoretic force in a liquid are more nebulous than in a gas [38].

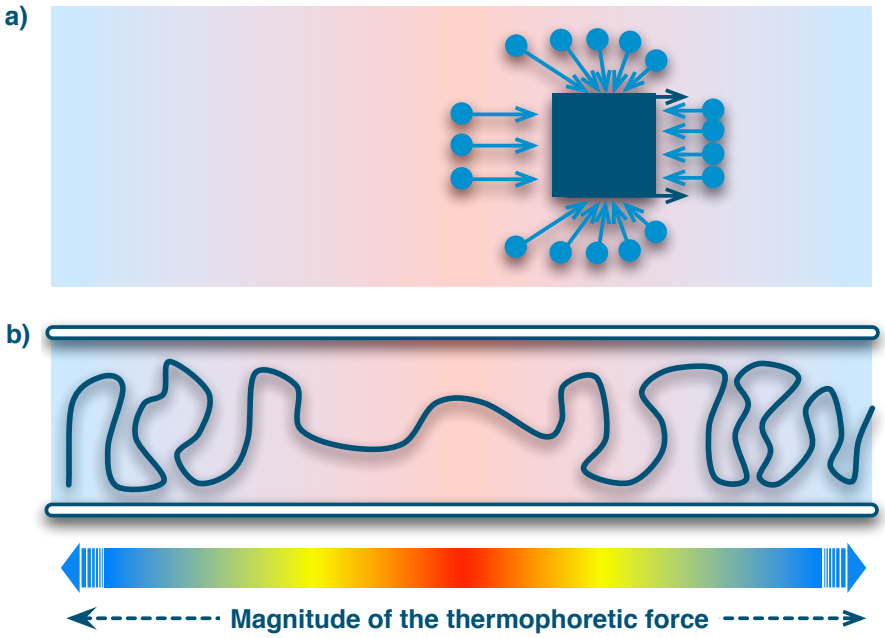

FIGURE 1.9 Thermophoresis: a) a particle suspended in a gas under a thermal gradient whose molecules acquire more momentum on the left than on the right resulting in a net velocity of the particle towards the right; b) a polymer being stretched by thermophoretic forces in a symmetric thermal gradient.

This thermophoretic transport of matter can be introduced in the mass flux equation alongside Brownian diffusion in the following way [38]:

$$J = -D\nabla c - cD_T\nabla T, \tag{1.29}$$

where D is the diffusion coefficient, c the concentration, and D_T is much like a thermophoretic mobility. Indeed, the steady state velocity a particle acquires under thermophoresis is given by $v_T = -D_T\nabla T$. Assuming a uniform thermal gradient along a direction x and vanishing flux

($J = 0$), then Eq. 1.29 leads to:

$$\frac{dc}{dx} = -S_T c \frac{dT}{dx}, \tag{1.30}$$

where $S_T = D_T/D = -(1/c)dc/dT$ is the Soret coefficient, the usual measure of the strength of thermophoresis [38]. If $S_T > 0$, then the particles move from hot to cold (thermophobic), else if $S_T < 0$, they turn around (thermophilic). For macromolecules suspended in solution, the context in which the study of Chapter 4 is situated, there is no exact analytical expression for S_T that works in all cases. The problem stems from the fact that contrary to the electrophoretic mobility whose strength can be fully determined by calculating the net charge q_{net} of an electrolyte in an electrical field E, the Soret coefficient appears to depend on many factors including thermal conductivity of the solvent and the solvated particles, particle concentration and their charge distributions, the strength of the particle-solvent, particle-particle, and solvent-solvent interactions, and temperature [38]. The temperature dependence appears to be described by a universal relationship of the form [39]:

$$S_T(T) = S_T^{\infty}\left[1 - \exp\left(\frac{T^* - T}{T_0}\right)\right], \tag{1.31}$$

where S_T^{∞} is the high temperature limit of the Soret coefficient, T^* is the temperature at which the suspended particles go from being thermophilic to thermophobic, and T_0 gives the strength of the temperature dependence. Let us assume we are at a sufficiently high temperature such that $S_T \approx S_T^{\infty}$. We can calculate the magnitude of the thermophoretic force acting on a particle by simply requiring that in the steady state motion it equates the friction force:

$$f_T = \zeta v_T = -\zeta D_T \nabla T = -k_B T S_T \nabla T, \tag{1.32}$$

where $\zeta = k_B T/D$ is the friction coefficient of the particle. Like we did for establishing the size of thermal and Pincus blobs, we can equate the work done by thermophoretic forces to $k_B T$ to find the length scale l_T below which diffusion dominates and beyond which thermophoresis takes over: $f_T l_T = k_B T \rightarrow l_T = (S_T \nabla T)^{-1}$. For a segment of DNA close to physiological temperature and at the steepest point of the temperature gradient used in [40], the thermophoretic length scale is $l_T \sim 6\mu\text{m}$. For comparison, the length scale of diffusion is $l_D \sim 10\text{pm}$ which is many orders of magnitude smaller.

In the article presented in Chapter 4, we are not so much concerned about the origins of thermophoresis than its effects on a nano-confined polymer. I will therefore spare you the details of all the theories put forward to derive S_T [38]. From the very elegant theory for colloidal thermophoresis in dilute solutions and under moderate thermal gradients by Duhr and Braun [41], we get that

there are two main contributions to S_T: 1) stress tensor anisotropies in the hydration layer around the particles; 2) variable molecular interactions (electrostatic interactions often being dominant). In Chapter 4, we just assume there is a thermophoretic force of the form given by Eq. 1.32 that acts on all monomers of a nano-confined polymer such as the one described in the previous subsection and construct a model that describes well the observed monomer concentration profile in a study by Thamdrup *et al.* [40].

1.5 Physics of lipid bilayer vesicles

Lipid made membranes are major components of cellular organisms. For instance, the outer membrane of bacteria is their single most important organ where hundreds of processes take place. In eukaryotic cells, the type making up our bodies, lipid bilayer membranes are everywhere: the cells themselves are wrapped with one and so is the nucleus and most of the organelles, while the transport of proteins from the inside to the surface is done via small lipid bilayer sacks that we call vesicles [6]. These last smallish objects are the main focus of this section. Why, you might ask? For many reasons, to name a few:

- They naturally occur in the body and play important roles in the transport of cellular matter.
- They are simple prototypical systems whose rheological properties resemble those of cells with no nucleus such as erythrocytes and platelets [42, 43].
- They are synthesized and used for research and pharmacological purposes, often as drug carriers [44, 45].

Thus a better understanding of the properties and behaviours of vesicles can potentially impact many research areas. My personal contribution here, which is presented in Chapter 5, pertains to the rheological properties of small vesicles as they are extruded in nano-channels. The question that was asked, of interest to the synthesis community, is: can we predict the final size of vesicles obtained after multiple extrusions? You will of course get the chance to read the answer, but before doing so, an introduction to the physics of lipid bilayer vesicles, how they self-assemble, how they're described, and how they flow, is necessary.

1.5.1 Self-assembly of lipid bilayers and vesicles

The remarkable thing about vesicles is that they form out of self-assembled lipid bilayer membranes. Under the proper conditions, put some lipids in solution, wait, and voilà, vesicles appear. But I guess *How?* is the key question. Indeed, how is it that ordered objects like vesicles appear out of an apparently disordered suspension of lipids without an external intervention? Doesn't this go against the laws of thermodynamics since this ordering should lower the entropy of the system? One answer to this question was provided when we introduced the concept of free-energy for open systems in section 1.3.2: the entropy of lipids can be lowered as long their energy of interaction is also lowered. Lipids are what we call amphiphilic molecules: the head part, often made of a phosphoric group, is polar or charged such that it likes the company of water (hydrophilic) whereas the tails are hydrocarbon chains who prefer to be side-by-side than close to water (hydrophobic) (see Fig. 1.10). Thus when the tails are hidden from water and the heads exposed, the total potential energy of the lipids is minimized. However, since the energy is minimized from the point of view of the lipids, it means the entropy of the surrounding environment increases. Indeed, the water molecules around the tails of free floating lipids organize themselves in a shell-like structure to minimize interactions with the hydrocarbon chain. When, the tails are hidden, water molecules gain in freedom of movement and thus in entropy. If one were to look at the system lipids+solvent, entropy is maximized.

Suspend some lipids in water at room temperature and they will seek to self-assemble. Of course, they don't do it out of their own volition. The "seeking" action is done by Brownian diffusion, a purely random process. This means that if the concentration of lipids is too low, they might never meet up to form stable ordered structures. The latter are numerous, spherical micelles, cylindrical micelles, bilayer sheets, and vesicles being the prominent examples. Assuming the concentration of lipids is sufficiently high to form any of these, whether one observes only micelles or some vesicles depends mostly on the geometry of the lipids. Single tail lipids, whose volume is well described by a cone as in Fig. 1.10b, tend to aggregate into micelles (Fig. 1.11a) while two tails lipids, those that are most found in cellular membranes and whose volume is well described by a cylinder as in Fig. 1.10a, will more readily form lipid bilayer (LB) sheets that can potentially close into vesicles (Fig. 1.11b). This can be easily explained using geometrical arguments only: while it is possible for "conical" single tail lipids to fully occupy the spherical volume of a micelle, like the slices of a pizza can be arranged in a disk, no configuration of "cylindrical" two tails lipids can do so [46]. However, it is certainly not impossible for single tail lipids to also assemble into

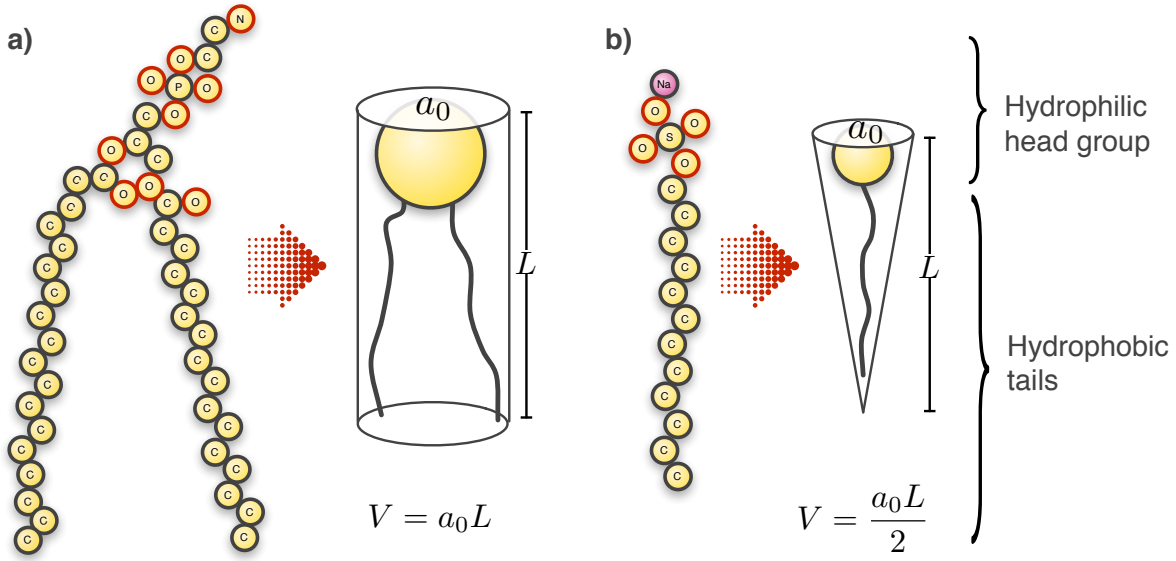

FIGURE 1.10 Lipids of length L are made of a hydrophilic head group that occupies an area a_0 and hydrophobic tails. Physicists are often more interested in a coarse grained description than in the chemical details of lipids. They wish to capture relevant physical and geometrical properties in the simplest object one can conceive. In a) we see a typical synthetic two tail lipid, 1-palmitoyl-2-oleoyl-*sn*-glycero-3-phosphocholine (POPC), and in b), a small one tail lipid, sodium dodecyl sulfate (hydrogen atoms were omitted for clarity).

bilayers and ultimately into vesicles. For the rest of this section we will focus on the properties of bilayers and vesicles.

The more spacing there is in a self-assembled lipidic structure, the more chances there are for water molecules to slip in and the more unfavourable the structure becomes in terms of energy (remember tails don't like water). Edges in a LB sheet are often some of the most costly zones: the outer leaflet needs to curve considerably to close the structure and the restrictions imposed by the geometry of the lipids prevents a dense packing of the tails thus increasing the area covered by the head groups and the spacing between the lipids (Fig. 1.11b). It might then be more favourable for the lipid sheet to close into a vesicle even if the entire surface is now curved because this curvature does not cost as much. Of course, one needs a large enough sheet to form a vesicle of minimal size set by this energy cost difference, since the smaller the vesicle is, the more curved it is [46]. We will discuss curvature effects in greater details below.

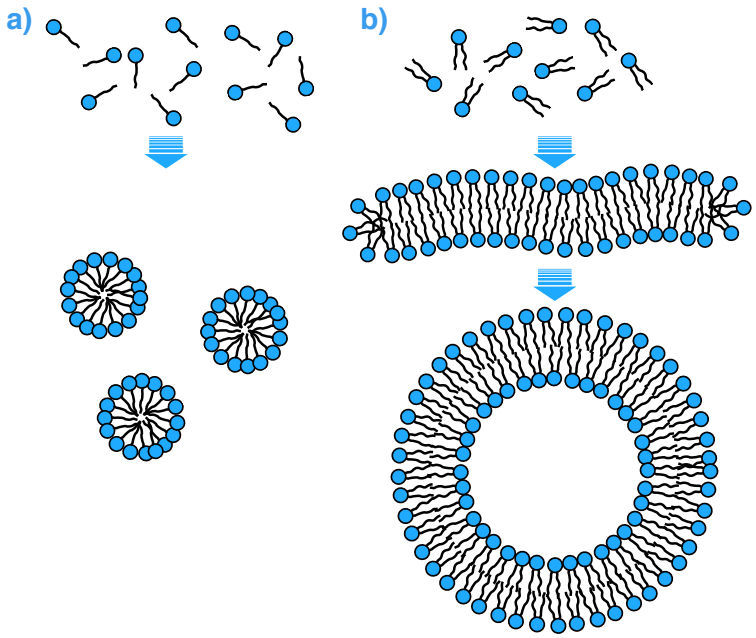

FIGURE 1.11 a) Single tail lipids tend to aggregate in micelles although bilayers are possible. b) Two tails lipids aggregate in lipid bilayers which then can possibly close to form vesicles.

1.5.2 Elasticity of lipid bilayers

Membranes in general are elastic in nature. Just inflate a balloon and you will be met with resistance. In this specific case, the balloon is made of reticulated polymers, in other words rubber, which resists being stretched. A lipid bilayer membrane (LBM) is also elastic but not for the same reasons. Take a look at Fig. 1.12: a LBM in a stress-less state with area per lipid a_0 can be stretched such that its area per lipid increases to a value a greater than a_0, resulting in a higher probability of water infiltration and making the new state undesirable; it can also undergo bending, a deformation hindered by the streric repulsions in the membrane. In short, the membrane resists being deformed. How much resistance? Well for sure your average balloon has got more of it than a vesicle for example. A LBM is fairly fragile and cannot sustain shearing, but it has the amazing ability to heal itself since it is fluid: the lipids in it are free to diffuse along the two dimensional surface created and constantly rearrange themselves. If one stretches a LBM slowly increasing the force, a point will be reached beyond which the nucleation of holes will be favourable, but if the imposed stress is released, the nucleated holes will close (assuming the force is not so high that the membrane was torn to pieces). This fluidity is essential for many processes in our bodies and makes complex life possible as it allows cells to function, change shape, grow, and divide.

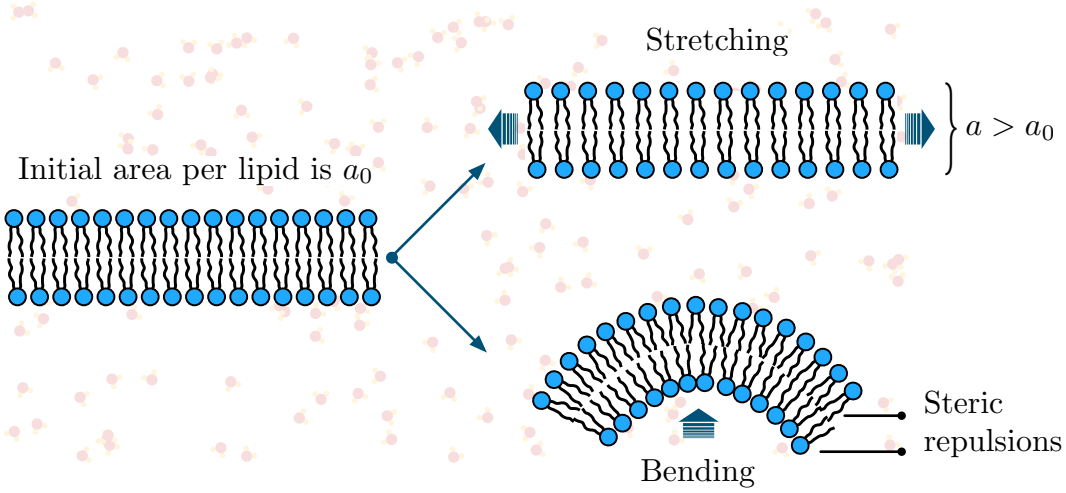

FIGURE 1.12 A lipid bilayer in a stress-less state with area per lipid head equal to a_0 can be stretched or bent which increases the area per lipid a to a value greater than a_0 in at least of the leaflets.

Mathematically, Wolfgang Helfrich came up with a free-energy term that combines both bending and area compressibility energies for a LBM [47]:

$$F_{\mathrm{LB}} = \oint dS \frac{1}{2} k_c \left[\frac{1}{R_1} + \frac{1}{R_2} - c_0 \right]^2 + \frac{1}{2} K_A \left[\frac{a - a_0}{a_0} \right]^2, \tag{1.33}$$

where local contributions to the energy are integrated over the entire surface. The first term accounts for bending: k_c is the bending constant, R_1 and R_2 are the principal local curvature radii, and c_0 is the spontaneous curvature. We neglect the Gaussian curvature term $\sim 1/R_1 R_2$ since its contribution to the total energy of the membrane is independent of size and shape for the geometries considered here [47]. As the membrane is bent, the curvature departs from equilibrium and follows a quadratic elastic response. The second term accounts for area compressibility: K_A is the area compression constant, a is the local area per lipid, and a_0 is the stress-free value. There is also a quadratic elastic response when the membrane is stretched or compressed in its plane. The ratio $\alpha = (a - a_0)/a_0$ is a measure of the area expansion. The magnitude of the response tension in the membrane γ_m is simply given by the derivative of this second term with respect to a:

$$\gamma_m = K_A \alpha. \tag{1.34}$$

In reality, Evans and Racwiz have shown that this relationship is more complex for very small tensions where one needs to take into account the flattening of undulations in the membrane which

means bending plays a role [48]. LB membranes can usually sustain being stretched without nucleating holes up to a tension γ_m^*, or equivalently until the critical area expansion α_c is reached. Let us consider Eq. 1.33 for a perfectly spherical vesicle made of N lipids with $c_0 = 0$ and radius R, the simplest system. In this specific case $R_1 = R_2 = R$ and assuming the area per lipid to be uniform, the integral over the surface just yields a $4\pi R^2$ factor such that:

$$F_{\text{sph}} = 8\pi k_c + 2\pi R^2 K_A \alpha^2. \tag{1.35}$$

One readily observes that the curvature energy is independent of size. If $k_c \sim 10^{-19}\text{J}$, $K_A \sim 10^{-1}\,{}^{\text{N}}/_{\text{m}}$, $R \sim 10^{-6}\text{m}$, and $\alpha \sim 10^{-2}$, all reasonable estimates [48], then the curvature term in the above is of order 10^{-18}J whereas the area expansion term is roughly of order 10^{-16}J. The curvature term being two orders of magnitude lower than its companion, it becomes negligible. Only for the smallest vesicle sizes, $10^{-8} - 10^{-7}\text{m}$, does the curvature become important. Hence, if the vesicle is osmotically inflated ,with ΔP being the pressure difference between the inside and the outside, only the surface tension matters in the elastic response of a sufficiently large vesicle and we get that the total energy is:

$$E_{\text{tot}} = -\Delta P \int dV + \gamma_m \oint dS. \tag{1.36}$$

The equilibrium is found by minimizing the above considering a small variation in volume and area which gives $\Delta P dV = \Delta P 4\pi R^2 dR = \gamma_m 8\pi R dR = \gamma_m dS$ and leads to Laplace's equality:

$$\gamma_m = \frac{\Delta P R}{2}. \tag{1.37}$$

The surface tension in the LB membrane of the vesicle is directly proportional to pressure and its radius. This has interesting implications for life because it imposes a rough upper limit to the size of cells. The latter need to sustain an osmotic pressure differential $\Delta P \sim 300\text{Pa}$ [5] because of their content rich in solutes of all sort (proteins, salts, *etc.*). Assuming a maximal tension $\gamma_m^* \sim 0.001\,{}^{\text{N}}/_{\text{m}}$ we find $R_{\max} \approx 7\mu\text{m}$, a value quite close to the size of the cells in our bodies. What happens now if we push a suspension of vesicles in an extruder made of narrow-channels? How do they respond? Under what conditions do they not break and freely flow? These questions are those tackled in the article making up Chapter 5. But I invite you to a small introduction to the rheological properties of vesicles in narrow-channels before jumping to the latter.

1.5.3 Rheology of vesicles in narrow channels

In Chapter 5, entitled *Predicting the final size of small vesicles produced by pressure extrusion through nano-channels*, a model that allows the prediction of the final size of vesicles produced by multiple passages through an extruder is developed based on the flow of small vesicles in narrow-channels nanoscopic in size. It mostly relies on Robijn Bruinma's theory [49]. He proposed that once in the narrow-channel, the vesicles adopt a sphero-cylindrical shape (see Fig. 1.13) and described the steady-state motion of these objects under a constant pressure differential. He did not consider the entry and exit phases as these are intractable analytically and one has to resort to numerical solutions of the full Navier-Stokes equations with approximate constitutive equations for the vesicle membrane [50, 51], or simulations [52, 53].

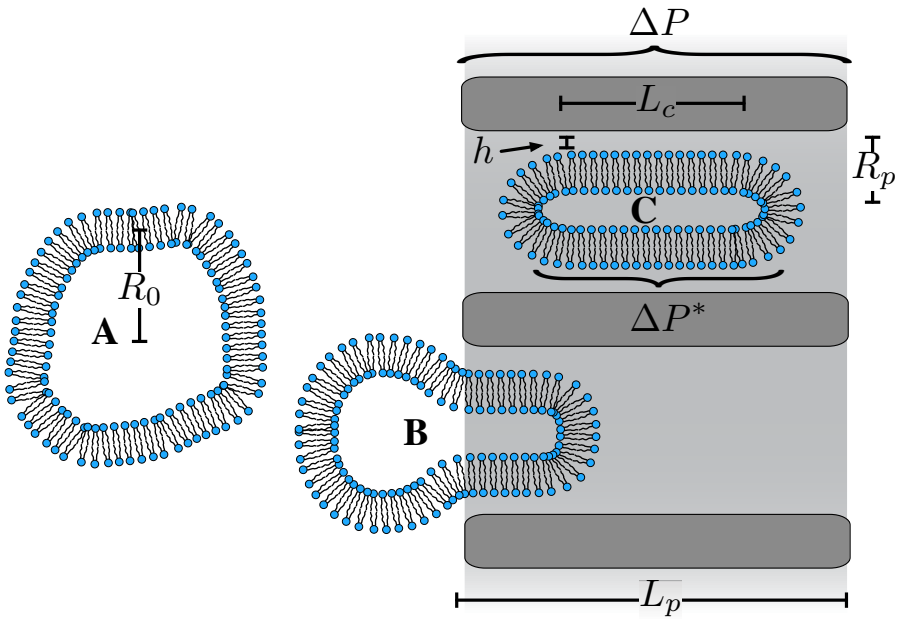

FIGURE 1.13 Extrusion of vesicles in narrow channels: vesicles of radius R_0 with potential loose in the membrane (A) are pushed into an array of nano-capillaries of length L_p and radius R_p by a pressure differential ΔP, first adopting a pear shape during the entrance phase (B) and then travelling in a sphero-cylindrical shape of cylinder length L_c within (C). There is a lubrication layer of thickness h between the sphero-cylindrical vesicle and the capillary wall and a pressure drop ΔP^* is established across the length of the oblong object.

Let us first consider Navier-Stokes equations that describe the flow of an incompressible New-

tonian fluid of viscosity η like water [54]:

$$\rho\left(\frac{\partial \mathbf{v}}{\partial t}+\mathbf{v}\cdot\nabla\mathbf{v}\right)=-\nabla P+\eta\nabla^2\mathbf{v}+\mathbf{f}, \tag{1.38}$$

$$\nabla\cdot\mathbf{v}=0, \tag{1.39}$$

where $\mathbf{v}$ is the velocity field. Eq. 1.38 is essentially Newton's equation of motion applied to a fluid. The left-hand side is the inertial term made of the "traditional" acceleration expressed as a time derivative of the flow velocity accompanied by what is known as convective acceleration, a time-independent acceleration of the fluid with respect to space. A common example of convective acceleration would be the water speeding up as it exits the nozzle of a hose: since the flow rate is required to be constant, the water that enters the constriction of the nozzle has to accelerate. On the right-hand side of Eq. 1.38 we have the pressure gradient ∇P that drives the flow along with viscous friction $\eta\nabla^2\mathbf{v}$ and possible external forces embodied in $\mathbf{f}$. For most flow problems, Navier-Stokes equations are hard if not impossible to solve analytically. Hence, we often have recourse to scaling arguments to gain some general information about the system studied and numerical tools to obtain full solutions.

Let us consider an object of side length L travelling at a velocity U in an otherwise quiescent fluid, or equivalently for the fluid moving at a mean velocity U in the vicinity of the object fixed in space, the inertial term of Eq. 1.38 can be written as $\rho|v\cdot\nabla v|\sim\rho U^2/L$ in the particle's referential. Indeed, the flow profile changes roughly over the extent of the particle but not in time. Similarly one can approximate the viscous friction term to be $\eta|\nabla^2 v|\sim\eta U/L^2$. The ratio of the inertial term over the viscous term defines a Reynold's number Re that characterizes the flow [54]:

$$\mathrm{Re}=\frac{\rho|v\cdot\nabla v|}{\eta|\nabla^2 v|}\approx\frac{\rho U L}{\eta}. \tag{1.40}$$

L defines the important length scale for the study of flow around or in a particular geometry. For the flow around a sphere or inside a tube this length would be the diameter for example. At high Reynold's number, fluid flow is dominated by inertia and might present some turbulences, while at lower values, fluid flow is said to by laminar and dominated by viscous friction. Given an initial impulse, the energy is quickly dissipated in the latter case whereas it is not in the former. The onset of turbulence is anywhere in the range $\mathrm{Re}\approx[10^3,10^5]$ depending on the system studied. Let us illustrate the difference between turbulent and laminar flows using an example from Philip Nelson's book [5]: "A $30\mathrm{m}$ whale, swimming in water at $10\mathrm{ms}^{-1}$, has $\mathrm{Re}\approx 3\times10^8$. But a $1\mu\mathrm{m}$ bacterium, swimming at $30\mu\mathrm{ms}^{-1}$, has $\mathrm{Re}\approx 3\times10^{-5}$." Same fluid yet a 13 orders of magnitude

difference in Re. The whale can thus glide through water while an *E. Coli* bacterium only moves when its flagella are active. For most biological objects on the micron to nanometer scale, $\mathrm{Re} < 1$ and fluid flow is laminar.

Here we are interested in nanometric vesicles flowing down narrow nano-channels of circular cross-section for which Reynold's number $\mathrm{Re} \sim 10^{-2}$ using parameters in [55]. The flow is thus laminar. The solution to Navier-Stokes equations for a pressure driven flow (ΔP) in a channel of radius R_p and length L_p yields [54]:

$$\eta U = K \frac{\Delta P}{L_p} = \frac{R_p^2}{8} \frac{\Delta P}{L_p}, \tag{1.41}$$

where U is the mean flow velocity. Eq. 1.41 defines Poiseuille flow and has been written in the form of Darcy's law. Assuming there is a linear density n of sphero-cylindrical vesicles along the length of the channel, each travelling at velocity U, and a pressure drop ΔP^* across each one (see Fig. 1.13), then the effective pressure drop in Eq. 1.41 is no longer ΔP but $\Delta P - nL_p \Delta P^*$, leading to a modified Poiseuille flow:

$$\eta U = \frac{R_p^2}{8} \left[\frac{\Delta P}{L_p} - n \Delta P^*(U) \right]. \tag{1.42}$$

For a sphero-cylindrical vesicle to flow down a narrow channel, there needs to be a lubrication layer between it and the wall of thickness $h(U)$ as shown on Fig. 1.13. One can equate the dissipated power in the lubrication layer surrounding each sphero-cylindrical vesicle of side length $L_c \gg h(U)$, $\dot{E}_{\mathrm{diss}} \approx \eta U^2 / h(U) 2\pi R_p L_c$, with the driving power provided by the pressure drop, $\dot{E}_{\mathrm{driv}} = \pi R_p^2 \Delta P^*(U) U$, which leads to [49]:

$$\Delta P^*(U) \approx 2\eta \frac{U L_c}{R_p h(U)}, \tag{1.43}$$

Inserting the above in Eq. 1.42 gives a Darcy like expression that reduces to Eq. 1.41 when no vesicle is present within the channel:

$$\eta U \approx K' \frac{\Delta P}{L_p} = \frac{R_p^2/8}{1 + nR_p L_c / 4h(U)} \frac{\Delta P}{L_p}. \tag{1.44}$$

Unsurprisingly, the flow through the nano-channels is reduced when vesicles are present. An expression for $h(U)$ in terms of known values and observables remains to be found. In the rest frame of an object of length L travelling close to a flat surface, the flow in the lubrication layer is essentially steady. Eq. 1.38 therefore reduces to $\nabla P = \eta \nabla^2 \mathbf{v}$ with no acceleration ($|\nabla P| \approx$

$\eta U/h^2$). If the frontal angle of attack α is positive, the object feels a pressure that lifts it away from the surface approximately given by $P_{\text{lift}} = f(\alpha)|\nabla P|L \approx f(\alpha)\eta UL/h$ where $f(\alpha) \approx \alpha L/2h$ in the small angle approximation [54]. The faster and closer to the surface the object moves, the stronger is this lift pressure.

In the case of our sphero-cylindrical vesicles squeezed in nano-channels, the surface is all around and the lift pressure acts radially close to the frontal part where $\alpha > 0$. Since vesicles are deformable objects, this results in further squeezing until the tension in the LBM compensates or rupture occurs. We can quickly come to an approximate solution for $h(U)$ using scaling arguments and dropping all numerical factors: let us assume that close to the front the lift pressure is counteracted by the tension γ_f in the LBM over a length $L \sim R_p$ of the vesicle. Using Laplace's law [54] we get that $\gamma_f \approx P_{\text{lift}} R_p \sim \alpha\eta U R_p^3/h^3$ such that the lubrication layer's thickness is approximated as $h \sim R_p(\eta U/\gamma_f)^{1/3}$. The dimensionless ratio $\eta U/\gamma_f$ is the capillary number characterizing the relative strengths of viscous drag and interfacial tension.

Robijn Bruinsma performed a more thorough calculation of $h(U)$ [49] and found a form similar to our simple approximation. The differences are in the power, $2/3$ instead of $1/3$, and the numerical factor, 2.05 in is case. He first found that interfacial shear stresses between the fluid in the lubrication layer and the LBM of the vesicle induced the formation of a linear tension gradient in the latter such that:

$$\gamma(z) = \gamma_f - \frac{\eta U}{h(U)} z, \tag{1.45}$$

where z is along the major axis of the vesicle in the channel, $z = 0$ being equal to the frontal end of the cylindrical portion where the tension is γ_f. He then described the flow near the front and used Helfrich's free-energy concepts to ultimately numerically solve for $h(U)$ [49]:

$$h(U) \approx 2.05 R_p \left(\frac{\eta U}{\gamma_f}\right)^{2/3}. \tag{1.46}$$

When the flow velocity is high enough, or equivalently when the pressure drop is strong enough, Bruinsma's model leads to $\gamma_f \approx R_p \Delta P(U)^*/2$. Using the latter together with Eqs. 1.43 and 1.46, and substituting ΔP^* in Eq. 1.42, one finds [49]:

$$\eta U \approx K' \frac{\Delta P}{L_p} = \frac{R_p^2}{8 + 0.233 n L_c^3/R_p^2} \frac{\Delta P}{L_p}. \tag{1.47}$$

The above is a true Darcy law where the permeability K' is independent of the fluid velocity U, unlike in Eq. 1.44, provided that we assume L_c to remain mostly unchanged when the velocity varies which is reasonable as long as $h(U) \ll L_c$.

In Chapter 5, it is shown for the first time, qualitatively if not quantitatively, that the main elements of Bruinsma's model presented above hold in MD simulations of the extrusion of small vesicles in narrow channels.

1.6 Numerical tools

I have employed a large set of numerical tools and implemented many others while conducting the studies whose results are presented in the following chapters. Chapters 2, 4, and 5 all include data acquired through running MD simulations while Monte-Carlo (MC) simulations were used in chapter 3. I have modified and customized the ESPResSo [56] and HOOMD-Blue packages [57, 58] for the former, and have written my own code for the latter. The raw data were mostly analysed using routines written in the Python language. I cannot stress too much how useful and powerful this language is with many incredible modules free and available online such as Numpy and Scipy for array manipulations of all sorts, Matplotlib for plotting purposes, and MDAnalysis for loading massive particle trajectory files from MD simulations and easily manipulate the enclosed information. However, in this section, I will mostly focus on those tools whose description will help better understand the subsequent articles: MD and MC simulations, and the triangulation scheme used in Chapter 5 to estimate the area occupied by each lipid in a bilayer membrane.

1.6.1 Molecular Dynamics simulations

A Molecular Dynamics (MD) simulation is essentially a virtual experiment, *in silico* as opposed to *in vitro* or *in vivo*. The steps required to prepare and run such a simulation are very straightforward: put the desired particles in a box, specify how they should interact, and integrate Newton's equations of motion! However, "straightforward" does not mean "easy", since there is much work that goes into programming all of these steps for them to run efficiently on a computer. Not too long ago, anyone who's desire was to run MD simulations had to get their hands dirty. Fortunately for us, nowadays a great number of free and open MD tool sets are available on-line which makes it easier for the new generation of researchers to do science, not computer science. Nevertheless, some would argue that there was a great pedagogical value in writing your own MD. I personally think it's a very good thing that we now have access to highly optimized code, but I still recommend to have a look at the books from D. C. Rapaport [59] and M.P. Allen and D.J. Tilsdey [60] covering the essentials of MD simulations.

Once you understand what you are doing, the proper tool has to be chosen. When I started my Master degree a few years ago, I coded my own MD to finally end up using a code developed by a colleague. I now have migrated to the ESPResSo and HOOMD-Blue packages, and toyed with LAMMPS. The system studied dictated the tool to be used: a single polymer chain system containing just a few tens or hundreds of particles as in Chapters 2 and 4 is well suited for ESPResSo, whereas a vesicle extruded in a nano-channel as in Chapter 5 where the number of particles needed is between a quarter to half a million is the ideal system for HOOMD-Blue. The question is why? The answer lies in what type of hardware is used by the code in this specific case. ESPResSo a highly versatile old-school package in the sense that it can run in parallel on the CPUs of your machine while HOOMD-Blue is a next generation package which fully utilizes the power of GPUs (graphics cards) whose advantage is mostly apparent for larger systems. In fact, a single NVIDIA® GeForce ® GTX 580 graphics card can integrate roughly 800 time steps per second (TPS) for a typical Lennard-Jones liquid of 64000 particles using HOOMD-Blue whereas the efficient LAMMPS package accomplishes the same task in the same amount of time using roughly 64 CPU cores. The reason for this discrepancy can be understood very simply considering the historical development of the architecture of both compute units: the CPU was created with control, precision, and flexibility in mind which means adding a core is a costly design procedure whereas the GPU has evolved as a natural parallel processor with now hundreds of cores to allow it to compute the position of millions of polygons many times each seconds when playing video games. It is this ability that scientists now leverage for other purposes. In terms of monetary cost, one might be able to acquire a small cluster containing 64 CPU cores for at least $30000 while a workstation containing four of the formerly mentioned graphics cards costs roughly $5000. At equal performance, four clusters are then necessary and we are talking about a twenty-five-fold difference in price [4]. The lesson here: one has to be very wise in his choice of MD package and hardware since time and money are very important variables in science.

In the rest of this subsection, I will elaborate on the physics behind MD simulations of systems in the canonical or NVT ensemble, in other words, connected to a heat bath. I will of course discuss the simulation of polymers and lipid bilayer vesicles, the systems studied in the following chapters.

[4] 4×64 CPU cores $= 4 \times$ GTX 580 $\rightarrow 4 \times \$30000 = \$120000 \gg \$5000$

The physics of MD in the canonical ensemble

The simulation of a system in all its atomic details is computationally intensive which means we are usually limited to short time intervals and small sizes. Since in soft matter physics we are often more interested in the thermodynamics properties of systems at the mesoscopic scale where atomic details become irrelevant, one resorts to coarse-graining. Hence atoms are clumped together in super-particles, interactions are modelled as mean forces and the lost degrees of freedom are accounted for by adding friction and noise. Let us imagine we have a system of N particles in the canonical ensemble. We can write Newton's second law for the i-th particle of mass m_i at position $\vec{r}_i$ using Langevin's approach:

$$m_i\ddot{\vec{r}}_i = -\nabla U(\vec{r}_i) - \zeta_i\dot{\vec{r}}_i + \vec{R}_i + \vec{F}_{i,\text{ext}}, \tag{1.48}$$

where $U_i(\vec{r}_i)$ is the potential energy of the particle whose derivative gives a net force, ζ_i is the friction coefficient of the particle which multiplied by the velocity gives a friction force, $\vec{R}_i$ is a random force (noise), and $\vec{F}_{i,\text{ext}}$, a potential external force. To satisfy the fluctuation-dissipation theorem, the random force $\vec{R}_i$ is on average equal to zero, $\langle\vec{R}_i(t)\rangle = 0$, and its time correlation function is $\langle\vec{R}_i(0)\cdot\vec{R}_i(t)\rangle = 2dk_BT\zeta_i\delta(t)$ where d is the dimensionality one works in. Hence, normally distributed random numbers with variance $2dk_BT\zeta_i$ and zero mean are usually generated in simulations to satisfy these conditions. Langevin dynamics as described by Eq. 1.48 thus naturally imposes a temperature T to the system while it provides forces that jostle the particles resulting in diffusion. Through this approach, one can simulate the equilibrium properties of colloids and polymers without explicitly including the solvent as long as hydrodynamic interactions can be neglected, thus providing great gains in simulation speed.

Numerically, each particle stores its position $\vec{r}_i$, velocity $\vec{v}_i$, and acceleration (or net force) $\vec{a}_i$. Then Eq. 1.48 is often integrated using the *Velocity-Verlet* algorithm which traditionally follows these four steps given a time step Δt [59]:

- Calculate the velocity a half time step in the future: $\vec{v}(t+\Delta t/2) = \vec{v}(t) + \vec{a}(t)\Delta t/2$
- Update the position: $\vec{r}(t+\Delta t) = \vec{r} + \vec{v}(t+\Delta t/2)\Delta t$
- Update $\vec{a}$ by calculating the total force acting on the particle using the RHS of Eq. 1.48
- Update the velocity: $\vec{v}(t+\Delta t) = \vec{v}(t+\Delta t/2) + \vec{a}(t+\Delta t)\Delta t/2$

The advantage of the above over other integration schemes such as the *Leapfrog* algorithm [59], a basic Verlet variant, is that all the parameters defining the future of the particle can be fully determined using present values thus sparing memory usage (only $3N$ vectors are stored at all times).

The friction term in Eq. 1.48 involves the velocity of the particle with respect to the center of mass of the entire system. This means that momentum propagation over large distances, in other words flow, is impossible. To allow Non-Equilibrium Molecular Dynamics (NEMD) simulations to be performed, a local scheme can be used to introduce friction in the equation of motion: the velocity of the particle is simply calculated with respect to its immediate neighbourhood leading to a friction term $-\zeta_i v_{i,\mathrm{local}}$. It happens to be the thermostat developed for Dissipative Particle Dynamics (DPD) that is also well suited for NEMD [61].

Details of polymer simulations

Chapters 2 and 4 present articles where coarse-grained MD simulations of polymers were conducted using the ESPResSo MD package. The integration scheme followed Langevin dynamics as described in the previous subsection where the form of the potential energy $U(r)$ in Eq. 1.48 needs to be specified. Fig. 1.14 illustrates the general aspect of a coarse-grained model polymer: a series of beads connected by springs. All beads interact through pairwise interactions to reproduce EVI. The Lennard-Jones (LJ) interaction (see Eq. 1.8) is often used to model these for reasons exposed in section 1.4.2. Here we write its generalized form:

$$U_{\mathrm{LJ}}(r) = \frac{A}{(r - r_{\mathrm{off}})^{12}} - \frac{B}{(r - r_{\mathrm{off}})^{6}}, \tag{1.49}$$

where A, B, and the offset distance r_{off} can be tuned to reproduce various behaviours. The first term on the RHS of the above is the repulsive part and the second, the attractive part. Usual values of the parameters are $A = 4\epsilon\sigma^{12}$, $B = 4\epsilon\sigma^{6}$, and $r_{\mathrm{off}} = 0$ where ϵ sets the energy scale of the system and σ does the same for length. In fact, the units in coarse-grained MD are often given in terms of ϵ and σ with additional units of mass m and time τ. The springs making up the bonds in the chain can be modelled using a simple harmonic potential of the form:

$$U_{\mathrm{harm}}(r) = \frac{k}{2}(r - r_{\mathrm{eq}})^2, \tag{1.50}$$

where k is the spring rigidity and r_{eq}, the equilibrium distance. But the harmonic spring is infinitely extensible provided a strong enough stretching force which does not reflect the finite ex-

tensibility of a true polymer. This shortcoming led to the search for an alternative. Let us recall the notion of thermal blob that establishes the scale of a sub-unit of a real polymer chain for which EVI are dominated by thermal fluctuations (see section 1.4.2). Then a model polymer can be thought of as a series of such thermal blobs with springs that represent the finite extensibility of the ideal sub-units and beads that simulate the EVI between the blobs. The potential energy of the finitely extensible non-linear elastic (FENE) springs is derived from the elasticity of an ideal chain (see Eq. 1.20):

$$U_{\mathrm{FENE}}(r) = \begin{cases} -\frac{1}{2}kr_0^2 \ln\left[1 - \left((r - r_{\mathrm{eq}})/r_0\right)^2\right] & \text{for } r - r_{\mathrm{eq}} \leq r_0 \\ \infty & \text{for } r - r_{\mathrm{eq}} > r_0 \end{cases}, \tag{1.51}$$

where k and r_{eq} keep their definitions, and r_0 is the maximal extension. It is worth mentioning that close to its minimum, the above reduces to an harmonic potential of the form given by Eq. 1.50.

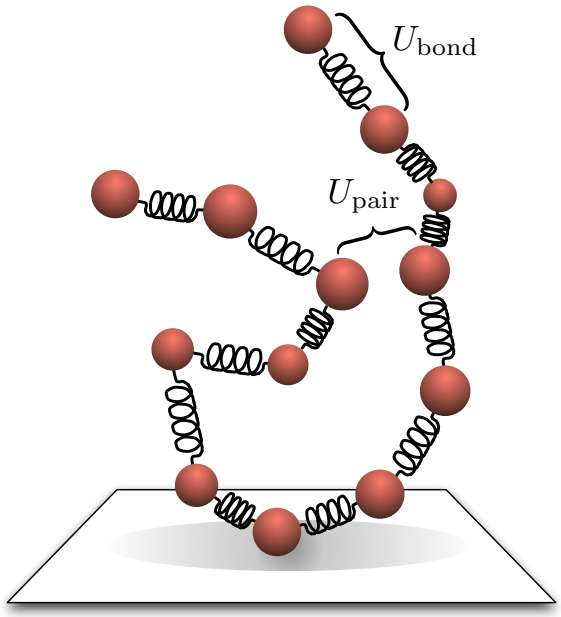

FIGURE 1.14 A simple coarse-grained polymer in MD simulations: a series of beads all interacting through some pair potential U_{pair} connected by springs of potential energy U_{bond}.

In Chapter 2 the Kremer-Grest approach [21] to the MD simulation of a model polymer in a heat bath is adopted. The LJ pair potential between all beads is given by Eq. 1.49 with the usual sets of parameters while the bonds are modelled using the FENE potential with $k = 30\epsilon/\sigma^2$,

$r_0 = 1.5\sigma$, and $r_{\text{eq}} = 0\sigma$. In this specific case, the LJ potential was truncated at $r_{\text{cut}} = 2^{1/6}\sigma$ to keep only its repulsive part for EVI. In Chapter 4, temperature sensitive EVI were required so that a model polymer proposed by Ciesla *et al.* [62] was used. The parameters of the LJ potential as defined by Eq. 1.49 are then $A = \epsilon\sigma^{12}$, $B = 2\epsilon\sigma^6$, and $r_{\text{off}} = 0$. The bonds are modelled as harmonic springs with $k = 16.67\epsilon/\sigma^2$ and $r_{\text{eq}} = 1\sigma$. For temperature dependent EVI the LJ potential is truncated at $r_{\text{cut}} = 2^{1/6}\sigma$ to span both the repulsive and attractive parts.

Details of lipid bilayer vesicle simulations

The article of Chapter 5 contains data from MD simulations of lipid bilayer vesicle extrusion. We wanted a true self-assembling model fluid bilayer that would enclose a roughly constant volume of fluid while forming a vesicle and would exhibit an hydrodynamic response as flow was to be studied. We thus opted for Goetz and Lipowsky's model [63] as it was simple enough to implement and had all the necessary attributes.

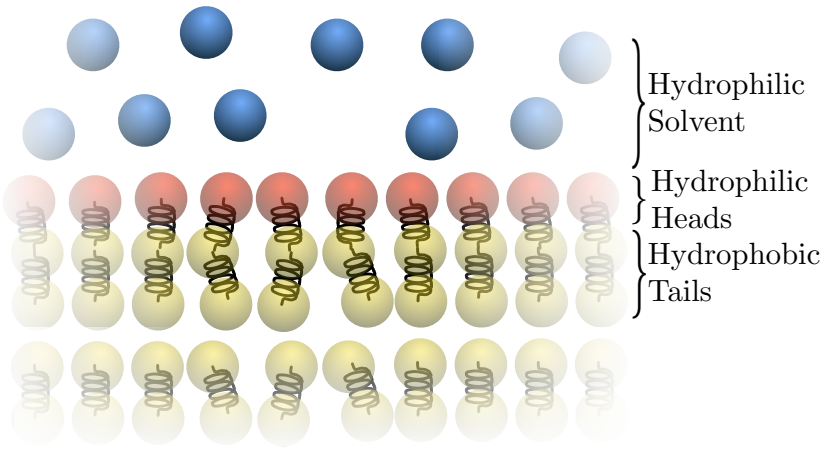

FIGURE 1.15 Two-dimensional representation of Goetz and Lipowsky's model of a bilayer that was simulated. The lipids are small three beads chains: one bead for the hydrophilic head and two bead for the hydrophobic tail, all linked with harmonic spring. The lipids are immersed in a hydrophilic solvent.

A representation of the main constituents of the simulated bilayer system is shown in Fig. 1.15. The lipids are essentially small three beads polymers, one bead for the hydrophilic head and two beads for the hydrophobic tail. Of course this is overly simplistic compared to the lipid shown in Fig. 1.10a, but simplicity here translates into speed since for a given system size the number

of particles is greatly reduced. The lipids bathe in a solvent also made of hydrophilic beads. The hydrophobic-hydrophilic interaction is modelled using a soft core potential of the form:

$$U_{\text{soft}} = 4\epsilon \left(\frac{\sigma_{\text{SC}}}{r} \right)^9, \tag{1.52}$$

where ϵ and $\sigma_{\text{SC}} = 1.05\sigma$ are related to the LJ potential. Thus defined, the soft core potential exhibits a repulsive response similar to the LJ potential at close range, but remains so at long range. All other pair interactions are modelled by a LJ potential of the form given by Eq. 1.49 with the usual parameters. Both of these potentials are truncated at $r_{\text{cut}} = 2.5\sigma$ where they have essentially reached their asymptotic limit of zero. Thus for $2^{1/6}\sigma < r < r_{\text{cut}}$, the interaction between the heads and the solvent is attractive while it is repulsive between tails and solvent which makes the bilayer configuration favourable. The beads of a lipid are bound together using harmonic springs with a potential energy defined by Eq. 1.50 where the rigidity $k = 5000\epsilon/\sigma^2$ and $r_{\text{eq}} = \sigma$. Such strong bonds are used to limit the fluctuations in length of the lipids.

Simulated lipid bilayer vesicles are extruded through a narrow channel that connects two reservoirs (see Fig. 1.13). The channel was made of solvent beads bonded to FCC lattice sites using stiff harmonic springs. This allowed the full thermostating of the system without any violations of the fluctuation-dissipation theorem. The solvent and vesicle were pushed in the channel by applying a pressure differential to the system in the form of an external force acting on all particle in a thin slab at the start of the entrance reservoir. To allow for flow, the system's temperature was kept constant using the local DPD thermostat.

The simulations whose data are presented in Chapter 5 were all set up using ESPResSo with the *mbtools* package included [64]. They contained anywhere between 250 000 and 500 000 particles whose trajectories had to be integrated over a few million time steps. To speed up the process considerably, the initial snapshot of the systems were sent to HOOMD-Blue for execution on GPUs. Simulation speed went from between 2 and 4 TPS using ESPResSo on octo-core machines to 20 TPS using HOOMD-Blue on the NVIDIA® TESLA® 1060 GPUs of the *angel* cluster of Sharcnet (www.sharcnet.ca). As of this writing, preliminary benchmarks on newly acquired NVIDIA® GeForce ® GTX 580 graphics cards shows execution speeds of 60 TPS! In this specific case the advantage of GPUs over CPUs for many particles MD is made very clear.

1.6.2 Monte-Carlo simulation of a stretched polymer

Using statistical mechanics, in the canonical or NVT ensemble, one can calculate the average value of an observable $Y(\vec{x})$ in a given system in the following way ($\vec{x}$ is a state vector):

$$\langle Y \rangle = \frac{1}{\mathcal{Z}} \int Y(\vec{x}) \exp\left[-\beta \mathcal{H}(\vec{x})\right] d\vec{x}, \tag{1.53}$$

where $\mathcal{H}(\vec{x})$ is the total energy of the system and $\mathcal{Z} = \int \exp\left[-\beta \mathcal{H}(\vec{x})\right] d\vec{x}$ is the partition function with $\beta = 1/k_B T$ [12]. The problem is that this integral is often pretty nasty and impossible to solve analytically. However, the solution can be well approximated using various numerical methods, those of interest here being of the Monte-Carlo (MC) type [65]. In particular, we will discuss the use of MC simulations to calculate equilibrium properties of coarse-grained polymer chains such as their sizes, as was done in Chapter 3.

We are interested in Markov chain MC methods corresponding to an exploration of configuration space where subsequent steps or changes of state are correlated. The correlation vanishes for non contiguous steps. Concerning single isolated polymer chains and their equilibrium properties, on-lattice and off-lattice MC methods exist with various types of moves possible to explore phase space. Many of these are detailed in Landau and Binder's book [65]. Whichever method one decides to use, the criterion to decide whether a move is accepted or refused is quite often the one proposed by Metropolis *et al.* [66]: given a change of state $\vec{x} \rightarrow \vec{x}'$, if the corresponding change in energy $\Delta\mathcal{H} = \mathcal{H}(\vec{x}') - \mathcal{H}(\vec{x})$ is negative, the energy is lowered and the move is accepted, else it is accepted with a probability $\exp\left[-\beta\Delta\mathcal{H}\right]$. In terms of thermodynamics, states of energy much greater or much lower than the thermal energy $k_B T$ are improbable and do not persist in time as the heat bath will respond by absorbing the excess energy or giving some back.

In the article of Chapter 3, stretched ideal semi-flexible heteropolymers as depicted in Fig. 1.16 are studied. The total energy of such a chain is found using the discrete Kratky-Porod model:

$$\beta\mathcal{H}(\vec{\alpha}, \vec{K}, \vec{\psi}, f, z) = -\beta f z - \sum_i K_i \cos(\alpha_i - \psi_i), \tag{1.54}$$

where the definitions for all variables can be found in Fig. 1.16. The first term on the RHS of the above is the work done by the stretching force f to extend the chain by an amount z, while the second term on the RHS is a sum of all local bending energies along the chain. These originate from steric repulsions between subsequent monomers along the backbone of the chain as illustrated in Fig. 1.6. Both the bending stiffness K_i and the preferred angle ψ_i between subsequent monomers

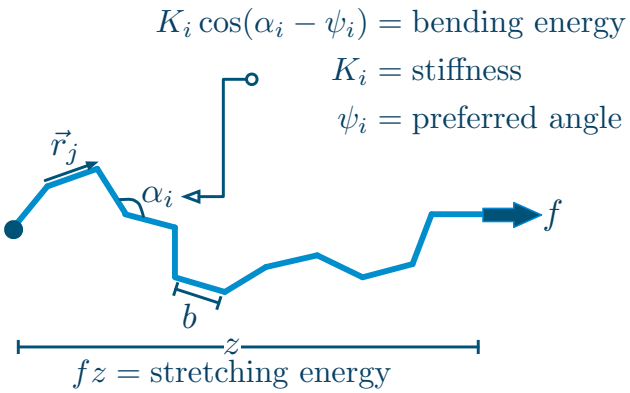

FIGURE 1.16 Model Kratky-Porod heteropolymer made of monomers of size b being stretched in the z direction by a force f: there is a local preferred angle ψ_i between subsequent monomers and an associated bending stiffness $K_i = l_{p,i}/b$ related to the local persistence length $l_{p,i}$ of the chain. Each monomer's orientation and direction is given by a vector vertex $\vec{r}_j$ of length b connecting two vertices.

can vary along the chain as is the case for DNA [25]. When $K_i = K$ and $\psi_i = \psi$ for all i in Eq. 1.54, the semi-flexible chain is homogeneous.

For given sets $\{K_i\}$ and $\{\psi_i\}$ with an applied external force f, we would like to calculate the resulting mean extension z of a heteropolymer chain made of N monomers of size b. While this cannot be done analytically, MC simulations can find the answer quite easily. To produce the data of Chapter 3, MC simulations with pivot moves were used to explore the phase space of the system with speed and efficiency. Two types of such moves were used: what I called *small* pivots and *big* pivots. Here are the steps to perform a *small* pivot move which mainly explores small deviations of the α_i:

- The system is in state $\vec{x}$ with energy $\mathcal{H}(\vec{x})$ given by Eq. 1.54.
- A vertex $1 \leq j < N+1$ along the chain is selected as the pivot point O.
- A set of small random Euler angles with mean zero are generated from which a rotation matrix $\mathbf{R}$ around O is constructed.
- Vertices $j+1$ and/or $N+1$ are rotated, α_i associated with vertex j is recalculated and so is the extension z.
- The energy $\mathcal{H}(\vec{x}')$ is calculated and the Metropolis criterion applied.

- If the new state is accepted all other vertices between $j+1$ and $N+1$ are rotated, else nothing is done.

The steps for a *big* pivot move are similar but they only affect the extension z:

- The system's initial state is $\vec{x}$ of energy $\mathcal{H}(\vec{x})$.
- A vertex $1 \leq j < N$ is chosen and the vector $\vec{r}_j$ from j to $j+1$ is calculated.
- A set of Euler angles in the interval $[0, 2\pi]$ is generated from which a rotation matrix $\mathbf{R}$ around $\vec{r}_j$ is constructed.
- Vertex $N+1$ is rotated and the extension z recalculated.
- The energy $\mathcal{H}(\vec{x}')$ is calculated and the Metropolis criterion applied.
- If the new state is accepted all other vertices between $j+2$ and $N+1$ are rotated, else nothing is done.

Using a few hundreds of thousands of these moves, one can obtain precise values of the static properties of ideal semi-flexible heteropolymers with hundreds of monomers in the matter of minutes for a given applied force f when executing the MC simulations on only one CPU core. Notice that excluded volume interactions are not accounted for here. These would slow down the calculations considerably as a large number of moves would be rejected due to monomer overlap. Also, pivot moves cannot realistically reproduce the dynamical properties of polymer chains, only static properties such as mean size can be calculated.

1.6.3 Surface triangulation

A surface triangulation algorithm called the *Crust* by Nina Amenta [67] was used to analyse the data from MD simulations of extruded vesicles presented in the article of Chapter 5. In particular, it was used to reconstruct both the exterior and interior surfaces of the vesicle and to extract the area occupied by each lipid head. Since we know the area per lipid is related to the tension in the lipid bilayer membrane (see Sect. 1.5), tracking the former allows to follow the latter.

Once the surface was triangulated using the aforementioned algorithm of which I will not discuss the details, knowledge of the heads' positions and their respective connection maps was

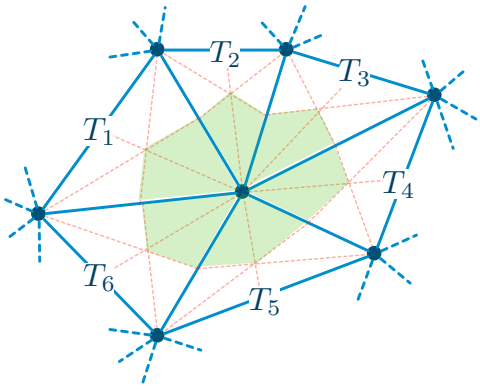

FIGURE 1.17 Triangulation of the surface of a lipid bilayer. A patch is shown where the vertices are the heads, the blue full lines represent the local connection map, and all medians of the triangles are drawn in thin red dotted lines. The green shaded area is the one occupied by the central lipid head. The T_i s denote the triangles that have the latter as a vertex.

used to find the area a_i occupied by each one and depicted by the green shaded area in Fig. 1.17 which is given by:

$$a_i = \frac{1}{3}\sum_j a(T_j), \tag{1.55}$$

where the areas $a(T_j)$ of all triangles to which a particular head i belongs are summed and then divided by three. Indeed, each vertex of a triangle can be assume to occupy a third of its area on the basis that all three medians of a triangle (red dotted lines in Fig. 1.17) divide its area in six equal parts. In the article of Chapter 5, two- and three-dimensional stress profiles of sphero-cylindrical vesicles travelling down a narrow-channel are shown (Fig. 6 therein). The stress was calculated has explained above.

1.7 References

[1] P Oswald. *Rheophysics: the deformation and flow of matter*. Cambridge University Press (2009).

[2] E Schrodinger. *What is life?* Cambridge University Press Cambridge (1944).

[3] JR Loofbourow. *Borderland problems in biology and physics*, ***Rev. Mod. Phys.* 12**, 267 (1940).

[4] SM Gruner, JS Langer, P Nelson, V Vogel. *What future will we choose for physics?*, ***Physics Today* 48**, 25 (1995).

[5] P Nelson, M Radosavljevic, S Bromberg. *Biological physics*. WH Freeman and Co. (2004).

[6] H Flyvbjerg, J Hertz, MH Jensen, OG Mouritsen, K Sneppen. *Physics of Biological Systems: From Molecules to Species*. Springer (1997).

[7] J Shendure, H Ji. *Next-generation dna sequencing*, ***Nat. Biotechnol.* 26**, 1135–1145 (2008).

[8] Various. *Insight: Lab on chip*, ***http://www.nature.com/nature/supplements/insights/labonachip/index.html*** (accessed 19 August 2011).

[9] JW Yoo, DJ Irvine, DE Discher, S Mitragotri. *Bio-inspired, bioengineered and biomimetic drug delivery carriers*, ***Nat. Rev. Drug Discovery* 10**, 521–535 (2011).

[10] JH Lee, J Jang, J Choi, SH Moon, S Noh, J Kim, JG Kim, IS Kim, KI Park, J Cheon. *Exchange-coupled magnetic nanoparticles for efficient heat induction*, ***Nat. Nanotechnol.* 6**, 418–422 (2011).

[11] A Einstein. *On the movement of small particles suspended in stationary liquids required by the molecular-kinetic theory of heat*, ***Annalen der physik* 17**, 549–560 (1905).

[12] JP Sethna. *Statistical mechanics: entropy, order parameters, and complexity*, volume 14. Oxford University Press (2006).

[13] B Greene. *The Fabric of the Cosmos: Space, Time, and the Texture of Reality*. Knopf (2004).

[14] M Rubinstein, RH Colby. *Polymer physics*. Oxford University Press, USA (2003).

[15] I Teraoka. *Polymer Solutions: An Introduction to Physical Properties: an introduction to physical properties*. Wiley-Interscience (2002).

[16] GR Strobl. *The physics of polymers*. Springer (2010).

[17] PG de Gennes. *Scaling concepts in polymer physics*. Cornell University Press (1979).

[18] JE Jones. *On the determination of molecular fields. ii. from the equation of state of a gas*, ***Proc. R. Soc. Lond. A* 106***738***, 463–477 (1924).

[19] F Latinwo, CM Schroeder. *Model systems for single molecule polymer dynamics*, ***Soft Matter*** (2011).

[20] Nobel Foundation. *Paul J. Flory — Nobel lecture*, ***http://nobelprize.org/chemistry/laureates/1974/flory-lecture.html*** (accessed 1 August 2011).

[21] GS Grest, K Kremer. *Molecular dynamics simulation for polymers in the presence of a heat bath*, ***Phys. Rev. A* 33**, 3628 (1986).

[22] DR Helinski, DB Clewell. *Circular DNA*, ***Annu. Rev. Biochem.*** **40**, 899–942 (1971).

[23] JP Mulvenna, C Wang, DJ Craik. *CyBase: a database of cyclic protein sequence and structure*, ***Nucleic Acids Res.*** **34**, D192 (2006).

[24] S Geggier, A Vologodskii. *Sequence dependence of dna bending rigidity*, ***PNAS*** **107**, 15421 (2010).

[25] Z Zhou, B Joós. *Sequence-dependent effects on the properties of semiflexible biopolymers*, ***Phys. Rev. E*** **77**, 061906 (2008).

[26] KC Neuman, A Nagy. *Single-molecule force spectroscopy: optical tweezers, magnetic tweezers and atomic force microscopy*, ***Nat. Methods*** **5**, 491–505 (2008).

[27] GaryW Slater, Y Gratton, M Kenward, LC McCormick, F Tessier. *Deformation, stretching, and relaxation of single-polymer chains: Fundamentals and examples*, ***Soft Matter*** **1**, 365–391 (2003).

[28] P Pincus. *Excluded volume effects and stretched polymer chains*, ***Macromolecules*** **9**, 386–388 (1976).

[29] Y Shen, L Zhang. *Elastic behavior of ring polymer chains*, ***J. Polym. Sci., Part B: Polym. Phys.*** **43**, 223–232 (2005).

[30] JF Marko, ED Siggia. *Stretching dna*, ***Macromolecules*** **28**, 8759–8770 (1995).

[31] D Stigter, C Bustamante. *Theory for the hydrodynamic and electrophoretic stretch of tethered b-dna*, ***Biophys. J.*** **75**, 1197–1210 (1998).

[32] J Kindt, S Tzlil, A Ben-Shaul, WM Gelbart. *Dna packaging and ejection forces in bacteriophage*, ***PNAS*** **98**, 13671 (2001).

[33] GB Salieb-Beugelaar, KD Dorfman, A van den Berg, JCT Eijkel. *Electrophoretic separation of dna in gels and nanostructures*, ***Lab Chip*** **9**, 2508–2523 (2009).

[34] YM Wang, JO Tegenfeldt, W Reisner, R Riehn, XJ Guan, L Guo, I Golding, EC Cox, J Sturm, RH Austin. *Single-molecule studies of repressor–dna interactions show long-range interactions*, ***PNAS*** **102**, 9796 (2005).

[35] T Odijk. *Scaling theory of dna confined in nanochannels and nanoslits*, ***Phys. Rev. E*** **77**, 060901 (2008).

[36] S Jun, D Thirumalai, BY Ha. *Compression and stretching of a self-avoiding chain in cylindrical nanopores*, ***Phys. Rev. Lett.*** **101**, 138101 (2008).

[37] JC Maxwell. *On stressed in rarefied gases arising from inequalities of temperature r. soc*, ***Phil. Trans. R. Soc.*** **170**, 231–40 (1879).

[38] R Piazza, A Parola. *Thermophoresis in colloidal suspensions*, ***J. Phys. Condens. Matter*** **20**, 153102 (2008).

[39] S Iacopini, R Rusconi, R Piazza. *The "macromolecular tourist": Universal temperature dependence of thermal diffusion in aqueous colloidal suspensions*, ***Eur. Phys. J. E*** **19**, 59–67 (2006).

[40] LH Thamdrup, NB Larsen, A Kristensen. *Light-induced local heating for thermophoretic manipulation of dna in polymer micro-and nanochannels*, ***Nano Lett.*** **10**, 826–832 (2010).

[41] S Duhr, D Braun. *Why molecules move along a temperature gradient*, ***PNAS*** **103**, 19678 (2006).

[42] V Vitkova, M Mader, T Podgorski. *Deformation of vesicles flowing through capillaries*, ***Europhys. Lett.*** **68**, 398 (2004).

[43] H Noguchi, G Gompper. *Shape transitions of fluid vesicles and red blood cells in capillary flows*, ***Proceedings of the National Academy of Sciences of the United States of America*** **102**, 14159 (2005).

[44] A Jesorka, O Orwar. *Liposomes: technologies and analytical applications*, ***Annu. Rev. Anal. Chem.*** **1**, 801–832 (2008).

[45] B Maherani, E Arab-Tehrany, R Mozafari, C Gaiani, M Linder. *Liposomes: A review of manufacturing techniques and targeting strategies*, ***Current Nanoscience*** **7**, 436–452 (2011).

[46] JN Israelachvili, DJ Mitchell, BW Ninham. *Theory of self-assembly of lipid bilayers and vesicles*, ***Biochim. Biophys. Acta, Biomembr.*** **470**, 185–201 (1977).

[47] W Helfrich. *Elastic properties of lipid bilayers: theory and possible experiments*, ***Z. Naturforsch*** **28**, 693–703 (1973).

[48] E Evans, W Rawicz. *Entropy-driven tension and bending elasticity in condensed-fluid membranes*, ***Phys. Rev. Lett.*** **64**, 2094–2097 (1990).

[49] R Bruinsma. *Rheology and shape transitions of vesicles under capillary flow*, ***Physica A: Statistical and Theoretical Physics*** **234**, 249–270 (1996).

[50] C Quéguiner, D Barthès-Biesel. *Axisymmetric motion of capsules through cylindrical channels*, ***J. Fluid Mech.*** **348**, 349–376 (1997).

[51] Y Lefebvre, D Barthès-Biesel. *Motion of a capsule in a cylindrical tube: effect of membrane pre-stress*, ***J. Fluid Mech.*** **589**, 157–182 (2007).

[52] G Gompper, DM Kroll. *Driven transport of fluid vesicles through narrow pores*, ***Phys. Rev. E*** **52**, 4198 (1995).

[53] DJ Quinn, I Pivkin, SY Wong, KH Chiam, M Dao, GE Karniadakis, S Suresh. *Combined simulation and experimental study of large deformation of red blood cells in microfluidic systems*, ***Ann. Biomed. Eng.*** pages 1–10 (2011).

[54] B Lautrup. *Physics of continuous matter: Exotic and everyday phenomena in the macroscopic world*. CRC (2009).

[55] BJ Frisken, C Asman, P Patty. *Studies of vesicle extrusion*, ***Langmuir*** **16**, 928–933 (2000).

[56] HJ Limbach, A Arnold, BA Mann, C Holm. *Espresso–an extensible simulation package for research on soft matter systems*, ***Comput. Phys. Commun.*** **174**, 704–727 (2006).

[57] JA Anderson, CD Lorenz, A Travesset. *General purpose molecular dynamics simulations fully implemented on graphics processing units*, ***J. Comput. Phys.*** **227**, 5342–5359 (2008).

[58] JA Anderson, A Travesset. *Molecular dynamics on graphic processing units: Hoomd to the rescue*, ***Comput. Sci. Eng.*** **10** (2008).

[59] DC Rapaport. *The art of molecular dynamics simulation*. Cambridge Univ Pr (2004).

[60] MP Allen, DJ Tildesley. *Computer Simulation of Liquids*, volume 408. Oxford Science Publications (1989).

[61] T Soddemann, B Dünweg, K Kremer. *Dissipative particle dynamics: A useful thermostat for equilibrium and nonequilibrium molecular dynamics simulations*, ***Phys. Rev. E*** **68**, 046702 (2003).

[62] M Ciesla, J Pawlowicz, L Longa. *Molecular dynamics simulation of the lennard–jones polymers in a good solvent*, ***Acta Phys. Pol. B* 38**, 1727 (2007).

[63] R Goetz, R Lipowsky. *Computer simulations of bilayer membranes: self-assembly and interfacial tension*, ***J. Chem. Phys.* 108**, 7397–7409 (1998).

[64] IR Cooke, K Kremer, M Deserno. *Tunable generic model for fluid bilayer membranes*, ***Phys. Rev. E* 72**, 011506 (2005).

[65] DP Landau, K Binder. *A guide to Monte Carlo simulations in statistical physics*. Cambridge Univ Pr (2005).

[66] N Metropolis, AW Rosenbluth, MN Rosenbluth, AH Teller, E Teller, others. *Equation of state calculations by fast computing machines*, ***J. Chem. Phys.* 21**, 1087 (1953).

[67] N Amenta, M Bern, M Kamvysselis. *A new voronoi-based surface reconstruction algorithm*, ***Proceedings of the 25th annual conference on Computer graphics and interactive techniques*** pages 415–421 (1998).

2

Entropic elasticity of dilated and contorted idealized circular chains

M Bertrand, M Forget, B Joós. *Physical Review E* (2010).

PHYSICAL REVIEW E **81**, 061803 (2010)

Entropic elasticity of dilated and contorted idealized circular chains

Martin Bertrand, Martin Forget, and Béla Joós*
Institut de physique Ottawa-Carleton, Campus de l'Université d'Ottawa, Ottawa, Ontario, Canada K1N 6N5
(Received 18 November 2009; revised manuscript received 20 April 2010; published 28 June 2010)

Thermal energy provides random motion to particles that leads to the well-known entropic force, which favors the clumping of linear and circular molecules. We evaluate the entropic force which resists the radial dilation and subsequent twisting out of plane of circular polymers by developing mechanical models and performing molecular dynamics simulations. We find that dilating a circular chain is analogous to stretching its linear counterpart. We also find that the torque applied to an already dilated ring and the resulting twist out of plane are related by a linear relationship for a wide range of deformed configurations and, using this result, we are able to predict the angular fluctuations of such a macromolecule.

DOI: 10.1103/PhysRevE.81.061803 PACS number(s): 82.35.Lr, 87.15.H−, 87.15.La, 87.14.E−

I. INTRODUCTION

Entropic forces play an important role in both soft and condensed matter physics, and biological physics. Indeed, whether it be the elasticity of rubber or the self-assembly of lipid bilayers, many materials often owe their unique properties to forces that are entropic in nature. Anytime thermal motion, or Brownian motion, is observed, one cannot neglect entropy as part of the free energy for the system under study. A classical problem involving entropic forces is the linear polymer in solution under stretch. Its entropic elastic response has been widely studied (see the review by Slater *et al.* [1]) and is a great subject matter for physics courses. A short description of the phenomenology goes as follows: thermal motion pushes the unconstrained linear chain in solution toward its most probable state, the random coil. Stretching the chain moves it into a lower entropy configuration. The thermal motion of the monomers fights this tendency creating the entropic recoil force. There are well-established expressions which relate this force to the chain's deformation and are unique for both freely jointed chains (FJC) and wormlike chains (WLC) when excluded volume interactions (EVI) are neglected [1]. But when EVI are included, one has to use scaling arguments that lead to different expressions for all force regimes. The entropic forces associated with circular chains have not received such an attention. In this paper, we present simple expressions that describe the entropic elastic response to applied external forces for prototypical circular polymers modeled as Gaussian chains with EVI (bead-spring model).

Circular polymers are of particular interest in soft matter [2–5] and biological physics. For example, we find circular DNA strands in many organisms [6], circular chains in the structure of macromolecules such as proteins, and cyclic peptides are often used in the pharmaceutical industry [7]. Of all circular molecules, DNA loops have been the most extensively studied and modeled as wormlike chains with both bending and twist rigidities [8,9]. A circular chain can be deformed by external forces in many different ways: it can be stretched, dilated, bent, and contorted. Entropic and mechanical elastic responses should be observed for all types of deformations. In the case of elastic rings modeling DNA loops dominated by mechanical forces, Panyukov and Rabin [8] provide a nice framework to describe shape changes due to external forces.

We focus on isolated simple idealized circular chains subjected to *dilation*, such as would result from a circular chain wrapped around a bulk object. A *twisting out of plane* is applied to the circular chain, which can be seen as a forced writhe and will be referred to as a *torsion* to avoid any ambiguity with an axial twist [10]. We develop simple relations for such deformations and compare them with molecular dynamics simulations on the bead-spring model. The next section introduces some useful theory. In Sec. III, the models are developed. Section IV presents the MD simulations and discusses the results in the light of our predictions.

II. ENTROPIC ELASTICITY

An isolated system connected to a heat bath of constant temperature T will always try to minimize its free energy A given by the following:

$$A = U - TS, \tag{2.1}$$

where we find the internal energy of the system U, a result of the interactions between the particles, and the entropy S, a measure of how probable the current conformation of the system is. In order to minimize the free-energy, it is clear that the entropy has to be maximized and thus the system will always tend toward its most probable conformation, driven to reconfigure by thermal motion. For a FJC made of N segments of length b in a thermal bath ($U=0$), under no constraint, this means it will clump in a shape that we call a random coil, with an average square end-to-end distance $\langle h^2\rangle = Nb^2$ [11] (more generally we find $\langle h^2\rangle = N^{2\nu}b^2$ where ν is the Flory exponent and is equal to 1/2 for a FJC [11]). It follows that it will resist any change of shape imposed by a constraint applied on a given coordinate x with an entropic recoil force, much like a spring:

*bjoos@uottawa.ca

$$f_{\text{recoil}} = -\frac{\partial A}{\partial x} = -\frac{\partial U}{\partial x} + T\frac{\partial S}{\partial x}. \tag{2.2}$$

Here, the derivative of the potential energy U should vanish leaving us with a force of entropic origin only. For example, if one pulls on both ends of a linear FJC (stress ensemble) with a force f in opposite directions (equivalently one can pull on one end with the other pinned in place), the chain develops an entropic recoil force equal to f and the mean end-to-end distance as a function of the force $\langle h(f)\rangle$ is given by the well-known relation [1]:

$$H = \frac{\langle h(F)\rangle}{h_{\max}} = \coth(F) - \frac{1}{F}, \tag{2.3}$$

where $h_{\max}=Nb$ is the maximal extension of the chain and $F=fb/k_bT$ is the scaled force or rather a ratio of a "stretching energy" over the thermal energy. The inversion of the series expansion of the above expression and subsequent interpolation of the solution produce an approximation of the entropic force in terms of the chains deformation [1]:

$$F(H) \cong \frac{3H - H^3}{1 - H^2}, \tag{2.4}$$

For very small deformations ($H \ll 1$) Eq. (2.4) can be reduced to Hooke's law $f \cong k\langle h\rangle$, where the spring constant is $k=3k_bT/Nb^2$. The entropic rigidity of the linear chain is directly proportional to temperature: the "warmer" it is, the stiffer it becomes.

For a real chain with EVI one observes a deviation from Eq. (2.3) for all but forces $F>1$. In the small forces regime ($F<N^{-\nu}$), scaling arguments still lead to Hooke's law:

$$\langle h\rangle \cong N^{2\nu}bF, \tag{2.5}$$

whereas in the intermediate forces regime ($N^{-\nu}<F<1$), they lead to a power law relationship [1]:

$$\langle h\rangle \cong NbF^{1/\nu-1} \tag{2.6}$$

If the chain is in a good solvent the Flory exponent is $\nu=0.588$.

III. MODELS

A. Dilating a circular chain

We here wish to calculate the entropic elastic response of a dilated circular chain as shown in Fig. 1. The system here studied resembles the two-dimensional (2D) planar polymeric loops studied by Camacho *et al.* in [12]. Like its linear counterpart, a circular chain will also clump in the entropically favorable coil conformation with a radius of gyration $R_{g,0} \propto bN^{\nu}$ (the proportionality constant is 0.29 for a Gaussian chain with $\nu=1/2$ [11]). Thus, if it is deformed in any given way, it will resist. In particular, if a force f_r is exerted on every components of a loop in a radial direction from the center of mass as shown in Fig. 1, we expect it will reach an equilibrium ring conformation with a radius of gyration $R_g(f_r)$ up to a maximum $R_{g,\max}=h_{\max}/2\pi=Nb/2\pi$. At equilibrium, we will assume that the entropic recoil force can be

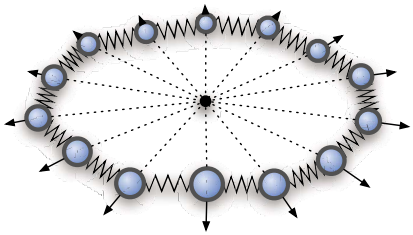

FIG. 1. (Color online) Dilating a polymer ring: a force f is exerted on the constituents of the chain in a chosen plane and in a radial direction from the center of mass.

assimilated to a uniform linear tension in the ring λ while a radial force per unit length $\tilde{f}_r=Nf_r/2\pi r$ is acting on it, where r is the radius of the ring ($r \approx R_g$). If a loop of circumference $l=2\pi r$ is stretched by an amount dl beyond equilibrium, the work done by the radial force $W_r=\tilde{f}_r dA=\tilde{f}_r 2\pi r dr$ has to be equal to the work done by the entropic force $W_e=\lambda dl=\lambda 2\pi dr$ such that we get a Laplace relation:

$$\lambda = \frac{Nf_r}{2\pi}. \tag{3.1}$$

As we go toward maximal extension, we propose the average circumference of the loop $\langle l\rangle$ approaches the end-to-end distance $\langle h\rangle$ of a linear chain pulled with a force f equivalent to the linear tension λ in the loop. In this regime, Eq. (2.3) would apply with a ratio on the left hand side of,

$$R = R_g(\Lambda)/R_{g,\max}, \tag{3.2}$$

and a scaled tension,

$$\Lambda = \lambda b/k_bT = Nf_r b/2\pi k_bT. \tag{3.3}$$

The analogy to a linear chain being stretched should still hold for intermediate extensions, with the relation between R and Λ being described by a power law:

$$R(\Lambda) \propto \Lambda^{\alpha}, \tag{3.4}$$

where the exponent α can be determined by experiment or simulation. However, it is clear that as we approach minimal extension the analogy does not apply. As the force decreases toward zero, the radius of the ring tends toward its undeformed radius of gyration $R_{g,0}(R_{g,0}/R_{g,\max} \sim N^{\nu-1})$. Of the functional form of the relation $R_g(\Lambda)/R_{g,\max}$ vs Λ for the weaker forces not much can be predicted, although one might observe a Hooke's type of relation analogous to the one introduced for the extension of a linear chain for $F \ll 1$. We will not focus on this regime for which the deformation is hard to separate from thermal fluctuations.

B. Twisting a dilated circular chain out of plane

What happens now if a chain dilated as in Fig. 1 is subject to a subsequent torsion, e.g., what is the entropic response to this additional deformation? To answer this question, let us imagine a circular chain dilated by a radial pressure $\tilde{f}_r$ that we twist out of plane as we would a towel as shown in Fig.

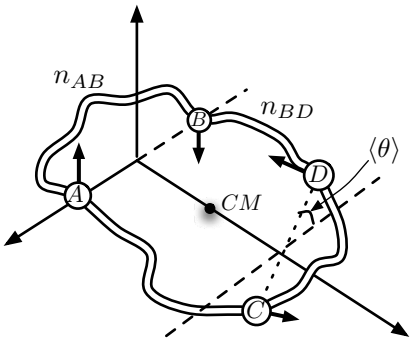

FIG. 2. Polymer loop under torsion: the pair AB is conveniently positioned on an axis such that one can clearly see what average angular displacement $\langle\theta\rangle$ is measured. If A and B are distant by d_A and d_B from their center of mass, and we find corresponding distance d_C and d_D for C and D, then the following is true about external torsion forces applied to the pairs and the resulting torque τ: $\tau=f_A d_A+f_B d_B=f_C d_C+f_D d_D$.

2: upon a ring of N elements, beads in our case, we select four of these ($i=\{A,B,C,D\}$), two pairs, AB and CD, on which we want to apply a torque of equal magnitude τ, with $n=n_{AB}$ beads between A and $B(n_{CD}=n_{AB})$ and n_{AC} beads between A and $C(n_{AC}=n_{BD})$. Vectors $\vec{d}_A$ and $\vec{d}_B$ run from the middle of the pair AB to A and B, respectively, while vectors $\vec{d}_C$ and $\vec{d}_D$ do the same for the pair CD. Vectors $\vec{s}_{AB}$ and $\vec{s}_{CD}$ run from the center of mass to the middle of opposite pairs. The direction of the force $\vec{f}_A$ is given by the cross product $\vec{d}_A\times\vec{s}_{AB}$ and its magnitude is equal to $\tau/2d_A$. All other forces are determined similarly thus setting the following equalities: $f_A d_A=f_B d_B$, $f_C d_C=f_D d_D$, and $\tau=f_A d_A+f_B d_B=f_C d_C+f_D d_D$.

The average angle $\langle\theta\rangle$ as depicted in Fig. 2 is then a measure of the amount of torsion (angular deformation) and can be plotted against the applied torque τ for a given set of parameters (n,f_r,N,k_bT) where n is short for n_{AB}. In the small angle limit, we predict the ring will contort until the entropic tension λ in the chain produces a torque equal to the one applied. The challenge is in evaluating the value of λ and its component along the direction of the forces producing the torque $\lambda_\parallel$, for a given angular displacement θ.

We refer the reader to Fig. 2 for the following discussion. Let us take point A since it is clear that all four points (A,B,C,D) are equivalent. The ring is dilated by a linear pressure $\tilde{f}_r$ that triggers the response of a uniform entropic tension λ we assume to be tangential to the curve at all points and normal to the force from which originates the pressure. Thus, A is pulled along an arc toward B and C by a force λ for both. As the ring is contorted, the tension pulling toward B does not produce any torque on A since it is by definition perpendicular to the twisting force f_A at all times. So is the dilation force f_r acting on A. We are thus left with the tension vector $\vec{\lambda}$ tangential to the arc that leads from A to C as the only candidate to produce a force $\lambda_\parallel$ that will oppose f_A. To evaluate $\vec{\lambda}$ and the component $\lambda_\parallel$ we place ourselves in the referential of C and first define the following:

$$d=d_A=d_C=R_g\sin\left(\frac{n}{N}\pi\right), \tag{3.5}$$

$$l=2R_g\cos\left(\frac{n}{N}\pi\right), \tag{3.6}$$

where d is half the length of the chords AB and CD, and l is the length of the chord AC (also BD) when the ring is at rest with a radius of gyration R_g. We assume here that this radius stays roughly constant as the loop gets twisted. These lengths so defined allow to write the following three vectors:

$$\vec{CA}=[d(1-\cos\theta),d\sin\theta,l], \tag{3.7}$$

$$\vec{CMA}=(-d\cos\theta,d\sin\theta,l/2), \tag{3.8}$$

$$\hat{f}_A=(-\sin\theta,-\cos\theta,0), \tag{3.9}$$

where $\vec{CA}$ is the vector going from C to A, $\vec{CMA}$ is the vector going from the center of mass to A, and $\hat{f}_A$ is the unit vector giving the direction of f_A. These vectors are defined in terms of an angular displacement θ. The cross product of $\vec{CA}$ and $\vec{CMA}$ gives a vector $\vec{p}_A$ normal to the twisting plane in A: $\vec{p}_A=\vec{CA}\times\vec{CMA}$. Another cross product of this new vector with $\vec{CMA}$ yields a vector $\vec{t}_A$ tangent to the curvature of the chain in A, following the arc going from A to C: $\vec{t}_A=\vec{p}_A\times\vec{CMA}$. This last vector allows to determine the tension vector we are hunting for: $\vec{\lambda}=\lambda\hat{t}_A$. We then can calculate $\lambda_\parallel$, the component of interest here, with the dot product $\lambda_\parallel=-\lambda\hat{t}_A\cdot\hat{f}_A$ which gives:

$$\lambda_\parallel=\frac{\lambda\sin\theta}{\left[\cos^2\left(\frac{n}{N}\pi\right)(2\cos\theta+1+\cos^2\theta)+\sin^2\theta\right]^{1/2}}, \tag{3.10}$$

where values for d and l were replaced by their definitions given in Eqs. (3.5) and (3.6). This component of the tension opposes and matches the force f_A acting on A at equilibrium. In the small angular displacement approximation ($\theta\ll1$), the second order Taylor series of the above expression gives the following polynomial approximation:

$$\lambda_\parallel\cong\frac{1}{2}\lambda\sec\left(\frac{n}{N}\pi\right)\theta. \tag{3.11}$$

Since the torque τ on the pairs AB and CD is equal to $2f_A d_A$, the preceding statement and Eq. (3.5) and (3.11) allow to write:

$$\tau\cong\kappa\theta=\lambda R_g\tan\left(\frac{n}{N}\pi\right)\theta. \tag{3.12}$$

The above equation is in the form Hooke's law for torsional elasticity where the elastic constant κ depends on three factors: size, entropic tension, and the points where torsional forces are applied. The third term in κ is a tangent function of the ratio n/N, which makes the entropic torque minimal as $n\to0$ and tend to infinity as $n\to N/2$: the entropic tension

induced in the arcs AC and BD of the ring grows as $n \to N/2$ until one reaches a point when the bonds between the beads making up the chain start to be stretched and the purely entropic response vanishes.

We know that the size of the ring R_g increases with the dilation force and the number of elements in the chain which leads to a dependence in λ and N. Thus we can rewrite Eq. (3.12) in a more practical form with the following substitutions, $R_g = \frac{Nb}{2\pi} R(\Lambda)$ and $\lambda = \frac{k_b T}{b}\Lambda$:

$$\tau \cong \kappa\theta = \frac{N}{2\pi} k_b T \Lambda R(\Lambda) \tan\left(\frac{n}{N}\pi\right)\theta, \tag{3.13}$$

where the product $\Lambda R(\Lambda)$ can be determined from the study of ring dilation (Sec. III A).

With Eq. (3.13), one can estimate the twist fluctuations when no torque is applied on the polymer ring. Using the equipartition of energy, one can argue that the twist is an actual degree of freedom and that the elastic energy of twist is related to the thermal energy as follows:

$$E_{\text{twist}} = \frac{1}{2}\kappa\langle\theta^2\rangle \cong \frac{1}{2}k_b T. \tag{3.14}$$

This equality then leads to an estimate of the root-mean-square value of the angular deviation:

$$\theta_{\text{rms}} \cong \sqrt{\frac{k_b T}{\kappa}} = \left[\frac{N}{2\pi}\Lambda R(\Lambda)\tan\left(\frac{n}{N}\pi\right)\right]^{-1/2}. \tag{3.15}$$

It is worth noting that throughout this last section, λ is assumed to be unchanging for a given dilation force. The fact that part of the entropic tension in the chain counteracts an additional applied torque on the points A,B,C,D implies that the tension itself needs to change as the ring is twisted for it to reach a new equilibrium configuration. The local lost of tension to counteract the dilation will be compensated by a redistribution of the load in segments AC and BD which is bound to change the physics of our problem and render the above model useless once a certain torsion angle is attained.

IV. MOLECULAR DYNAMICS SIMULATIONS OF DILATED AND CONTORTED LOOPS

This article presents data obtained from molecular dynamics (MD) simulations of single polymer chains either in a linear or circular configuration, all executed with ESPRESSO [13]. We use the Kremer-Grest approach [14], which consists in modeling the chains like beads connected by springs. In our simulations springs are modeled using a finitely extensible non-linear (FENE) potential of the form $U_{\text{FENE}}(r_{ij}) = 0.5kR_0^2 \log[1-(r_{ij}/R_0)]$, where $k = 30\epsilon_{\text{LJ}}/\sigma^2$ and $R_0 = 1.5\sigma$. Additionally, all beads interact through the repulsive part of a truncated and shifted Lennard-Jones (LJ) potential of the form $U_{\text{LJ}}(r_{ij}) = 4\epsilon_{\text{LJ}}[(\sigma/r_{ij})^{12} - (\sigma/r_{ij})^6 + shift]$ so that EVI are recuperated ($r_{cut} = 2^{1/6}\sigma$, $shift = 0.25$). The equilibrium distance between two adjacent beads on a chain is observed to be $b \cong 0.97\sigma$. The equations are integrated using a Langevin thermostat so that the system appears to be connected to a heat bath of temperature T (thermal energy $k_B T$). All numerical values are in MD units, σ being the unit of length (LJ range), ϵ, of energy (LJ energy), and m, of mass. Thus time has units of $\sqrt{m\sigma^2/\epsilon}$, and force, ϵ/σ.

Stretching experiments on linear chains were preformed with one end fixed in space and the other being pulled by a constant force f, while dilation and twisting out of plane experiments were performed as described in Secs. III A and III B. It is worth mentioning that using springs to model bonds leads to a longitudinal elasticity of the chain and thus a mechanical elastic response will appear for large applied loads ($F \gg 1$). However, this response has been shown to be negligible in our simulations, the overall contour length increase of both linear and ring polymers being at maximum close to 1%.

A. Dilated loops compared to stretched chains

We simulated the dilation of a circular chain and compared the results to the extension of a linear chain with the same number of segments for a wide range of parameters: $N = [40, 200]$, $k_B T = [0.4, 1.2]$, and $\{F, \Lambda\} = [0, 10]$. It is interesting to note that our results are very much similar to what Camacho *et al.* get in [12] where the linear pressure is replaced by an intrinsic bending stiffness in the ring.

We calculated, for undisturbed chain configurations ($F = 0$), Flory exponents for the radius of gyration of undeformed linear chains and rings resulting in values of $\nu = 0.60 \pm 0.02$ and $\nu = 0.623 \pm 0.005$, respectively. These values are within each other's confidence interval and are only slightly different than the one obtained from mean-field calculations for linear polymers with EVI ($\nu = 0.588$ [11]). The discrepancies are probably due to the model used for simulating our polymers (Kremer-Grest MD) and have been documented for linear chains [15]. We also found a ratio of $R_g/\langle h\rangle = 0.29$ for the ring's radius of gyration over the linear chain's end-to-end distance which, interestingly, corresponds to the theoretical prediction for ideal Gaussian chains, $R_{g,0}/bN^{1/2} = 0.29$.

We computed the entropic component of the recoil force ($T\frac{\partial S}{\partial x}$) by plotting f vs T [see Eq. (2.2)] at fixed values of the deformation ratio for both circular and linear chains of length $N = 100$. Figure 3 shows that the entropic force matches almost exactly the recoil force itself, showing that the increase of potential energy for high loads as seen in the inset of Fig. 3 (maximum of 0.5%) is of negligible incidence on the total force, and demonstrating that the entropic force is linearly dependent upon temperature.

Figure 3 also clearly shows that there is a good match between the elastic response of a polymer loop being dilated and a linear chain being stretched. In fact, the two response curves really start to diverge only when the load becomes smaller than the thermal force ($\{F, \Lambda\} < 1$). The intermediate loads regime for ring dilation (region between the vertical dotted lines in Fig. 3) was fitted with a power law, and although the parameters slightly vary with chain size N, the following fit formula is an approximation that covers well the range of sizes we are studying in here:

$$R(\Lambda) \cong 0.52\Lambda^{0.29}, \quad \text{for } 1 < \Lambda \leq 4. \tag{4.1}$$

In the high-loads regime ($\{F, \Lambda\} > 4$), Eq. (2.3) makes a good fit of the data and can be used to finish the construction of a piecewise function of $R(\Lambda)$ for $\Lambda > 1$:

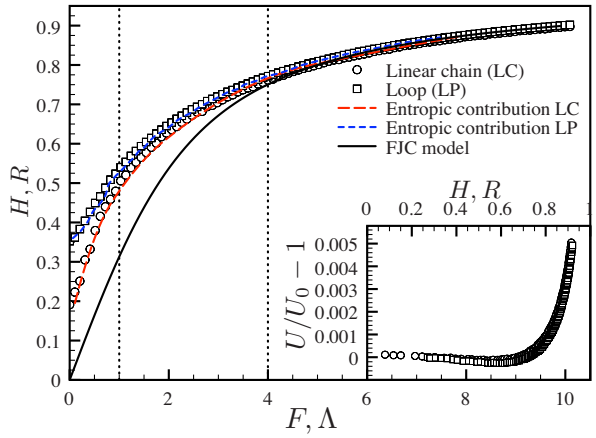

FIG. 3. (Color online) Comparison of a linear chain being stretched to a ring being dilated ($N=100$). The amount of *Stretch* (H,R respectively) in function of the scaled force F or tension Λ is shown in the main view along with entropic contributions and the theoretical curve for a FJC. The inset shows the increase in potential energy as the chains are deformed.

$$R(\Lambda) \cong \coth(\Lambda) - \frac{1}{\Lambda}, \quad \text{for } \Lambda > 4. \tag{4.2}$$

The function made of Eqs. (4.1) and (4.2) should prove to be a good tool to estimate the entropic component of the rigidity of mildly to strongly dilated polymer rings and be highly useful to complete the model for twisting rings out of plane [see Eq. (3.13)].

B. Circular chains under torsion

1. Angular displacement vs applied torque

Torsion experiments were performed as described in Sec. III B. We explored the following parameter space: $N=[20,200]$, $n=[5,35]$, $\Lambda=[1,8]b$, $k_bT=[0.4,1.2]$. The results obtained are quite remarkable, the hallmark of which is probably the presence of a linear relationship between the angular displacement and the applied torque over a rather wide range of values for $\langle\theta\rangle$ (see Fig. 4 for an example). It, thus, seem that the approximate formula we proposed to describe this same relationship in Eq. (3.13), used in conjunction with the fits given in 4.1 and 4.2, applies to a greater extent than we initially thought. In fact, in Fig. 4 one can observe how close the prediction is to the actual data from simulations, a deviation of 8.7% being observed in this particular case. In fact, a thorough comparison between the predicted slope κ^{-1} in this linear regime and the simulation results, throughout our parameter space, revealed deviations around or lower than 10% as long as the ring dilation corresponds to the intermediate or high-loads regimes ($\Lambda \gtrsim 1.5$). It is then clear that the counteracting torque originates from the entropic tension in the ring. Given a polymer ring dilated by an intermediate or high load, one can use Eq. (3.13) to either predict how much the molecule can contort if the applied forces are known or find the magnitude of those forces for a given contorted configuration.

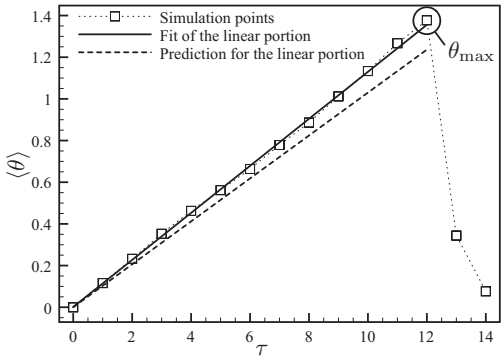

FIG. 4. Characteristic curve of the relationship between the average angular displacement $\langle\theta\rangle$ and the applied torque τ on both the pairs of beads AB and CD. Here it is shown for $N=100$, $n=5$, $\Lambda=5.0b$, and $k_bT=1$. The slope κ^{-1} of the linear portion is 0.113 while Eq. (3.13) predicts 0.103, a value that deviates by 8.7%. The maximum twist angle θ_{max} beyond which the ring enters an overtwisted regime is pointed out.

2. Maximum contortion

Figure 4 shows that there is a maximum angular displacement θ_{max} that can be achieved in our simulations, to which corresponds an applied torque τ_{max}. Beyond this limit, the ring enters a regime of over-contortion leading to a shape of writhe equal to 1, which is out of the scope of this study. We cannot provide any quantitative prediction for the values of θ_{max} due to limitations in our simple model. However, we'd like to propose an explanation as to why we observe that the most influential parameter is the ratio n/N, i.e., the position of the twisting points in proportion to the chain length. Indeed, as this ratio increases, the overall trend is to see the maximum angular displacement decrease. We suppose this is mostly due to the stretching of chain segments AC and BD in Fig. 2: as the ring is contorted, the entropic tension in those same segments increases, and the inhomogeneity this introduces in the tension along the circumference of the ring brings on its collapse. Let us use expressions 3.5, 3.6, and 3.7 to write down an approximation for the stretch ratio l'/l:

$$\frac{l'}{l} = \sqrt{\frac{1}{2}\tan^2\left(\frac{n}{N}\pi\right)(1-\cos\,\theta)} - 1. \tag{4.3}$$

We then assume that passed a "stretch" threshold, the ring collapses. For the sake of this argument, we fix this threshold as low as 1% and assume it is uniform for all n/N. The above equation can then be solved for θ which should give a trend for θ_{max} vs n/N. This is confirmed in Fig. 5 where we see qualitative agreement between values obtained from simulations and the predicted trend.

3. Angular fluctuations with no net angular displacement

Equation (3.15) at the end of Sec. III B approximates θ_{rms} for rings upon which no torque is applied. It so happens that in such a conformation the mean angular displacement $\langle\theta\rangle$ is zero and that θ_{rms} is equal to σ_θ, the standard deviation of θ. We, therefore, compared θ_{rms} to σ_θ obtained from simula-

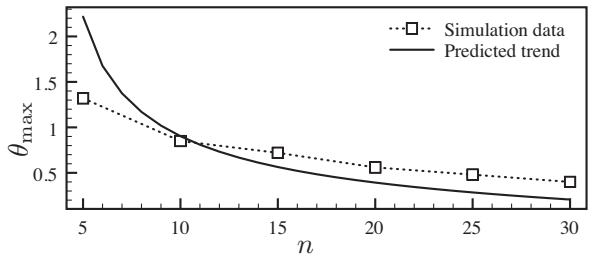

FIG. 5. Qualitative agreement of the maximum twist angle from simulations with the predicted trend as a function of n. The size of the loop is $N=100$ and the thermal energy is $k_bT=1$.

tions for various permutations of the parameters n, N, and k_bT, through all dilation regimes ($\Lambda=[1.0b, 8.0b]$). For any given dilation value with n and N fixed, our model predicts angular fluctuations independent of temperature, a behavior that simulation data confirms. We then fixed the temperature, scaled the data and the model by the appropriate asymptotic values for very high loads $\Lambda \gg 1$, $\sigma_{\theta,\min}$ and $\theta_{\mathrm{rms,min}}$ respectively, and found that they are thus in excellent agreement in both the intermediate and high-loads regimes. Hence, for a given dilation load, the model is able to predict values obtained from simulations within a prefactor $\theta_{\mathrm{rms,min}}/\sigma_{\theta,\min}$, which has a strong dependence on the ratio n/N, and a weak one on N alone that we will neglect here. We plotted the prefactor in function of n/N and found the relationship to be approximately linear. We fitted the curve and used the resulting coefficients to adjust our model:

$$\theta'_{\mathrm{rms}} = \left(0.55\frac{n}{N} + 0.72\right)^{-1} \theta_{\mathrm{rms}}. \tag{4.4}$$

The angular fluctuations thus approximated are consistent with what we measure from simulations as shown in Fig. 6. We believe that the prefactor in Eq. (4.4) is due to the approximations made in our model, in particular to the reduced number of degrees of freedom since we only consider the four A,B,C,D beads and not the entire chain. Nonetheless, Eq. (4.4) is a valuable tool to get a very good estimate of the angular fluctuations in a dilated ring.

V. CONCLUSION

We presented a study on circular chain dilation with subsequent twisting out of plane of which the two highlights are: (1) the dilation of a ring is analogous to stretching a linear chain of the same size; (2) when twisting out of plane a dilated ring, a linear relationship is found between the entropic response torque and the angular displacement. We proposed simple mechanical models for both types of deformation. Our analysis suggests that the entropic response to both dilation and contortion originates from an entropic tension along the contour of the polymer loop. The models provide a surprisingly good approximation to the results from simulations of bead-spring chains. Aside from its intrinsic interest as a thermally driven force, our study complements our understanding of the entropic spring so prevalent whenever polymers are present. Entropic rings may be less prevalent. But they may provide some insight into the rigidity of certain folded proteins where loops are present resulting from hydrogen-like bonds, for instance, linking different segments together [16,17].

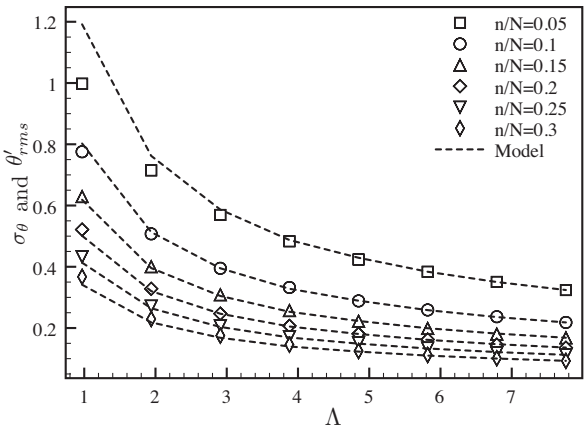

FIG. 6. Comparison of the twist fluctuations θ'_{rms} derived from our model (dotted lines) to the standard deviation of the twist σ_θ obtained from simulations (symbols) when no torque is applied on the dilated ring: the model accurately predicts the observed behavior for a large interval of the ratio n/N across all dilation load Λ regimes except for the lowest values of the load and ratio.

ACKNOWLEDGMENTS

BJ would like to thank Michael F. Thorpe for a useful discussion. The work has been funded in part by the Natural Sciences and Engineering Reserach Council (Canada) and "Le fonds québécois de la recherche sur la nature et les technologies" (FQRNT).

[1] G. W. Slater, Y. Gratton, M. Kenward, L. McCormick, and F. Tessier, Soft Matter **1**, 365 (2003).
[2] S. P. Obukhov, M. Rubinstein, and T. Duke, Phys. Rev. Lett. **73**, 1263 (1994).
[3] M. Müller, J. P. Wittmer, and M. E. Cates, Phys. Rev. E **53**, 5063 (1996).
[4] S. Brown and G. Szamel, J. Chem. Phys. **108**, 4705 (1998).
[5] G. Zifferer and W. Preusser, Macromol. Theory Simul. **10**, 397 (2001).
[6] D. Helinski and D. Clewell, Annu. Rev. Biochem. **40**, 899 (1971).
[7] J. Mulvenna, C. Wang, and D. Craik, Nucleic Acids Res. **34**, D192 (2006).
[8] S. Panyukov and Y. Rabin, Phys. Rev. E **64**, 011909 (2001).

[9] S. Medalion, S. Rappaport, and Y. Rabin, J. Chem. Phys. **132**, 045101 (2010).
[10] J. Marko and E. Siggia, Macromolecules **27**, 981 (1994).
[11] I. Teraoka, *Polymer Solutions: an Introduction to Physical Properties* (Wiley, New York, 2002).
[12] C. Camacho, M. Fisher, and R. Singh, J. Chem. Phys. **94**, 5693 (1991).
[13] H. Limbach, A. Arnold, B. Mann, and C. Holm, Comput. Phys. Commun. **174**, 704 (2006).
[14] G. S. Grest and K. Kremer, Phys. Rev. A **33**, 3628 (1986).
[15] D. Rapaport, J. Phys. A **11**, L213 (1978).
[16] D. J. Jacobs, L. A. Kuhn, and M. F. Thorpe, in *Rigidity Theory and Applications*, edited by M. F. Thorpe and P. M. Duxbury (Kluwer Academic/Plenum, New York, 1999).
[17] D. J. Jacobs and S. Dallakyan, Biophys. J. **88**, 903 (2005).

3

Universal measure of the effect of sequence on the elasticity of heteropolymers

M Bertrand, D O'Keeffe, B Joós. To be submitted.

Universal measure of the effect of sequence on the elasticity of heteropolymers

Martin Bertrand, Daniel O'Keeffe and Béla Joós*
Institut de physique Ottawa-Carleton
Campus de l'Université d'Ottawa
Ottawa, Ontario, Canada, K1N 6N5
(Dated: December 29, 2011)

We describe a simple method to characterize the importance of sequence on the entropic elasticity of heteropolymers belonging to the same family. We predict the universal functional form of the variance of the thermally averaged extension versus the force and fit it to data obtained from various simulated heterogeneous Kratky-Porod chains being stretched. We use the extracted fit parameters to characterize the effect of sequence. This new tool that we present should be useful for those who wish to better judge whether sequence matters or not when measuring observables related to the entropic elasticity of semi-flexible biopolymers.

I. INTRODUCTION

Biopolymers such as DNA and proteins are often heterogeneous in nature, that is they are made of sequences of differing elements. The properties of these so called heteropolymers are often found to be composition-dependent which influences the entropy driven processes they are involved in [1–15], *e.g.* DNA stretching, loop formation, and packaging, protein folding, etc. With the advent of various experimental techniques, such as optical or magnetic tweezers and atomic force microscopy, the entropic elasticity of single biomolecules has been extensively probed ([16] and references therein) and results have been successfully compared to theoretical models describing the entropic response to stretch of a homogeneous flexible "freely-jointed chain" (FJC) or semi-flexible "worm-like chain" (WLC) [17]. But the effects of inhomogeneities in the sequence of elements on the entropic elasticity of heteropolymers are still not fully understood to date.

Sequence disorder in a semi-flexible chain like DNA typically arises from either variations in the bending rigidity along the backbone which results in a contour length dependent persistence length $l_p(s)$, where s is the distance along the chains' contour [9, 13–15, 18], and/or variations in the intrinsic local curvatures $c(s)$ [7, 8, 10–14]. These fluctuating properties give rise to an effective measured persistence length L_p that is sequence dependent which inevitably influences the entropic elasticity of heteropolymers, but to what extent? In particular, when are the effects of sequence maximized and, in opposition, when can we consider them to be negligible?

Numerous theoretical studies in the last two decades have been conducted to better understand the entropic elasticity of heteropolymers, all focusing on specific types of disorders [7, 8, 10–12] and/or given force intervals [13, 14]. Much of the work has also been directed at better understanding the effect of inhomogeneities in the composition of double-stranded DNA, motivated by all the key functions the molecule participates in and improving sequencing techniques. In general, the approach has been to try to find an effective persistence length $L_{p,\text{eff}}$ towards which L_p tends for long enough chains and with which one can describe the elasticity of heteropolymers such as DNA using the WLC model. In the present letter, we assume the existence of $L_{p,\text{eff}}$ and propose a simple measurement of the effects of sequence on the elastic response to stretch of biopolymers that exhibits universal properties for all types of disorders and for all applied forces. We first derive the variance in what we call "sequence-space" (s-space), the space of all possible sequences of elements given a family of molecules with similar properties, of the scaled thermally averaged or mean extension of heteropolymers as a function of the stretching force and with it, corroborate and complement many of the conclusions from previous studies, *i.e.* sequence is more important for short chains under moderate loads, it becomes irrelevant in the thermodynamic limit and under strong loads. We calculate this variance for simulated Kratky-Porod chains with disorder in either the preferred angles between subsequent monomers as in Bensimon *et al.* [11] or the bending constants which are analogous to variations in $c(s)$ and $l_p(s)$ respectively. We show that the derived variance fits the data very well and that the fit allows to extract both the effective persistence length $L_{p,\text{eff}}$, equivalent to the average $\langle L_p \rangle$ in s-space, and the variance $\text{Var}_L(L_p)$ of the persistence length in s-space for a family of polymers with contour length L, where L_p is the effective persistence length of a particular given sequence. The relative importance of sequence as measured by the ratio $\text{Std}_L(L_p)/\langle L_p \rangle$, where $\text{Std}_L(L_p) = \text{Var}_L(L_p)^{1/2}$, should prove to be a good test measurement to decide whether the specific sequence of a polymer needs to be accounted for in the description of properties and phenomena involving entropic elasticity.

* martbert@gmail.com

II. MODELLING THE EFFECT OF SEQUENCE ON THE ELASTICITY

We will now derive the variance in s-space of the scaled mean extension as a function of the applied stretching force (constant stress ensemble) for both heterogeneous FJCs and WLCs. Although most biopolymers are semi-flexible in nature and thus better described by the WLC model, we chose to include heterogeneous FJCs in our derivation for the sake of completeness. Let us start with models for the entropic elasticity of homogeneous FJCs and WLCs of contour length L and persistence length of a stress-free chain l_p. The scaled mean extension in the z-direction $\tilde{R}_z = R_z/L$ as a function of the scaled stretching force $F = fl_p/k_bT$ for each model is:

$$\tilde{R}_{z,\mathrm{FJC}} = \coth 2F - \frac{1}{2F}, \tag{1}$$

$$\tilde{R}_{z,\mathrm{WLC}} \cong \begin{cases} \dfrac{0.6667F + 0.8080F^2 + 0.10365F^3}{1 + 1.1118F + 1.1076F^2 + 0.10365F^3} & \text{for } F \leq 9 \\ 1 - \dfrac{1}{2\sqrt{F}} & \text{for } F > 9. \end{cases} \tag{2}$$

where the expression for the WLC model is an approximation derived by Zimm [19] to the "exact" numerical solution for the *extension vs force* relation of such a chain as calculated by Marko and Siggia in [17]. We then imagine disorder is introduced in the chains such that the persistence length becomes sequence dependent. The nature of the disorder here is irrelevant, but we are aware this might not always be the case. We assume that for a chain of a given length L many sequences are possible, as is the case for DNA, and that each sequence is characterized by its own effective persistence length L_p that we can substitute to l_p in the scaled force F as defined above. L_p should only converge to the global value $L_{p,\mathrm{eff}}$, in the thermodynamic limit. In the space of all possible sequences, we will assume that L_p is normally distributed with mean $\langle L_p\rangle = L_{p,\mathrm{eff}}$ and variance $\mathrm{Var}_L(L_p)$. If the average number of persistence lengths in a chain of length L is given by $\langle N_p\rangle = L/\langle L_p\rangle = Nb/\langle L_p\rangle$, we can expect $\mathrm{Var}_L(L_p) \cong \mathrm{Var}(l_p)/\langle N_p\rangle \sim 1/N$ where $\mathrm{Var}(l_p)$ is the variance of the local persistence length independent of L. Thus, as we explore the s-space, variations in L_p will inevitably introduce variations in the scaled mean extension $\tilde{R}_z$ measured for a given stretching force f. We calculate the variance of $\tilde{R}_z(f, L_p, k_bT)$ in s-space, using the Delta method which goes as follows: given $Y = g(X)$ a function of X, a normally distributed variable of mean μ and variance σ^2, if $g(X)$ can be approximated by a linear Taylor expansion around μ over the range of most likely values of X, then the variance of Y is approximated by:

$$\mathrm{Var}(Y) \cong \left[g'(X = \mu)\right]^2 \sigma^2. \tag{3}$$

Since $\tilde{R}_z$ is a function of the normally distributed random variable L_p, we derive the following variances in s-space for the FJC and WLC models:

$$\mathrm{Var}_{\mathrm{FJC}}(\tilde{R}_z) \cong \frac{\mathrm{Var}_L(L_p)}{4\langle L_p\rangle^2}\left[4F\,\mathrm{csch}^2(2F) - \frac{1}{F}\right]^2, \tag{4}$$

$$\mathrm{Var}_{\mathrm{WLC}}(\tilde{R}_z) \cong \frac{\mathrm{Var}_L(L_p)}{\langle L_p\rangle^2}\begin{cases} 16F^2\dfrac{(\sum_{i=0}^{4} a_i F^i)^2}{(\sum_{j=0}^{3} c_j F^j)^4} & \text{for } F \leq 9 \\ \dfrac{1}{16F} & \text{for } F > 9, \end{cases} \tag{5}$$

where the scaled force is redefined as $F = f\langle L_p\rangle/k_bT$ and the coefficients in the variance for the WLC are given by the following vectors $\mathbf{a} = (66.67, 161.6, 47.084748, 9.226923, 3.105354) \times 10^6$ and $\mathbf{c} = (20000, 22236, 22152, 2073)$. We will henceforth concentrate on the variance of the mean extension for the WLC model that well describes most biopolymers, but let us keep in mind that much of the discussion can be transposed to the FJC model. Eq. 5 is plotted in Fig. 1 where we can see that it fits very well data obtained from simulations of which we will discuss in details below. We find a striking characteristic shape which peaks when $f\langle L_p\rangle \cong k_bT$: it appears the effect of varying the sequence is most important for moderate stretching forces or conversely, moderate deformations. Then as $f\langle L_p\rangle$ comes to dominate over k_bT, the variance decays toward zero like $1/F$, in other words, as the extension saturates. This is in line with [10, 14] where it is reported that disorder in sequence is irrelevant under strong forces.

III. COMPARISON TO MC SIMULATIONS

As shown in Fig. 1, this variance that we use can be fitted to simulation data, and quite possibly experimental data, to not only extract the mean persistence length $\langle L_p\rangle$ of a family of heteropolymers, but also the variance $\mathrm{Var}_L(L_p)$ which tells how much this persistence length varies in the space of all possible sequences for this same family, a valuable information to better judge of the effect of sequence disorder. We performed Monte-Carlo (MC) simulations of heteropolymers modeled as discrete Kratky-Porod chains in the manner of Bensimon *et al.*: given a chain of N monomers or segments of length b ($L = Nb$) under the action of a force f, its energy ε can be written as:

$$\frac{\varepsilon}{k_bT} = -\sum_i K_i \cos(\alpha_i - \psi_i) - H\sum_i \cos\theta_i, \tag{6}$$

where α_i is the angle and ψ_i, the preferred angle between successive segments $i-1$ and i, θ_i is the angle between the segments and the direction in which the force is pulling, the field $H = fb/k_bT$, and K_i is a bending stiffness between successive segments and is related to the local persistence length $l_{p,i}$ by $K_i = l_{p,i}/b$. In our simulations we sample ψ from a half-Gaussian distribution of mean zero and variance σ_ψ^2, $P(\psi) =$

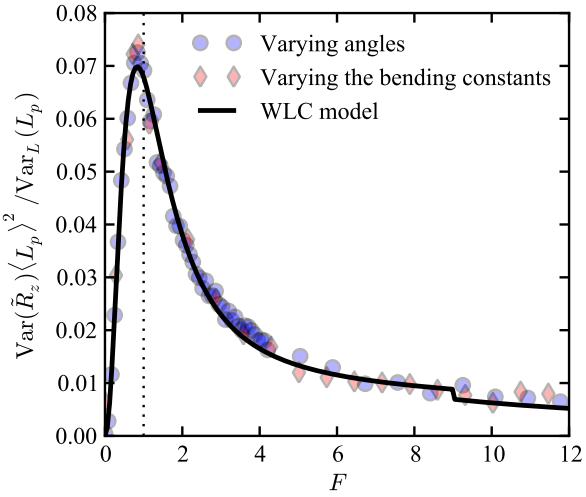

FIG. 1. The variance of the scaled mean extension in "sequence-space" as a function of a scaled force for a set of heteropolymers that behave according to the WLC model (continuous line). Fitted data and scaled accordingly is also shown for Monte-Carlo simulations of discrete Kratky-Porod chains with randomized preferred angles between successive segments (blue circle) and randomized bending constants (red diamonds).

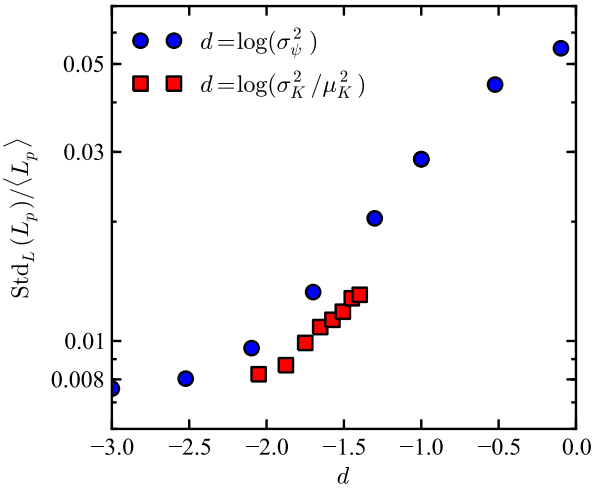

FIG. 2. Semi-log plot of the relative importance of disorder measured as the ratio $\mathrm{Std}_L(L_p)/\langle L_p\rangle$, where $\mathrm{Std}_L(L_p) = \mathrm{Var}(L_p)^{1/2}$ is the standard deviation of the stress-free persistence length in s-space, as a function of the strength of the sequence disorder d in either the preferred angles ψ, $d = \log(\sigma_\psi^2)$, or the bending constants K, $d = \log(\sigma_K^2/\mu_K^2)$. The data is from MC simulations of chains with $N = 600$. $K = 20$ when the preferred angles are randomized and $\mu_K = 15$ when it is the bending constants.

$\sqrt{2/\pi\sigma_\psi^2}\exp(-\psi^2/2\sigma_\psi^2)$ for $\psi > 0$, while fixing K to a constant value as is done in [11], or we sample K from a Gaussian distribution of mean μ_K and variance σ_K^2, $P(K) = 1/\sqrt{2\pi\sigma_K^2}\exp\left[-(K-\mu_K)^2/2\sigma_K^2\right]$, while fixing ψ at zero. The variance σ_K^2 has to be chosen carefully such that the probability of sampling a negative value of K is negligible. Variations in ψ and K are discrete analogues to variations in the spontaneous curvature $c(s)$ and persistence length $l_p(s)$ respectively of continuous filaments. In all MC simulations we have chosen $b = 1$ and $k_bT = 1$. Each MC run consisted of 5×10^6 steps and 80 different sequences were generated for each chosen disorder distribution. It is important to note that the variance can be measured with only a dozen sequences, but that for statistical smoothing we have simulated a larger number of these. We have verified that when varying the preferred angles we reproduce the predicted effective persistence length $L_{p,\mathrm{eff}} = \langle L_p\rangle$ as a function of the disorder as in Bensimon *et al.*: $\langle L_p\rangle$ decreases with increasing disorder in ψ, the chain thus appearing harder to stretch.

Fig. 2 essentially demonstrates how much varying the sequence affects the stress-free average or effective persistence length of a heterogeneous semi-flexible chain (N=600): no matter its origin, the greater the disorder is, the greater are the variations of L_p in s-space. While low disorder corresponds to variations in L_p of less than 1%, we observed variations as high as 6% with randomized preferred angles. But the quantities here are only relevant to the model we simulated. In reality, each family of heteropolymers shall need to be specifically characterized. The effect of disorder is plotted as the ratio of the standard deviation of L_p for chains of length L over the mean persistence length both in s-space $\mathrm{Std}_L(L_p)/\langle L_p\rangle$ as a function of the chosen disorder factor d, where $d = \log(\sigma_\psi^2)$ or $d = \log(\sigma_K^2/\mu_K^2)$ for randomized preferred angles or bending constants respectively (the variance in K is being divided by the mean K squared so as to represent the relative spread of the disorder in the bending constants). Since we wanted to keep the distribution of bending constants K Gaussian, the interval of disorder explored in varying K appears limited on the figure.

In Fig. 3 we show that $\mathrm{Var}(\tilde{R}_z)$ goes like N^{-1} and vanishes as $N\to\infty$. This corroborates previous predictions made in [13, 14]: in the thermodynamic limit, although the persistence length might need to be renormalized in function of the disorder, the sequence itself becomes irrelevant.

IV. CONCLUSION

Variations in the persistence length of specifically engineered short DNA chains have been recently measured

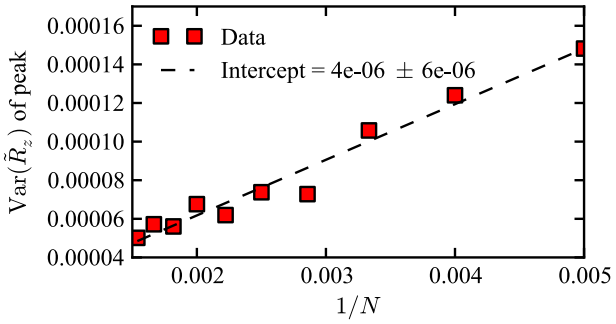

FIG. 3. The peak variance is clearly proportional to $1/N$ and goes to zero as $N \to \infty$. The data comes from a series of MC simulations for polymers of different lengths with preferred angles sampled from a half-Gaussian distribution of variance $\sigma_\psi^2 = 0.1$ and a bending constant $K = 20$.

as described in [9]. Using their results, we should be able to construct a family of chains upon which we could perform stretching experiments to confirm the usefulness of our variance. Furthermore, this new approach we presented in this letter for measuring the effect of sequence on a given observable of the chain related to its entropic elasticity by calculating a variance in s-space is one that could potentially be applied to a number of problems. For example, one could consider directly extending our study to the constant strain ensemble by fixing the extension and measuring fluctuations in s-space of the entropic force response. Also, the entropic elasticity being related to the relaxation time of a chain, one could measure the effects of sequence on any time related issue such as pore translocation of DNA, DNA looping, DNA packaging, and protein folding by using such a variance.

The work has been funded in part by the Natural Sciences and Engineering Research Council (Canada), and by a scholarship from "Le fonds québécois de la recherche sur la nature et les technologies" (FQRNT) to MB.

[1] P. Hagerman, Annu. Rev. Biophys. Biophys. Chem. **17**, 265 (1988).
[2] D. Crothers, Haran, T.E., and J. Nadeau, J. Biol. Chem. **265**, 7093 (1990).
[3] A. Travers, *DNA-Protein Interactions* (1993).
[4] B. Audit, C. Thermes, C. Vaillant, Y. D'Aubenton-Carafa, J. Muzy, and A. Arneodo, Phys. Rev. Lett. **86**, 2471 (2001).
[5] C. Vaillant, B. Audit, and A. Arneodo, Phys. Rev. Lett. **95**, 068101 (2005).
[6] E. Segal, Y. Fondufe-Mittendorf, L. Chen, A. Thåström, Y. Field, I. Moore, J.-P. Wang, and J. Widom, Nature **442**, 772 (2006).
[7] J. Moukhtar, E. Fontaine, C. Faivre-Moskalenko, and A. Arneodo, Phys. Rev. Lett. **98**, 178101 (2007).
[8] J. Moukhtar, C. Vaillant, B. Audit, and A. Arneodo, Europhys. Lett. **86**, 48001 (2009).
[9] S. Geggier and A. Vologodskii, Proc. Nat. Acad. Sci. USA **107**, 15421 (2010).
[10] P. Nelson, Phys. Rev. Lett. **80**, 5810 (1998).
[11] D. Bensimon, D. Dohmi, and M. Mézard, Europhys. Lett. **42**, 97 (1998).
[12] Y. Popov and A. Tkachenko, Phys. Rev. E **76**, 021901 (2007).
[13] Z. Zhou and B. Joós, Phys. Rev. E **77**, 061906 (2008).
[14] Z. Zhou and B. Joós, Phys. Rev. E **80**, 61911 (2009).
[15] S. Muhuri and M. Rao, J. Stat. Mech: Theory Exp. **2010**, P02005 (2010).
[16] K. Neuman and A. Nagy, Nature methods **5**, 491 (2008).
[17] J. Marko and E. Siggia, Macromolecules **28**, 8759 (1995).
[18] J. Van Noort, T. Van Der Heijden, M. De Jager, C. Wyman, R. Kanaar, and C. Dekker, Proc. Nat. Acad. Sci. USA **100**, 7581 (2003).
[19] D. Stigter and C. Bustamante, Biophys. J. **75**, 1197 (1998).

4

Thermophoretic stretch of nano-confined polymers: model and simulations

M Bertrand, B Joós. Submitted for publication.

Thermophoretic stretch of nano-confined polymers: model and simulations

Martin Bertrand and Béla Joós*
Institut de physique Ottawa-Carleton
Campus de l'Université d'Ottawa
Ottawa, Ontario, Canada, K1N 6N5
(Dated: December 19, 2011)

We present a novel approach to model the effects of a non-uniform force field stretching a nano-confined polymer using blobs and the Flory free-energy. We use it to describe the thermophoretic stretch of polymers exposed to symmetric thermal gradients in nano-confined geometries as demonstrated in Thamdrup *et al.*, Nano Lett., 10, 2010. We validate our model with experimental data and molecular dynamics simulations. Excluded volume interactions are shown to play a key role especially when temperatures are close to the solvent's θ value.

Being able to manipulate single biopolymers is of utmost importance for the study of their properties. In particular, we often wish to extend these to perform force response measurements or to expose the backbone of the chains to study the binding activity of external agents such as enzymes with DNA. Some common techniques are: optical and magnetic tweezers, and atomic force microscopy [1]; fluid flow [2], and electrophoretic forces [3]. All these techniques require the binding of one or both ends of the polymers to specific sites or colloids, which is not always convenient. Confinement of biopolymers such as DNA to nano-channels can also result in uniaxial extension and has many advantages as reported in [4], none the least being able to forgo the binding procedure. However, polymer insertion becomes one of the main challenges which Thamdrup *et al.* [5] recently overcame by thermophoretic manipulation of single DNA molecules in both micro- and nano-channels. They successfully inserted double-stranded DNA (dsDNA) in nano-channels using thermophoretic forces originating from highly localized thermal gradients and also showed that, once in, DNA can be symmetrically stretched under thermophoresis (see Fig. 1). Although it is not the first time thermophoretic forces have been used to stretch DNA [6, 7], the particular way they do it in [5] facilitates the study of thermophoresis.

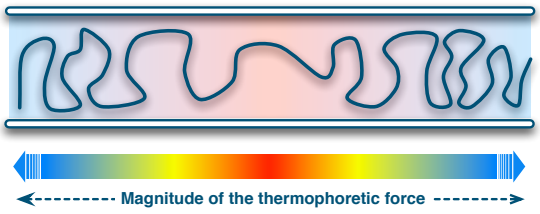

FIG. 1. A representation of the symmetric thermophoretic stretch of a polymer under a thermal gradient and confined to a nano-channel. The monomer concentration is lower in the central region and increases toward the ends.

The Soret coefficient $S_T = -1/c(\mathrm{d}c/\mathrm{d}T)$, where c is the particle concentration and T, the temperature, characterizes the strength of thermophoresis [8]. For particles suspended in gases in the quasi-hydrodynamic regime and under a thermal gradient, the general form of S_T has been analytically derived [9]. However, for colloids in solution, the picture is incomplete [8]. For instance, although an effective thermophoretic force proportional to the temperature gradient and acting on all suspended particles in a given solution can often be measured, its strength has been shown to be highly sensitive to molecular interactions whether they be particle-solvent or particle-particle [10–12]. In fact Duhr and Braun recently found evidences that support a theory of thermophoresis based on solvation entropy [13]. This leads to thermal diffusion from hot to cold (thermophobic behaviour), as expected, but also from cold to hot (thermophilic behaviour), which defies our naive intuition of the phenomenon.

We present a novel approach to describe nano-confined polymers symmetrically stretched by the action of a non-uniform force field originating in our case from thermophoretic forces as in Fig. 1. We construct a simple model that incorporates thermophoresis in a theory of blobs and Flory free-energy which accurately reproduces the observed monomer concentration profile. Temperature dependent excluded volume interactions (EVI) can also be included. We show that the particular shape of the monomer concentration profile such as the one reported in [5] can be obtained without the intervention of strong thermophoretic forces. To demonstrate this and give strength to our model, we fit the latter to data from molecular dynamics (MD) simulations in which we use a temperature profile similar to the one measured in [5] and an explicit thermophoretic force that we can tune. From a theoretical standpoint, we think the study of thermophoretic effects on nano-confined polymers, that is collections of linked monomers, can help shed light on the true nature of thermophoresis in viscous media. Indeed, the metastable state of equilibrium reached by the single polymer system studied here gives us a unique op-

portunity to look at collective effects in thermophoresis. From a practical standpoint, a better understanding of thermophoresis and temperature dependent EVI in the context of nano-confined biopolymers such as DNA or even proteins could potentially lead to interesting ways to gain better access to their mid part and its properties.

We consider a polymer of N segments (or monomers) of Kuhn length twice the persistence length $b = 2l_p$ and width d confined to a channel of diameter D_c with x being the coordinate along the channel's axis. We work within the hypothesis that $b < D_c < R_g$, a level of confinement that puts our polymer in either the *de Gennes* (dG) regime, with $b < D_c < b^2d/4$, or the *Extended de Gennes* (EdG) regime, with $b^2d/4 < D_c < R_g$ [14, 15]. We do not discuss the *Odjik* regime for $D_c < b$ [16].

Let us then imagine the polymer is composed of a series of N/g blobs of size $D \sim D_c$ containing g segments each. In each blob, the chain size follows the usual bulk statistics. We recall the well known Flory free-energy [17] that we write for a blob here:

$$\beta A_{\text{blob}} \cong \frac{D^2}{gb^2} + \frac{gb^2}{D^2} + v\frac{g^2}{D^3} + w\frac{g^3}{D^6}, \qquad (1)$$

where $\beta = 1/k_BT$. The four terms in Eq. 1 are, in order of appearance: the entropic cost of stretching (1) and compression (2), the two particles (3) and three particles (4) EVI terms where $v \approx \frac{T-\theta}{T}b^2d$ and $w \cong (bd)^3$ essentially give their respective strengths. The excluded volume v characterizes the solvent quality, that is the relative strength of the monomer-solvent, monomer-monomer, and solvent-solvent interaction energies [17]. As one raises the temperature across the θ value, solvent-monomer interactions come to dominate, we go from a poor solvent to a good solvent, and the whole polymer experiences a globule to coil transition or in other terms, it swells. When $T \gg \theta$, the chain is in an athermal solvent and $v \cong b^2d$. When $T \ll \theta$ we are dealing with a non-solvent and $v \cong -b^2d$. The local free-energy of the chain that we present in Eq. 1 corresponds to the dG regime of confinement. We know that the spatial density of monomers is roughly equal in both the dG and EdG regimes at $\rho \sim b^{-4/3}d^{-1/3}D^{-4/3}$ for a polymer in an athermal solvent [15], which means the evaluation of EVI should roughly be the same. Hence, even if blobs are assumed to take an anisotropic shape of length H and width D as in the EdG regime [15], the local free-energy should be correctly approximated by Eq. 1. In fact, it was shown in previous studies [15, 16] that for calculating static properties of confined polymers such as the extension, the dG and EdG regimes lead to equal results.

Let us establish a stable symmetric temperature gradient $T(x)$ in the system from the middle of the polymer as reported in [5] (if $x = 0$ is the midpoint of the chain, $T(x) = T(-x)$). We choose it to be of the following functional form that fits the true experimental profile:

$$T(x) = T_{\text{room}} + T_0 \exp\left[-\left(1 + \frac{c}{2}(x - x_0)^2\right)^{\alpha}\right], \qquad (2)$$

where x_0 is the midpoint, T_{room}, the room or reference temperature, and T_0, c, α are tunable parameters. In the experiment that lead to the observed monomer concentration profile of Fig. 7c in [5], the parameters that fit the thermal profile used are: $x_0 = 55.86\mu$m, $T_0 = 37.44$K, $c = 0.987\text{m}^{-2}$, and $\alpha = 0.175$. The chain is then stretched symmetrically and non-uniformly along x by local thermophoretic forces proportional to the temperature gradient $f_T(x) \propto -\nabla T(x)$ acting on all segments. The proportionality constant is equal to $S_T(T)/\beta$ where $S_T(T)$ is the temperature dependent Soret coefficient [8]. Indeed, thermophoresis experiments conducted on colloids show that S_T grows with temperature to an asymptotic limit of S_T^∞ [12]. For many colloids, S_T^∞ is reached close to room or physiological temperatures. Unfortunately, for segments of DNA we do not know if this is the case, but since experiments in [5] were conducted between 300K and 320K, we will assume $S_T \approx S_T^\infty$ such that:

$$f_T(x) \approx -S_T^\infty \frac{\nabla T(x)}{\beta(x)}. \qquad (3)$$

Thermophoretic forces push segments away from the polymer's center where forces are the strongest. One should thus expect the segment density to go up as we go from the middle of the chain to its ends. The experimental monomer concentration profile in Fig. 2 shows exactly this. Let us include thermophoretic forces in Eq. 1 and calculate this profile. It was shown that the action of external forces reduces the size of Pincus blobs [17, 18]. Here we assume that all blobs are of mean size $D \sim D_c$ and that it's the number of segments g per blob that varies. We then assume, by a mean-field type approach, that all g_i segments in the i-th blob whose center is positioned at x_i feel a temperature $T(x_i)$ and are subject to a thermophoretic force $f_T(x_i)$. Each blob is considered to be an entropic spring and the work done by thermophoretic forces on blob i is given by the sum of all f_Ts acting on all segments in the blobs from x_{i+1} to the nearest end of the polymer which is approximately:

$$W_{T,i} \sim DF_{T,i} = -DS_T^\infty \sum_{j=i+1}^{n_b/2} g_j \frac{\nabla T(x_j)}{\beta(x_j)}, \qquad (4)$$

where n_b is the number of blobs in the chain. We can then rewrite the free-energy of a blob now including the thermophoretic work:

$$\beta_i A_i \cong \frac{D^2}{g_i b^2} + \frac{g_i b^2}{D^2} + v\frac{g_i^2}{D^3} + w\frac{g_i^3}{D^6} - \beta_i W_{T,i}. \qquad (5)$$

In the center of the chain, where few monomers are found, the contribution of EVI to the free-energy of a

blob is overestimated in the above. However, as long as $|v| \ll D^3$, the error introduced should be negligible since the entropic term will come to dominate. Again we can minimize the free-energy with respect to D to find the equilibrium configuration which leads to the following polynomial:

$$c_0 g_i^4 + c_1 g_i^3 + c_2 g_i^2 + c_3 g_i + c_4 = 0, \qquad (6)$$

where $c_0 = 6w/D^7$, $c_1 = 3|v|/D^4$, $c_2 = 2b^2/D^3$, $c_3 = -\beta_i S_T^\infty \sum_j g_j \nabla T(x_j)/\beta(x_j)$, and $c_4 = -2D/b^2$. This polynomial can be solved numerically and recursively starting from the ends of the polymer where $g = 0$ and iterating over the blobs until the center of the chain is reached. Thermophoretic forces contribute to blob segregation. Therefore our model should be able to predict the segment concentration profile close to the middle part of the chain even in conditions where blob overlap is expected near the ends, as in the case of an ideal chain. In fact, as long as the thermophoretic work done on a particular blob is more important than thermal agitation around that position ($W_{T,i} > k_B T(x_i)$), the number of segments in that blob should be correctly estimated. If the chain is in an athermal solvent, strong EVI naturally segregate blobs and the model is expected to correctly predict the full extent of the segment concentration profile in quality if not in quantity.

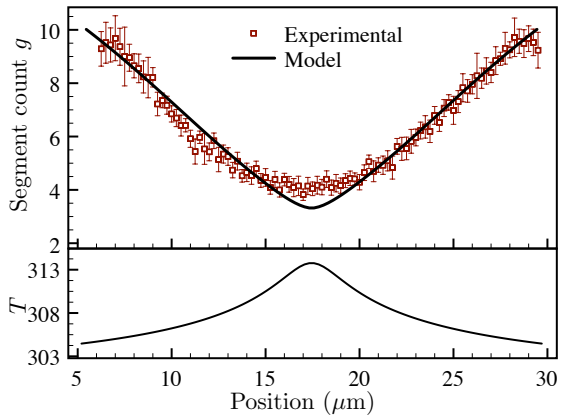

FIG. 2. Top panel: fit of our model of thermophoretic stretch to data of experiments on DNA taken from Fig. 7c in the paper by Thamdrup *et al.* [5]. Bottom panel: the temperature profile used. All parameters are specified in the text.

In Thamdrup *et al.* paper [5], they inserted and then thermophoretically stretched YOYO dyed T4 dsDNA strands of 166 kbp (contour length $L_c \approx 72\mu$m, Kuhn length $b \approx 120$nm, number of Kuhn segments $N_K \approx 600$, and width $d \approx 2$nm [19]) confined to a square nanochannel of side $D_c = 250$nm and under the thermal gradient defined previously. Fig. 7c in the paper shows a fluorescence intensity time trace of the experiment. We processed the image and extracted the segment concentration profile plotted in Fig. 2 where it has been renormalized using the known total number of Kuhn segments and assuming the blobs are the size of the channel's side of length D. We then fitted our model considering an athermal solvent with S_T^∞, n_b, and d as free parameters: the Soret coefficient is unknown while the number of blobs and the width of the DNA filament can at best be estimated. Clearly, we can reproduce the shape of the profile well. However, divergences are present which can be attributed to two main factors: first, the data from [5] used was preliminary, and data with better statistics could be expected in the future; second, the blobs contain very few monomers, especially those in the central region, where the limits of our Flory free-energy based model might be stretched. As a result of fitting the data, we found $n_b \cong 100$, a DNA width $d = 3.1 \pm 0.1$nm close to the estimated value in [19], and a Soret coefficient for a DNA Kuhn segment $S_T^\infty = 0.051 \pm 0.001\text{K}^{-1}$ which is only half of $\sim 0.1\text{K}^{-1}$ found for DNA filaments of length $L_c \sim b$ in Fig. 4c of [13]. Other factors which might influence the Soret coefficient here are the collective effects, that is the segments of DNA are connected to each other, and the strong confinement the DNA chain is under. Thamdrup *et al.* report a value of 50fN for the entropic recoil force of the T4 DNA fragments [5]. A thermophoretic force of comparable strength is needed to strongly stretch the central part as is the case here. We found $F_{T,0} \approx 44$fN as required.

We also fitted our model to the results of MD simulations. This was done in part to better evaluate its accuracy and in part to explore the effects of temperature dependent EVI. A bead-spring chain of N beads was placed in a cylindrical channel of radius R_c. Interactions in the system are those found in [20]: beads can interact through a Lennard-Jones (LJ) inspired potential $U_{\text{LJ}}(r) = \epsilon\left[(\sigma/r)^{12} - 2(\sigma/r)^6\right]$ and springs are modelled with harmonic potentials of the form $U_{\text{H}}(r) = k_s(r-\sigma)^2$ where $k_s = 16.67\epsilon/\sigma^2$. Thus, the MD chain is akin to single-stranded DNA (ssDNA) and not dsDNA. We set the unit of energy $\epsilon = 1$ ($k_B = 1$), the unit of length $\sigma = 1$, the unit of mass $m = 1$, and the unit of time $\tau = 1$. All observables from this point on are considered to be in the appropriate MD units. If the LJ potential is truncated at $r_{\text{cut}} = 2.5$, the chain thus simulated exhibits a globule-coil transition around $\theta = 2.18$ which allows the study of solvent quality effects. One can also truncate at $r_{\text{cut}} = 1$ to recuperate the behavior of a chain in an athermal solvent using purely repulsive interactions or avoid using the LJ potential altogether to simulate an ideal chain. Each segment of the chain has a length equal to its width $b = d = 1$ such that the volume is $b^3 = 1$. We modified the Langevin thermostat in the ESPREsSo package [21] to accommodate for a temperature profile as given by Eq. 2 and an explicit thermophoretic force of magnitude $-Ck_BT\nabla T$ acting on all particles in the sys-

tem where C is a tunable constant in units of k_B/ϵ. The middle bead was anchored with a soft harmonic spring in the middle of the channel where the temperature is set to be the highest to prevent longitudinal diffusion. The confinement parameter $D = 2(R_c - \sigma)$, as the monomers always interact with the channel wall via the repulsive part of the LJ potential.

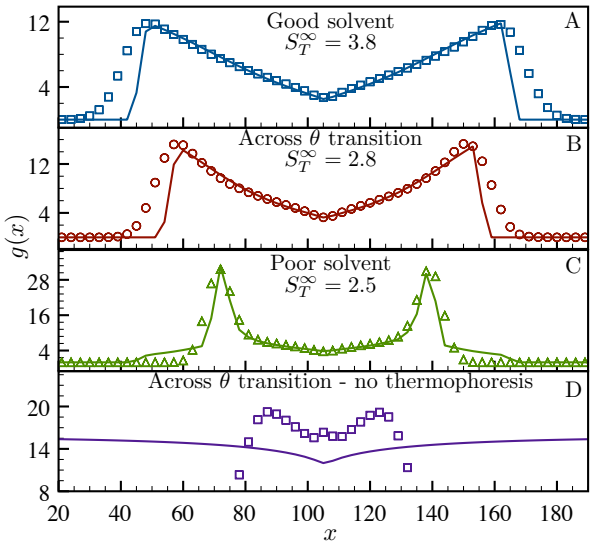

FIG. 3. Monomer concentration profiles for a MD simulation of nano-confined polymer in a symmetric temperature gradient in various solvent conditions: A) good solvent, $T_{\rm room} = 4.0$; B) across the θ-transition, $T_{\rm room} = 2.0$; C) poor to θ solvent, $T_{\rm room} = 1.0$; D) across the θ-transition, no explicit thermophoretic force. The symbols represent the data from simulations and the solid lines, the best fits. The confinement $D = 4.75$ and $C = 2.5$, while $N = 201$ and $b = 1$.

Fig. 3 shows the data from MD simulations in various solvent conditions (variable $T_{\rm room}$) and the corresponding best fits of our model. The values for the thermal profile were: $T_0 = 5.5$, $c = 0.987$, and $\alpha = 0.175$. The chains considered here are long compared to the width of the thermal profile ($L_c = 201$ vs $2\Delta_{T_{\rm max}/2} = 12.8$). The strength of thermophoretic forces was set to $C = 2.5$. The agreement between our simple model and simulation data is impressive. The Soret coefficients S_T^∞ obtained from fitting our semi-quantitative model to the simulation data are close to the chosen strength C as expected. In fact, S_T^∞ essentially scales the curve up and down but does not affect the shape much. The chains are quite extended in their mid part for strong enough thermophoretic forces and thus the effects of EVI should be negligible which means all densities should coincide. Although we do not explicitly show this in Fig. 3, both the data and our model adhere to this conclusion. Therefore, for experiments conducted with polymers that have contour lengths close to the width of this central region corresponding to a faster changing temperature gradient, EVI could potentially be neglected.

Comparing the ends of profiles A and C in Fig 3, we can clearly see collective effects: in a good solvent (A), end monomers appear thermophobic, the chain stretches, whereas in a poor solvent (C), they appear thermophilic as monomer clumping is observed due to the dominating monomer-monomer attractive interactions. The number of monomers per blob in good solvent conditions without any thermal gradient ($T(x) = 4.0$) is $g \approx 12$ and the full extent of the confined chain is $R_\parallel \approx 71$. In the cases studied here, no matter the solvent quality, the extension of the chain is always enhanced by thermophoresis and more importantly, the backbone is better exposed in the central region.

Fig. 3D shows that variable EVI alone do produce the characteristic shape of the concentration profile although they do not enhance stretch as much as with additional thermophoresis (see Fig. 3B). If our prediction falls short of the MD results quantitatively, it is because blobs are not clearly segregated close to the θ transition.

We have demonstrated that a simple model based on blobs and the Flory free-energy can reproduce the monomer concentration profile observed in both experiments and simulations of the thermophoretic stretch of nano-confined polymers such as DNA. The approach we have taken could be applied to other problems where a non-uniform field acts on a confined polymer. Moreover, we have shown that EVI can be decoupled from other contributions to thermophoresis in the specific system studied here, which allowed us to expose collective effects. Temperature dependent EVI alone could partly explain the concentration profiles. The effects of variable EVI should definitely be further explored in the future. We would like to extend this study by simulating semi-flexible polyelectrolyte chains since this could prove useful to improve our prediction of the shape of confined DNA under thermophoresis as presented in [5].

We acknowledge financial support from NSERC and Jonas N. Pedersen for useful discussions.

* bjoos@uottawa.ca

[1] K. Neuman and A. Nagy, Nat. Methods, **5**, 491 (2008).
[2] R. Larson, T. Perkins, D. Smith, and S. Chu, Phys. Rev. E, **55**, 1794 (1997).
[3] S. Smith and A. Bendich, Biopolymers, **29**, 1167 (1990).
[4] J. Tegenfeldt, C. Prinz, H. Cao, S. Chou, W. Reisner, R. Riehn, Y. Wang, E. Cox, J. Sturm, P. Silberzan, *et al.*, Proc. Natl. Acad. Sci. U.S.A., **101**, 10979 (2004).
[5] L. Thamdrup, N. Larsen, and A. Kristensen, Nano Lett., **10**, 826 (2010).
[6] M. Ichikawa, H. Ichikawa, K. Yoshikawa, and Y. Kimura, Phys. Rev. Lett., **99**, 148104 (2007).
[7] H. Jiang and M. Sano, Appl. Phys. Lett., **91**, 154104 (2007).

[8] R. Piazza and A. Parola, J. Phys. Condens. Matter, **20**, 153102 (2008).
[9] P. Epstein, Z. Physik, **54**, 537 (1929).
[10] R. Piazza and A. Guarino, Phys. Rev. Lett., **88**, 208302 (2002).
[11] S. Putnam and D. Cahill, Langmuir, **21**, 5317 (2005).
[12] S. Iacopini, R. Rusconi, and R. Piazza, Eur. Phys. J. E, **19**, 59 (2006).
[13] S. Duhr and D. Braun, Proc. Natl. Acad. Sci. U.S.A., **103**, 19678 (2006).
[14] W. Reisner, K. Morton, R. Riehn, Y. Wang, Z. Yu, M. Rosen, J. Sturm, S. Chou, E. Frey, and R. Austin, Phys. Rev. Lett., **94**, 196101 (2005).
[15] Y. Wang, D. Tree, and K. Dorfman, Macromolecules (2011).
[16] T. Odijk, Phys. Rev. E, **77**, 060901 (2008).
[17] M. Rubinstein and R. Colby, *Polymer physics* (Oxford University Press, USA, 2003).
[18] S. Jun, D. Thirumalai, and B. Ha, Phys. Rev. Lett., **101**, 138101 (2008).
[19] L. Thamdrup, A. Klukowska, and A. Kristensen, Nanotechnology, **19**, 125301 (2008).
[20] M. Ciesla, J. Pawlowicz, and L. Longa, Acta Phys. Pol. B, **38**, 1727 (2007).
[21] H.-J. Limbach, A. Arnold, B. A. Mann, and C. Holm, Comput. Phys. Commun., **174**, 704 (2006).

5

Predicting the final size of small vesicles produced by pressure extrusion through nano-channels

M Bertrand, B Joós. Submitted for publication.

Predicting the final size of small vesicles produced by pressure extrusion through nano-channels

Martin Bertrand and Béla Joós*
Département de Physique
Université d'Ottawa
Ottawa, Ontario, Canada, K1N 6N5
(Dated: December 12, 2011)

We propose a model that predicts the final sizes of lipid bilayer vesicles produced by pressure extrusion through nano-channels and we conduct large scale coarse-grained molecular dynamics simulations of the phenomenon. We show that, to a first approximation independent of pressure, vesicle size can be predicted by a simple geometrical argument that considers an invariable inner vesicle volume enclosed by a finitely extensible lipid bilayer. The pressure dependence is then incorporated in our model by arguing that the effective channel radius decreases with increasing pressure due to a thickening of the lubrication layer between the vesicles and the channel wall. We fit our model to the experimental data of Patty and Frisken [Biophys. J., **85**, 2003]. We predict that at high pressure, vesicle size significantly depends on channel length and therefore flow rate. The latter also explains why slightly larger vesicles are produced when the vesicle density in suspension is increased.

I. INTRODUCTION

Small lipid bilayer vesicles, or liposomes, are often synthesized for research and pharmacological applications [1–3]. One of the most popular techniques to produce such soft objects is the pressure extrusion of a vesicle suspension through an array of nano-channels [2, 4–7]. Related to this procedure, a long standing goal has been to be able to predict the average final size of the extruded liposomes given the parameters of the system which are: lipid nature, concentration of lipids in suspension, temperature, applied pressure, and radius of the nano-channels. Two models have been proposed: the first by Clerc and Thompson [8] refers to the Rayleigh instability [9] and predicts a final vesicle size larger than observed [5–7] and mostly independent of pressure; the second by Patty and Frisken[7] uses the analogy of blowing a bubble through a hole to describe the initial entry of large vesicles in the smaller nano-channels and derives a prediction from an analysis of the system in static equilibrium. Although this second model successfully fits their data, it requires two free parameters that are not clearly linked to the physics of vesicle pressure extrusion and looks at the problem from a static viewpoint. In contrast to this static description our model includes a dynamic (i.e. rheological) description of the extrusion.

Pressure extrusion involves multiple passages through nano-channels, and we can assume that in the final passages, vesicles flow in and out without breaking and their shape goes back and forth between a spheroid outside of the channels and a sphero-cylinder inside. The sphero-cylinder has a greater area than the sphere of equal volume. The final vesicles are of a size such that the lipid bilayer can tolerate this area difference. We show that to a first approximation, this prediction is valid. We then incorporate the effects of pressure in our simple geometrical argument using elements of a model of sphero-cylindrical vesicles flowing in narrow channels developed by Bruinsma [10] to predict the final sizes of extruded vesicles as pressure is increased. This idea was mentioned by Hunter and Frisken [5] but not exploited. Flow being involved here, it is expected that the length of the channels would be an important parameter in the process. Frisken *et al.* [6] find that at low pressure, doubling the length of the channels does not significantly influence the final sizes of the produced vesicles. Our model corroborates experimental evidence at lower pressures, but predicts that there is a length dependence at high pressure, which suggests further experimental investigation. Our model can also explain the small dependence in lipid concentration observed [6].

In addition to the rheological model, we performed out of equilibrium coarse-grained molecular dynamics simulations of vesicle extrusion to confirm our geometrical argument, to corroborate some main elements of Bruinsma's theory [10], and to describe the initial entry of a large vesicle in a nano-channel and its subsequent rupture. Although the extrusion of vesicles [11] and erythrocytes [12] has been simulated in the past, to the best of our knowledge no true bilayer vesicle in an explicit solvent has ever been simulated in such a context. We leverage the computing power of Graphical Processing Units (GPUs) to make this feasible in a relatively short time frame.

Our model and study should be useful to experimentalists considering pressure extrusion as a means to produce liposomes, but also to the large community studying the flow of diverse cells in and out of narrow channels such as

*bjoos@uottawa.ca

red blood and plasma cells flowing in narrow capillaries.

II. EXTRUSION MODEL

The production of liposomes through pressure extrusion consists in starting with a suspension of large and possibly multilamellar vesicles (MLVs) that is pushed by a pressure drop ΔP multiple times through an array of nano-channels of average radius R_p and length L_p as seen in Fig. 1 (typically 10-15 times [5–7]). For every passage through the extruder there is an ever diminishing drop in the average vesicle size (see Fig. 1 in the article by Frisken *et al.* [6]). Thus, towards the end of the entire extrusion procedure, most vesicles in suspension flow in and out of the nano-channels without rupturing. To a first approximation, we assume that in these last passages they transition from a relatively spherical shape outside the nano-channels to a sphero-cylindrical shape inside and back again while conserving volume as depicted in Fig. 1. Let us develop this argument.

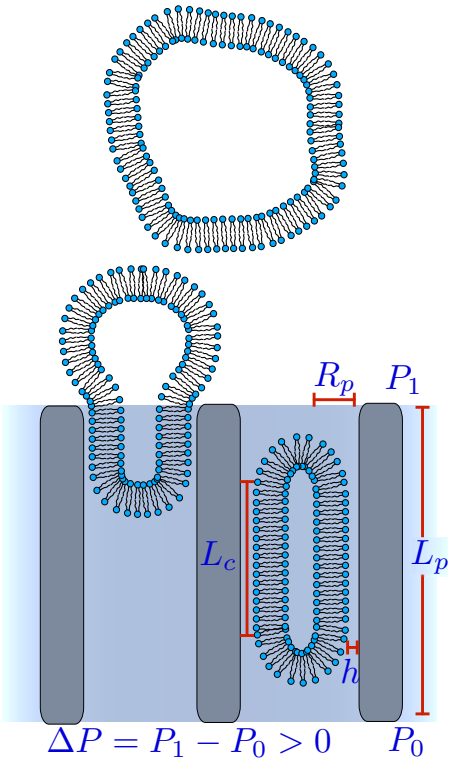

FIG. 1. In the final passages, vesicles flow through the extruder back and forth going from a roughly spherical shape outside to a sphero-cylindrical shape inside. Some key variables are highlighted.

A. Surface and volume conservation

We start with a vesicle of apparent initial spherical area $A_0 = 4\pi R_0^2$ enclosing a volume $V_0 = 4\pi R_0^3/3$. The membrane tension γ is related to its fractional surface expansion $\alpha = \Delta A/A_0$ by:

$$\alpha = \frac{k_b T}{8\pi k_c} \ln\left(1 + c\frac{\gamma A}{k_c}\right) + \frac{\gamma}{K_A}, \tag{1}$$

where K_A is the area compressibility, k_c, the bending rigidity, and $c \simeq 0.1$ is a constant related to surface undulations [13]. For high enough tension, $\gamma \cong K_A\alpha$. Let us assume that in the extrusion process the vesicle volume stays constant while its area expands. Then there exists a critical value α_c where the vesicle ruptures. This critical surface expansion α_c can have two contributions: 1) α_A related to the flattening of the excess area in the membrane; 2) α_γ related to the lysis tension in the bilayer which depends on the nature of the lipids (see Eq. 1). Thus $\alpha_c = \alpha_A + \alpha_\gamma$.

If the vesicle is pushed almost quasistatically in a nano-channel of radius R_p, it will do so without breaking as long as the surface expansion remains below a threshold characterized by α_c. Assuming the steady-state shape in the channel to be that of a sphero-cylinder of side length L_c and radius R_p (see Fig. 1 with $h = 0$) we can find the critical vesicle to channel radius ratio $R = R_0/R_p$ for which the vesicle barely remains intact by solving the following derived polynomial:

$$V_0 = \frac{4\pi R_0^3}{3} = \pi L_c R_p^2 + \frac{4\pi R_p^3}{3} = V_f, \tag{2}$$

$$(1+\alpha_c)A_0 = (1+\alpha_c)4\pi R_0^2 = 2\pi L_c R_p + 4\pi R_p^2 = A_f, \tag{3}$$

$$2R^3 - 3(1+\alpha_c)R^2 + 1 = 0. \tag{4}$$

Eq. 2 accounts for volume conservation and Eq. 3, for surface expansion, here assumed equal over the entire deformed vesicle. It will be shown in Sect. III that Eq. 4 alone gives a rough approximation of the final size vesicles obtained by pressure extrusion. The next subsection extends our model to account for the pressure dependence.

B. Pressure dependence

Between the surface of a sphero-cylindrical vesicle and the surface of the channel it is flowing through, there is a relatively thin lubrication layer of thickness h (see Fig. 1 and inset of Fig. 4 for a close-up in simulations) that grows with increasing vesicle velocity U. The vesicle essentially travels in a channel of effective radius $R_{\text{eff}} = R_p - h$ that decreases with U and solving Eq. 4 in this case gives the ratio $R' = R_0/R_{\text{eff}}$. Thus if we wish to get the corrected ratio $R = R_0/R_p$ for a given applied pressure ΔP we first need to calculate h. Bruinsma has

given an expression for h as a function of U[10]:

$$h \cong 2.05 R_p \left(\frac{\eta U}{\gamma_f}\right)^{2/3}, \tag{5}$$

where η is the solvent's viscosity and γ_f is the frontal membrane tension of the vesicle. The membrane tension γ is predicted to be linearly decreasing along the cylindrical part of the travelling sphero-cylindrical vesicle going from γ_f at the front cap ($z = 0$) to γ_r at the rear cap ($z = L_c$) such that:

$$\gamma(z) = \gamma_f - \frac{\eta U}{h(U)} z. \tag{6}$$

However, we will assume a uniform mean tension $\bar{\gamma}$ along the length of vesicle to simplify our calculations such that $\gamma_f \cong \bar{\gamma}$ in Eq. 5. Bruinsma also developed a Darcy type law to describe the flow of sphero-cylindrical vesicles in narrow channels. First, he assumed that each of the N vesicles in a channel of length L_p at a given time diminishes the pressure drop ΔP across the whole channel by an amount $\Delta P^*(U)$ such that Poiseuille's law becomes:

$$\eta U = \frac{R^2}{8}\left(\frac{\Delta P}{L_p} - n\Delta P^*(U)\right), \tag{7}$$

where $n = N/L_p$ is the linear density of vesicles in the channel. He then equated the energy dissipated in the lubrication layer to the work done by the pressure differential to drive the system and obtained a Darcy-like equation with a possible dependency upon velocity in the channel permeability K':

$$\eta U = K' \frac{\Delta P}{L_p} = \frac{R_p^2/8}{1 + nR_pL_c/4h(U)} \frac{\Delta P}{L_p}. \tag{8}$$

Ultimately, with the proper substitutions, one recuperates an expression in the form of Darcy's law, assuming the length L_c of the travelling sphero-cylindrical vesicles remains mostly unchanged with the thickening of the lubrication layer:

$$\eta U = K' \frac{\Delta P}{L_p} = \frac{R_p^2}{8 + 0.223 n L_c^3/R_p^2} \frac{\Delta P}{L_p}. \tag{9}$$

Since the mean flow velocity inside a channel is roughly equal to U, the above can be converted to a flow rate Q:

$$Q \cong \frac{\pi R_p^2 K'}{\eta} \frac{\Delta P}{L_p}. \tag{10}$$

Supposing the vesicles flowing back and forth in the extruder can only barely support it without rupturing, we can make $\bar{\gamma} = \gamma_l$, the lysis tension, and calculate the ratio $R = R_0/R_p$ at a given pressure ΔP iteratively until the solution converges using Eq. 9 for the velocity U (we get the same answers with Eq. 8):

$R(R_p, \Delta P, \alpha_c) = \{$

1. Calculate R' by solving Eq. 4 for a given α_c
2. Estimate L_c using Eq. 2
3. Estimate h using Eqs. 5 and 9
4. Calculate $R_{\text{eff}} = R_p - h$
5. Improve L_c using $R_p = R_{\text{eff}}$ with R' in Eq. 3
6. Improve h using the new value of L_c
7. Repeat steps 3 to 5 until h and L_c converge
8. Get R from h and R' $\}$

(11)

This is our complete model to predict the final size of extruded vesicles. Let us now discuss its agreement with experimental results.

III. MODEL AGREEMENT WITH EXPERIMENT

Let us consider vesicles made of POPC lipids such as in Patty and Frisken's study [7] with $K_A \cong 234$mN/m, $k_c \cong 1.43 \times 10^{-19}$J, $\gamma_l \cong 7.4$mN/m, $R_p = [25, 50]$nm, and $L_p = 6\mu$m. Using Eq. 1 we find $\alpha_\gamma \cong 0.04$. Solving Eq. 4 with this value for α_c gives $R = 1.23$ regardless of channel radius or applied pressure. In Fig. 2 we reproduced data that originate from pressure extrusion experiments performed by Patty and Frisken on POPC lipid vesicles [7]. Our value of R predicts the smallest vesicle sizes obtained by extrusion under strong pressure gradients whereas we would have expected a better prediction for the final sizes under the weakest pressures. With $\alpha_c \cong 0.10$ we achieve this. Consequently, the final vesicles must be deflated with an excess area accounting for roughly 6% of the observed expansion ($\alpha_A \simeq 0.06$) which is confirmed by the swelling they undergo at the end of the extrusion runs [14]. Although quite simplistic, we are convinced that our geometrical argument shows that to predict the final sizes of extruded vesicles one needs to describe how these objects flow through nano-channels.

Let us now include the pressure dependence. We fitted Eq. 11 to data from Patty and Frisken's paper [7]. We let α_c be a free parameter and used all other parameters therein except n that we fix to a value of $1/L_p \cong 1.67 \times 10^{-7}\text{m}^{-1}$, a single vesicle per channel which would correspond to a low lipid concentration. Fig. 2 shows the best fits and Table I gives the values for α_c as a function of the channel radius. The fits are in good agreement with the data. All expansion coefficients compare favourably with one another and are close to the upper limit $\alpha_c = 0.10$ considered in the geometrical argument for vesicles slightly deflated with some excess area. Our model seems to fail properly predicting the ratio R for the very lowest pressures especially

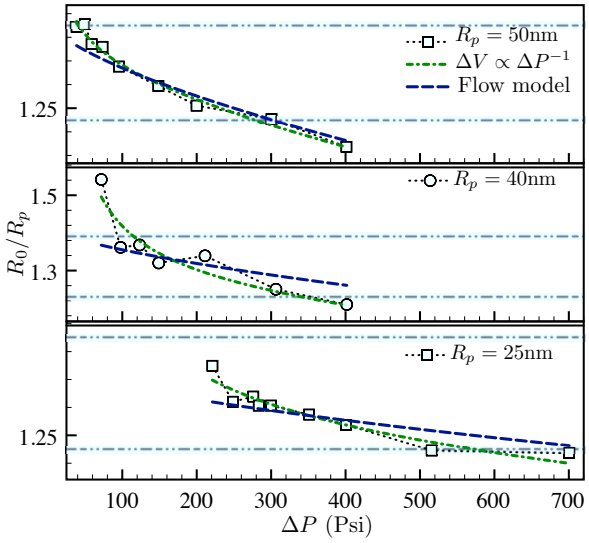

FIG. 2. Experimental data of final vesicle sizes expressed in terms of the ratio $R = R_0/R_p$ as a function of the pressure drop ΔP for three different channel sizes are reproduced from Patty and Frisken's paper [7]. The horizontal grey dot-dashed lines are those for $\alpha_c = 0.04$ at $R = 1.23$ and $\alpha_c = 0.10$ at $R = 1.39$. The blue dashed lines represent the fits of our flow model, while the green dot-dashed lines are those with the volume relaxation argument included.

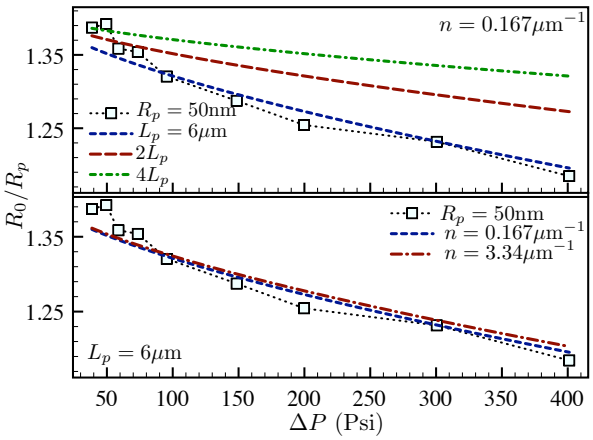

FIG. 3. Top plot: while doubling or even quadrupling the channel length does not change much the final vesicle sizes at lower pressures which corroborates previous findings [6], the difference is much more important at higher pressures. Bottom plot: Increasing the initial lipid concentration inevitably increases the number of vesicles in a given channel and reduces the flow rate which results in slightly bigger final vesicles as previously observed [6].

for $R_p = 40$nm. We think this is where one needs to pay careful attention to the first few passages in the extruder. It is quite possible that at lower pressures, the probability of forming large deflated vesicles with much excess area and reduced volume is greater. To account for this in our model we can potentially relax the volume by introducing a $\Delta V \propto \Delta P^{-1}$ which allows to better fit the data, but by doing so we need to introduce a free parameter hard to relate to the actual physics in the system. We show the resulting fits on Fig. 2 for the sake of completeness although we will not further use this volume relaxation argument in the following discussion.

TABLE I. The mean critical surface expansion α_c obtained while fitting data from Patty and Frisken's paper[7] is roughly 0.10.

Channel radius R_p (nm)	Critical surface expansion α_c
25	0.083 ± 0.002
40	0.111 ± 0.005
50	0.105 ± 0.003

We took our flow model with the values of α_c we obtained and doubled the channel length L_p as in the paper by Frisken *et al.* [6] where they report no significant change in the final vesicle sizes at low pressure. Given the apparent experimental uncertainties, we show in Fig. 3 (top plot) that our model recovers that result since all curves seem to converge at low pressure. Indeed, in this limit where the flow rate is weakest, vesicle size is mostly defined by the geometrical constraints. However, we predict that at higher pressures the final mean vesicle size strongly depends on channel length or flow rate if one prefers as they are related. In fact, if the reduced vesicle size R is plotted as a function of the flow rate Q proportional to the pressure gradient $\Delta P/(\text{Channel length})$, the theoretical predictions in Fig. 3 collapse unto a single curve (not shown). We therefore suggest to revisit the channel length doubling experiment at a higher pressure to test the validity of our prediction.

Interestingly, the flow rate dependence can also explain a result reported in the same paper [6], that is vesicle size weakly increases with lipid concentration. A higher lipid concentration results in an increase in n, the vesicle density in the channel, thus decreasing the flow rate Q as given by Eq. 10. By increasing n twenty fold, roughly the limit density of vesicles in a channel before they start interacting, our model predicts a slight increase in the average vesicle size as observed experimentally (see Fig. 3, bottom plot).

IV. CGMD SIMULATIONS OF THE EXTRUSION PROCESS

Our flow model presented in Sect. II predicts the final sizes of extruded vesicles based on an analysis of the last few passages in a pressure extrusion run where size is expected to vary only marginally. It combines a geometrical argument (Sect. II A) to elements of Bruinsma's descrip-

tion of sphero-cylindrical vesicles flowing down narrow channels (Sect. II B). Using a Coarse-Grained CGMD model, we thus decided to simulate small inflated and spherical lipid bilayer vesicles being pressure extruded in channels of different sizes to corroborate qualitatively if not quantitatively the various components of our model (Sect. IV A). We also simulated larger vesicles extruded in the same narrow channels to give a qualitative description of the initial extrusion passages (Sect. IV B).

In our CGMD simulations of lipid bilayer systems, we modelled all interactions using Goetz and Lipowsky's set of potentials [15] where σ is the unit of length, ϵ, of energy, τ, of time, and m, of mass. We chose a thermal energy $k_BT = 1.0\epsilon$ for all our simulations. We used lipids with one bead for the hydrophilic head and two beads for the hydrophobic tail. The lipids are fully flexible with no bending potential along their length. The hydrophilic solvent is of the Lennard-Jones (LJ) type with a density of $0.8\sigma^{-3}$ and shear viscosity $\eta = 1.98 \pm 0.16\sigma^{-2}\sqrt{m\epsilon}$ as calculated using Green-Kubo's formulation [16], in agreement with [17]. We characterized flat bilayers made of these short lipids and immersed in such a solvent. From the calculation of the microscopic stress tensor [15], we found $a_0 \cong 1.9\sigma^2$, the area per lipid at which the stress is zero with a bilayer thickness $l_{\mathrm{BM}} \cong 4.8\sigma$, and an area compressibility $K_A = 8.84 \pm 0.76\epsilon/\sigma^2$. We then calculated the bending rigidity using its relation to the area compressibility [18] $k_c = K_A l_{\mathrm{BM}}^2/48 = 4.24 \pm 0.36\epsilon$. As expected, our membranes are softer than those studied by Goetz and Lipowsky made of lipids with longer tails in a solvent of lower density at a slightly higher temperature [15, 18].

For the simulations of lipid bilayer vesicle pressure extrusion we constructed a system made of two reservoirs linked by a channel of radius R_p and length L_p. The vesicle started in one of the reservoirs and a pressure drop was applied across the system such that it penetrated the channel, travelled along its length, and ended up in the second reservoir. The walls consisted in solvent beads laid out on an FCC lattice with density $1.0\sigma^{-3}$ and anchored in space with stiff harmonic springs [19]. We used the non-conservative part of Dissipative Particle Dynamics (DPD) interactions to thermostat the system to a thermal energy $k_BT = 1.0\epsilon$ as they allow for momentum propagation [20], an essential feature to study flows (out of equilibrium dynamics). The anchored particles making up the wall interact with the rest of the system through DPD interactions such that realistic friction is reproduced in their vicinity. Indeed, simulations of the LJ fluid alone flowing under a pressure gradients yields a Poiseuille flow inside the channel with a negligible slip length, the velocity being essentially zero at the wall (data not shown).

The simulations, which contained from a quarter to half a million particles in total, were initialized using the ESPResSo pacakage [21] and executed on Graphical Processing Units (GPUs) using a customized version of the very fast and optimized HOOMD-Blue package [22, 23]. Simulations ran on Sharcnet's Angel cluster which contains 44 NVIDIA Tesla 1070 GPUs. Of course, even with a decent amount of computation power it always remained beyond our ability to simulate a suspension of multiple vesicles pressure extruded multiple times. But we can learn much from the study of the extrusion of a single vesicle.

A. Final passages simulated

The extrusion in nano-channels of small vesicles made of $n_l = 3000$ lipids was simulated. Vesicles were all initially set up such that the bilayer was under no stress due to a pressure difference between the inside and the outside (Fig. 7A). The outer layer was made of $n_{out} = 1841$ lipids with a mean area per lipid head $a_{out} = 1.86\sigma^2$ which corresponds to a radius of $R_{0,out} = 16.5\sigma$ while the corresponding values of the inner layer $n_{in} = 1159$, $a_{in} = 1.68\sigma^2$, and $R_{0,in} = 11.5\sigma$. The inner layer thus started more compressed than the outer layer. This is a consequence of requiring the area per lipid to be constant as measured in the mid-section of the bilayer ($a_{mid} \approx 1.75\sigma^2$). Overall the area per lipid of our vesicles is smaller than $a_0 = 1.9\sigma^2$ found for flat bilayer membranes. This is mainly due to the difference in geometry in the finite size of our systems.

1. *Geometrical argument.*

We tracked multiple observables throughout our simulations one of the most important being the local area per lipid a which is directly related to the stress in the bilayer. It was calculated from the triangulation of both the outer and inner layers using the Crust surface reconstruction algorithm [24] while accounting for lipid flips from one layer to the other. Following a and its mean $\bar{a}$ permitted to determine both the time and the spatial coordinates of a rupture event. The observation of many such events (Fig. 7C) leads to values of the expansion coefficient for both layers very close to one another: $\alpha_{c,out} \cong \alpha_{c,in} \equiv \alpha_c \cong 0.21$. Feeding this α_c into Eq. 4 gives a ratio $R = R_0/R_p = 1.62$. Taking $R_0 = R_{0,in}$ we find $R_{p,\mathrm{crit}} = 10.2\sigma$, the smallest channel radius into which the vesicle can penetrate and travel without breaking. Now in our simulations, even at the lowest pressures, there is a lubrication layer between the vesicle and the channel wall of minimal thickness close to the size of a LJ bead $h_{\min} \cong 1.1\sigma$. We thus need to compare the predicted critical radius with the minimal effective radius $R_{\mathrm{eff}} = R_p - h_{\min}$. Because our walls were set up on a lattice to maximize impermeability, we could not fine tune the radius to a very specific value, but when $R_p = 12.0\sigma$, that is $R_{\mathrm{eff}} = 10.9\sigma$, we could barely push vesicles in without breaking them while for $R_p = 11.5\sigma$, $R_{\mathrm{eff}} = 10.4\sigma$, it appeared impossible on the time scale of our simulations. Thus the true size limit is most prob-

ably very close to the one predicted by the geometrical argument.

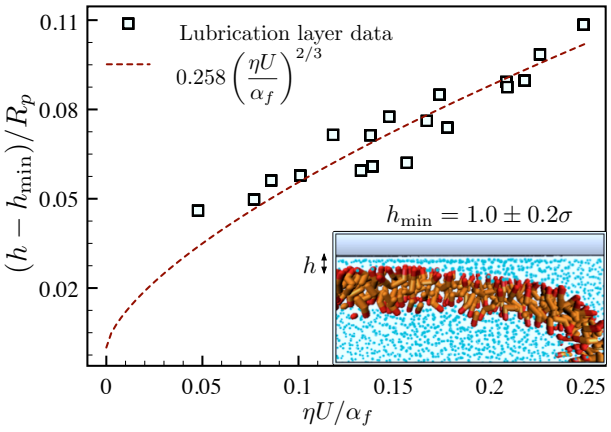

FIG. 4. The lubrication layer's thickness h grows with $\eta U/\gamma_f$ like predicted by Bruinsma [10]. Here we used α_f, the frontal area per lipid expansion of the outer layer of the membrane of our sphero-cylindrical vesicles travelling in channels that we assume goes like γ_f, the frontal tension in the membrane.

2. *The lubrication layer.*

We measured the thickness of the lubrication layer h and can assert that it does increase with the mean flow velocity U as predicted by Bruinsma [10]. To our knowledge, this is the first direct measurement of h for a vesicle flowing in a narrow channel. We show in Fig. 4 the cumulative data for vesicles flowing in channels of radii $R_p = \{13.0, 13.5, 14.0\}\sigma$ plotted using non-dimensional axes $(h-h_{\min})/R_p$ *vs* $\eta U/\alpha_f(U)$, where α_f is the frontal area per lipid expansion of the vesicles, $\eta = 1.98\sigma^{-2}\sqrt{m\epsilon}$ is the shear viscosity of the surrounding LJ fluid, and $h_{\min} = 1.0 \pm 0.2$ is the minimum thickness of the lubrication layer whose value was extracted by fitting the data. One can see that the expected power law behaviour with an exponent of 2/3 agrees well with our data. Furthermore, the minimal thickness $h_{\min}$ found corresponds to the approximate value we can directly extract from simulations at the lowest pressures (see Sect. IV A 1). Fluid particles within a distance $h_{\min}$ away from the channel wall move with a velocity roughly an order of magnitude slower than the vesicle and close to zero such that they essentially create a no-slip layer. This is in agreement with what we found for a simple LJ fluid flow.

3. *Darcy's law.*

The actual relationship between flow velocity and pressure may be written as $\eta U = K'(\Delta P - \Delta P_{\min})/L_p$ [6] where $\Delta P_{\min}$ is the minimum pressure to push a vesicle of given size in the channel and K' is defined in Eq. 8. We plotted, in Fig. 5, ΔP as a function of UL_p/K' for data from simulations of small vesicles made of $n_l = 3000$ lipids pushed in channels of radii $R_p = \{13.0, 13.5, 14.0\}\sigma$ and extracted the shear viscosity η of the fluid in the lubrication layer and a mean minimum pressure $\Delta P_{\min}$.

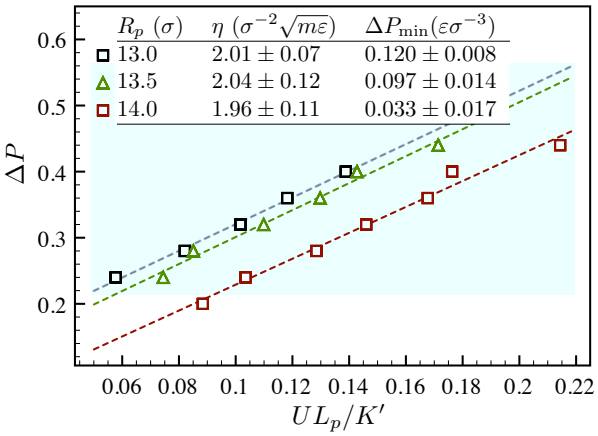

FIG. 5. Verifying that Darcy's law of the form $\eta U = K'(\Delta P - \Delta P_{\min})/L_p$ holds for our simulated vesicles. We here show linear plots of ΔP as a function of UL_p/K' for various channel radii $R_p = \{13.0, 13.5, 14.0\}\sigma$. The slope is the shear viscosity η and the intercept, the minimum pressure $\Delta P_{\min}$.

The table at the top of Fig. 5 summarizes the results. The shear viscosities reported in Fig. 5 are all within the margins of uncertainty of the expected value, a remarkable result given the number of physical quantities entering the calculation. Any small change to these produces important deviations in the value of η. As for the minimal pressure, one would expect it to decrease as the radius of the channel increases and this is what we observe: it is harder to push a vesicle of a given size in a smaller channel. However, we were not able to directly verify the accuracy of these predicted values in our simulations due to time constraints (very long and multiple massive simulations necessary).

4. *Tension profile along the vesicle.*

The frontal area expansion α_f used in verifying the validity of Eq. 5 in our simulations was obtained from profiles along the length of sphero-cylindrical vesicles such as those in Fig. 6a. Assuming we are in a linear regime where $\gamma \cong K_A\alpha$ we find that the profile for the outer layer of the membrane corroborates Eq. 6, that is tension decreases linearly along the cylindrical part of the vesicle in the channel going from the front to the back. The slope of the linear part should be, according to the same equation, $\eta U/K_A(h-h_{\min})$. We thus extracted from our data an approximate value for the area compressibility

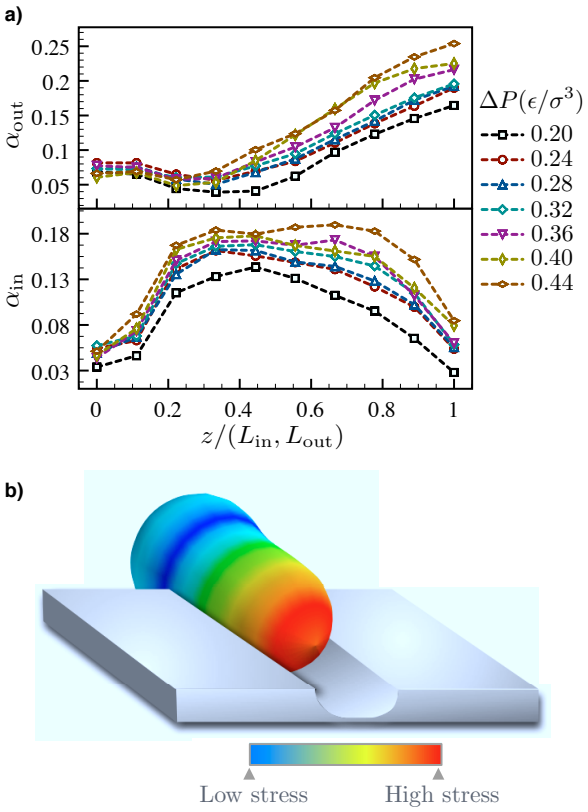

FIG. 6. a) Average tension profiles for the outer and inner layers of the membrane inferred from the change in area per lipid α as the sphero-cylindrical vesicles travel down the channel. The z coordinate along the length of the objects has been renormalized for ease of calculation and clarity. One can clearly observe, in the outer layer, the linear decrease of tension going from the frontal cap of the vesicle to its back. b) Heat map of the stress on the outer shell of the vesicle as it enters the channel: clearly pore nucleation and rupture is more probable close to the front cap and along the cylindrical portion of the vesicle.

modulus $K_A = 6.95 \pm 0.29\epsilon/\sigma^2$. Although this value is not exactly equal to $K_A = 8.84 \pm 0.76\epsilon/\sigma^2$ found for a flat bilayer (Sect. IV), it is of the same order of magnitude and still quite close. The discrepancy can be attributed to the different geometry considered, *e.g.* a vesicle *versus* a bilayer, and the fact that only the outer layer is involved here. Fig. 6a also shows the frontal tension increasing with the velocity as expected. Interestingly, the area expansion profile for the inner layer of the membrane does not follow its outer counterpart. Indeed, the area expansion appears roughly constant along the cylindrical part of the vesicle which means the hydrodynamic shear stresses the outer membrane is subjected to get damped in the bilayer and do not propagate to the inner heads. At the back of the vesicle, the hydrodynamic stress on the outer layer is at its lowest and the stresses on the two layers are comparable. As for the frontal part, the high curvature spaces out the outer heads while it compresses the inner heads which enhances the difference in stress. It is an interesting question whether this occurs or not in real nano-size vesicles flowing down narrow channels.

B. Initial passages simulated

To produce small vesicles by pressure extrusion, one starts with a suspension of rather large vesicles that break into smaller and smaller pieces with each passage through the extruder until the size stabilizes. Until now one could only guess what is the true mechanic of rupture of these large initial vesicles. For instance, it has been proposed that the rupture occurs at the neck of the channel in an axisymmetric fashion such that small hemispherical vesicles are expressed from the larger ones ("blowing a bubble" model of Patty and Frisken [7]). While this might be true for the very first passage, where vesicles are much larger than the channel radius, our simulations show that this might not be the case for vesicles of moderate sizes in the subsequent initial passages.

In our simulations, a rather large vesicle ($n_l = 10000$) approaching a small channel ($R_p = 12.0\sigma$) in a converging flow field eventually gets sucked-in due to the hydrodynamic friction with fluid particles speeding by as they enter the channel. Fig. 7D shows the vesicle as it is squeezing in the channel. Then one of two scenarios can happen: 1) the pressure is too weak and the vesicle reaches an equilibrium state; 2) the pressure is strong enough leading to rupture. When the vesicle ruptures, it always does so through pore nucleation whose probability is greater near the tip and decreases towards the neck as shown in Fig. 6b. Pores often nucleate in multiple sites at the same time which gives rise to flowing lipid sheets along the channel as shown in Fig. 7E. The sheets can then rip apart into smaller pieces in the channel and drift towards the other end where they fold again into floppy, partly deflated smaller vesicles. We think that the slightly higher than expected values of the critical surface expansion coefficient α_c that we found while analysing results from Patty and Frisken [7] are in part due to that loss of total internal volume or, equivalently, the creation of excess area. The polydispersity observed in the final sizes of vesicles produced by pressure extrusion [5–7] is most probably a direct consequence of the stochastic nature of the rupture of large vesicles penetrating into channels of small opening.

V. CONCLUSION

In the first part of this article, we have shown that the mean final size of vesicles produced by pressure extrusion depends on two elements: the geometrical constraints imposed on the vesicles due to volume conservation and finite extensibility, and the flow rate. It is known that

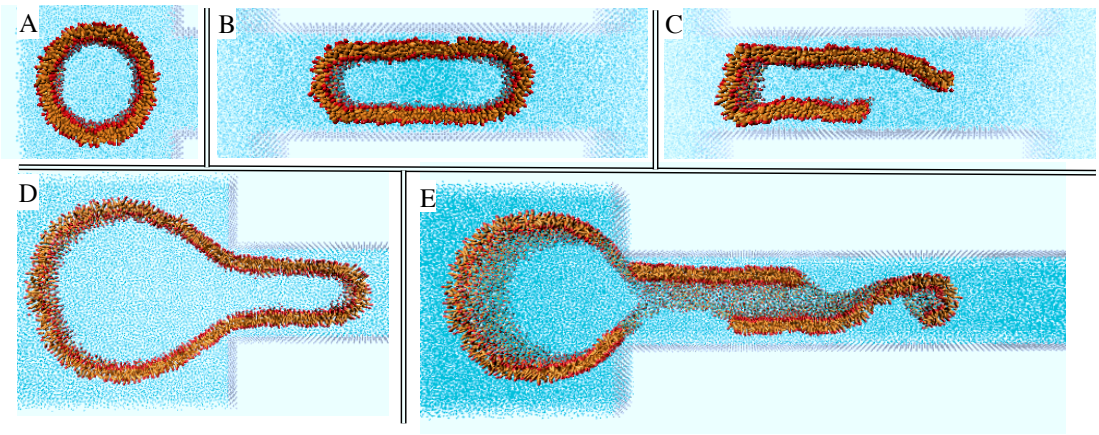

FIG. 7. Slices from 3D simulations of the pressure extrusion of vesicles in nano-channels. A) The initial shape of the vesicle for reference. B) A sphero-cylindrical vesicle flowing in the channel. C) A sphero-cylindrical vesicle breaking in a channel while pushed by a strong pressure difference. D) The typical shape of a vesicle as it is entering the channel. E) The rupture of a large vesicle at the entrance of a small channel.

beyond a critical area expansion α_c, a lipid bilayer vesicle ruptures and that the transition from a spherical shape outside the channel to a sphero-cylindrical shape inside is one that inevitably stretches its membrane if volume is to be conserved: a narrower channel results in greater area expansion. In addition, the faster a sphero-cylindrical vesicle travels inside the channel the more its membrane stretches since the channel appears smaller as a result of the thickening of the lubrication layer surrounding it [10]. Hence, as the flow rate increases, the size of vesicles that can go through a given channel without breaking decreases. Our model captures this behaviour and predicts the mean final size of vesicles obtained by pressure extrusion given the lysis tension γ_l and related approximate critical area expansion α_c of a lipid bilayer, the radius R_p and length L_p of the extruder's channels, and the applied pressure ΔP. Flow rate can be varied in multiple ways the easiest being a change in either the pressure gradient $\Delta P/L_p$ or the channel radius R_p. More subtly, Eq. 9 shows that an increase in lipid concentration results in a greater density of vesicles per channel which decreases the flow rate and produces slightly larger final vesicles. To test our model and in particular the flow rate dependence, we propose that the simple channel length doubling experiment performed at low pressure in the paper by Frisken *et al.* [6], where they observed no significant difference in the mean final size of extruded vesicles, should be repeated at high pressure where we predict a large vesicle size difference.

Fitting experimental data yields an effective critical expansion parameter α_c of the bilayer which includes both the unfolding component α_A and the expansion component α_γ. α_γ is usually known, so the fitting will yield α_A a measure of the degree of floppiness of the vesicle. α_A can then be used to estimate the content loss through the entire extrusion process, as volume loss is an important generator of excess area. This could potentially be useful in the context of drug encapsulation prior to extrusion.

The second part of our paper presents results from large scale non-equilibrium coarse-grained molecular dynamics simulations of nano-sized vesicles being extruded in narrow channels. Both lipids and solvent were explicitly included in the simulations, which to our knowledge is a first. Simulation cost has always been a major deterrent for doing so, but with the introduction of GPU-optimized code, it is now feasible on a reasonable time scale. One can even buy for a relatively low price a desktop workstation equipped with multiple GPUs that has the computing power of a small to medium size cluster of CPUs. The results of our simulations agree exceptionally well with Bruinsma's [10] description of a sphero-cylindrical vesicle flowing in a narrow channel and our own geometrical argument. We also used our simulations to try and give a qualitative description of the initial passages of large vesicles in the extruder. We showed that large vesicles did not rupture cleanly at the entrance of the channel but heterogeneously along the cylindrical part of the vesicle that is within the channel and with a greater probability towards the front cap. The fragments would then flow down the channel to close again into smaller and floppier vesicles.

Rupture in the channel of small extruded vesicles was frequently observed near the critical size. It is always accompanied by content loss and eventual closure of nucleated pores. A detailed study of this phenomenon will be presented in a subsequent paper. It should appeal to those interested in the encapsulation and release of drugs in the body, and to those studying the flow induced rupture of red blood cells in small capillaries since vesicles have similar rheological properties.

[1] A. Jesorka and O. Orwar, Annu. Rev. Anal. Chem. **1**, 801 (2008).
[2] D. Fenske, A. Chonn, and P. Cullis, Toxicol. Pathol. **36**, 21 (2008).
[3] B. Maherani, E. Arab-Tehrany, R. Mozafari, C. Gaiani, and M. Linder, Current Nanoscience **7**, 436 (2011).
[4] M. Hope, M. Bally, G. Webb, and P. Cullis, Biochim. Biophys. Acta **812**, 55 (1985).
[5] D. Hunter and B. Frisken, Biophys. J. **74**, 2996 (1998).
[6] B. Frisken, C. Asman, and P. Patty, Langmuir **16**, 928 (2000).
[7] P. Patty and B. Frisken, Biophys. J. **85**, 996 (2003).
[8] S. Clerc and T. Thompson, Biophys. J. **67**, 475 (1994).
[9] L. Rayleigh, Proceedings of the London Mathematical Society **1**, 4 (1878).
[10] R. Bruinsma, Physica A: Statistical and Theoretical Physics **234**, 249 (1996).
[11] G. Gompper and D. Kroll, Phys. Rev. E **52**, 4198 (1995).
[12] D. Quinn, I. Pivkin, S. Wong, K. Chiam, M. Dao, G. Karniadakis, and S. Suresh, Ann. Biomed. Eng., 1(2011).
[13] W. Rawicz, K. Olbrich, T. McIntosh, D. Needham, and E. Evans, Biophys. J. **79**, 328 (2000).
[14] B. Mui, P. Cullis, E. Evans, and T. Madden, Biophys. J. **64**, 443 (1993).
[15] R. Goetz and R. Lipowsky, J. Chem. Phys. **108**, 7397 (1998).
[16] M. Kenward and G. Slater, Eur. Phys. J. E **14**, 55 (2004).
[17] K. Meier, A. Laesecke, and S. Kabelac, J. Chem. Phys. **121**, 3671 (2004).
[18] R. Goetz, G. Gompper, and R. Lipowsky, Phys. Rev. Lett. **82**, 221 (1999).
[19] F. Tessier and G. Slater, Macromolecules **38**, 6752 (2005).
[20] T. Soddemann, B. Dünweg, and K. Kremer, Phys. Rev. E **68**, 046702 (2003).
[21] H. Limbach, A. Arnold, B. Mann, and C. Holm, Comput. Phys. Commun. **174**, 704 (2006).
[22] J. Anderson, C. Lorenz, and A. Travesset, J. Comput. Phys. **227**, 5342 (2008).
[23] A. Anderson, J and A. Travesset, Comput. Sci. Eng. **10** (2008).
[24] N. Amenta, M. Bern, and M. Kamvysselis, Proceedings of the 25th annual conference on Computer graphics and interactive techniques, 415(1998).

6

Other contributions

Besides the papers presented in this thesis, during the course of my doctoral studies I also contributed to the following submitted paper with members of Dr. Andrew Pelling's group:

L. Guolla, **M. Bertrand**, K. Haase, and A.E. Pelling "Force Transduction and Strain Dynamics in Actin Stress Fibres in Response to Nanonewton Force" Journal of Cell Science, Under Revision/Review (2011).

I developed a routine that allowed to considerably speed up the analysis of the strain along the length of actin fibres in the cell's cytoskeleton.

My research was also presented at a number of conferences listed below:

M. Bertrand and B. Joós "Lipid Bilayer Vesicle extrusion through nanopores: a coarse grained molecular dynamics study", American Physical Society (APS), March 2011, Dallas TX

B. Joós, **M. Bertrand**, and S. Ouellet "Vesicle Extrusion in nanopores", Canadian Association of Physicists (CAP), June 2010, Toronto ON

M. Bertrand, B. Joós, and D. O'Keeffe "The effect of sequence-dependent persistence length on the elastic response of polymers", Canadian Association of Physicists (CAP), June 2010, Toronto ON

B. Joós, **M. Bertrand**, and S. Ouellet "Vesicle Extrusion in nanopores", American Physical Society (APS), March 2010, Portland OR

M. Bertrand, M. Forget, and B. Joós "The Entropic Rigidity of Circular Polymers", American Physical Society (APS), March 2010, Portland OR

7

Conclusion

As scientists, our greatest hope is that some of what we did will serve as a nucleation site for other studies to come. To put it more bluntly: we want to be relevant. Throughout the last four years, I have tackled a variety of problems related to the deformation of soft materials, sowing the seeds for future research endeavours. I have been particularly successful with the Molecular Dynamics study of the rheology and deformation of lipid bilayer vesicles (Chapter 5) as both an undergraduate and a graduate student are working with Dr. Béla Joós and I on new problems using some of the investigative tools I have developed. As for the deformation of linear macromolecules such as DNA, thermophoretic stretch (Chapter 4) enthuses some of my colleagues, enough that future collaborations are quite possible. In this last section of the thesis, I'll recall some of the main conclusions of the papers presented in previous chapters, describe where the research should be taken, and discuss ongoing work.

Deformed polymers

Chapters 2, 3, and 4 are all about the deformation of linear macromolecules such as DNA, RNA, and proteins. Reading these, you have learned, or will learn, about the entropic response of a polymer ring to dilation with subsequent contortion (Chapter 2), the effect of backbone sequence on the entropic elasticity of a polymer (Chapter 3), and the deformation of a nano-confined polymer subject to thermophoretic forces (Chapter 4). Let me digress on these three topics.

Chapter 2 presents a study of the entropic elasticity of circular real chains dilated and subsequently twisted out of plane. The work done falls in the category of fundamental polymer physics as it completes our knowledge about the response to simple deformations of a real circular chain. Fundamental research does not always lead directly to applications, but it certainly might reveal itself useful in yet unforeseen situations. Only time will tell.

Chapter 3 presents a study of the effect of sequence on the entropic elasticity of a heteropolymer. Many biopolymers are heterogeneous, that is they are made of a sequence of elements sampled from a defined set, the most notable being DNA. The properties relevant to their entropic elasticity that are affected by sequence are the persistence length and the intrinsic curvature. As I was perusing the literature on the topic, it became clear that there was no simple way to characterize the importance of sequence in the entropic elastic response to an applied external force of a family of heteropolymers, *i.e.* polymers of the same length but different sequences. I thus derived, within the model of the entropic elasticity of semi-flexible chains, a very simple equation for the variance of the extension as a function of the applied force in what I called sequence space and, with this new tool, was able to measure the effect of sequence when both the persistence length and the intrinsic curvature varied along the backbone of a model polymer. Of course, the goal would now be to verify whether this is useful in the context of experiments. One could start by using data of the persistence length of distinct dinucleotides steps in DNA[1] to build realistic sequences instead of using arbitrarily randomized bending rigidities as was done. Simulations conducted with these would be more revealing of what is to be expected in reality. Also, as is mentioned in the paper, any phenomenon related to the entropic elasticity could be investigated. I would suggest looking into the effect of sequence on DNA translocation as it could potentially benefit those working in this hot research area.

Chapter 4 presents a study of the configuration of nano-confined polymers symmetrically stretched by thermophoretic forces. A symmetric thermal gradient is established in the pore with its warmer midpoint corresponding to that of the confined chain. Monomers are then pushed away from the central region towards the extremities by thermal forces, a behaviour that we call thermophobic. This was done experimentally and a related simple one dimensional model was even presented at the 2011 APS March convention in Dallas, Texas. It is from discussions with the presenter, Jonas N. Pedersen, that I had an idea for a more realistic and complete model which I then constructed and is the highlight of the paper we submitted on the topic. I compared it to

[1] Geggier, S. and Vologodskii, A., *Sequence dependence of DNA bending rigidity*, PNAS, **107** (2010), p. 15421

some preliminary experimental data on DNA and found a Soret coefficient, which characterizes the strength of thermophoresis, close to the expected value. I also was able to describe the configurations of a simulated polymer in a solvent whose temperature is close to its θ value. The thermophoretic manipulation of polymers in micro- and nano-fluidics devices is still in its infancy and many questions are still unanswered. As natural extensions of the study I conducted, two things could be further explored: the effects of explicit electrostatic interactions and the origins of the thermophoretic force. Indeed, this last issue is not addressed in our paper and it would certainly be interesting to see what can be done with the theory proposed by Duhr and Braun[2]. As for electrostatic interactions, the questions are: do the ions move under thermophoresis, and if they do, does it create a charge depletion towards the central part thus contributing to chain extension? Interesting research ahead.

Deformation and flow of vesicles

Chapter 5 presents my first foray in the marvellous world of self-assembled lipid bilayer membranes. The question answered therein is one that my supervisor was juggling with for a number of years: can we predict the final sizes of vesicles produced by pressure extrusion through nanochannels? Models to do so have already been proposed by Clerc and Thompson[3], and Patty and Frisken[4]. However, the first fails to predict the pressure dependence and is inaccurate, while the second introduces free parameters whose physical origins are unclear. I thus constructed an alternative model using a method I call *connect the dots*: all the pieces necessary are there in the work of talented scientists and just need to be connected. It does a great job at predicting the final size of extruded vesicles given only physically relevant parameters. The main elements of my model came from Bruinsma's description of sphero-cylindrical vesicles flowing down narrow capillaries[5]. Being a computational physicist, it was only natural then that I verify their veracity through some massive molecular dynamics simulations. Chapter 5 also presents the results of these. In these simulations, a large number of rupture events were observed and characterized which should lead to an article on rupture mechanics in vesicle extrusion. In addition, the simulation methodology

---

[2] Duhr, S. and Braun, D., *Why molecules move along a temperature gradient*, PNAS, **103** (2006), p. 19678

[3] Clerc, S. and Thompson, T., *A possible mechanism for vesicle formation by extrusion*, Biophys. J., **67** (1994), p.475-477

[4] Patty, P. and Frisken, B.J., *The pressure-dependence of the size of extruded vesicles*, Biophys. J., **85** (2003), p. 996-1004

[5] Bruinsma, R., Physica A, *Rheology and shape transitions of vesicles under capillary flow*, **234** (1996), p. 249-270

and analysis routines developed are now being used by two students working with Dr. Béla Joós and I. Alison Harman (M.Sc. candidate) is looking into the flow of vesicles in larger channels focusing particularly on the rupture and loss of content, while Ben Barlow (B.Sc. candidate) is trying to simulate the deformation of vesicles when pushed on by the tip of an atomic force microscope (AFM). The first project should appeal to those studying the rupture of red blood cells in the blood vessels of diseased patients and those looking into the delivery of vesicle encapsulated drugs. With the second project, there is a possible experimental collaboration and we hope to better understand the viscoelastic response of cells mechanically deformed by the tip of an AFM. Ultimately, I would also like to simulate more realistic lipid bilayers using the MARTINI coarse graining procedure.

Final words

I do not think anybody's journey through doctoral studies is an easy one. In my case I started out as an old teenager, maybe a bit lost and egocentric, and now emerge as a young man father of two with sometimes more responsibilities than I'd wish for. This transformation was not without pains. I remember some very hard moments where I really thought I wouldn't make it. But I was supported and persevered through the storms. I do not regret any of the decisions taken and am coming out more passionate than ever about science, either as a communicator or a researcher. I thought that the end of my master degree was the start of it all. Strangely, I feel the same now.